The Aeroplane Spin Motion and an Investigation into Factors Affecting The Aeroplane Spin

A thesis submitted for the degree of Doctor of Philosophy

by

Rein Inge Hoff

Brunel Flight Safety Laboratory

College of Engineering, Design and Physical Sciences

Brunel University London

November 2014

Abstract

A review of aeroplane spin literature is presented, including early spin research history and lessons learned from spinning trials. Despite many years of experience in spinning evaluation, it is difficult to predict spin characteristics and problems have been encountered and several prototype aeroplanes have been lost. No currently published method will reliably predict an aeroplane's spin recovery characteristics.

Quantitative data is required to study the spin motion of the aeroplane in adequate detail. An alternative method, Vision Based State Estimation, has been used to capture the spin motion. This alternative method has produced unique illustrations of the spinning research aeroplane and data has been obtained that could possibly be very challenging to obtain using traditional methods.

To investigate the aerodynamic flow of a spinning aeroplane, flights have been flown using wool tufts on wing, aft fuselage and empennage for flow visualization. To complement the tuft observations, the differential pressure between the upper and lower horizontal tail and wing surfaces have been measured at selected points. Tufts indicate that a large-scale Upper Surface Vortex forms on the outside wing. This USV has also been visualized using a smoke source. The flow structures on top of both wings, and on top of the horizontal tail surfaces, have also been studied on another aeroplane model. The development of these rotational flow effects has been related to the spin motion. It is hypothesized that the flow structure of the turbulent boundary layer on the outside upper wing surface is due to additional accelerations induced by the rotational motion of the aeroplane.

The dynamic effects have been discussed and their importance for the development of the spin considered. In addition, it is suggested that another dynamic effect might exist due to the additional acceleration of the turbulent boundary layer due to the rotational motion of the aeroplane. It is recommended that future spin recovery prediction methods account for dynamic effects, in addition to aerodynamic control effectiveness and aeroplane inertia, since the spin entry phase is important for the subsequent development of the spin. Finally, suggestions for future research are given.

Disclaimer

This report has been prepared at the Brunel Flight Safety Laboratory, Brunel University London, as part of a research degree and this report is prepared for research purposes only.

Absolutely no information, and none of the instructions, contained in this report are for operational use.

The spin characteristics depend on many variables and a slight change in configuration might alter the spin behaviour. Aeroplanes used in this research project, and aeroplanes discussed and referenced in the text, might be modified for research or test purposes, or might be experimental prototypes at an early development stage that might or might not have been certified at a later stage. Even if known aeroplane models are discussed in this report, the reader should be warned that the information might not be applicable or accurate. In some cases the aeroplanes have been modified for research or test purposes and are not representative of similar models even if the same name, type and model designation is used. Similar aeroplanes may have very different flight and spin characteristics.

This report is not a guide or source of information on how to fly, do a flight test or how to perform spinning. The information in this report is not a substitute for formal flight training from a recognized source of hands-on stall, spin, aerobatic flight or flight test instruction. Pilots should never perform aerobatic flight, stalls, post-stall manoeuvres or intentional spinning without proper flight instruction from a qualified flight instructor. Always use appropriate safety equipment and always adhere to the information and instructions in the official documentation from the aeroplane manufacturer or operator. Aerobatic flight and spinning can be very dangerous and life threatening.

Contents

Page No.

List of tables

List of figures

Abbreviations

AAIB	Air Accidents Investigation Branch
ADP	Air Data Probe
AHRS	Attitude and Heading Reference System
AI	Aileron In (Aileron set with the spin direction)
BCAR	British Civil Airworthiness Requirements
BFSL	Brunel Flight Safety Laboratory
CAA	Civil Aviation Authority
CAD	Computer Aided Design
CAS	Calibrated Air Speed
CCD	Charge-coupled Device (camera image sensor)
CEP	Circular Error Probable
CFD	Computational Fuid Dynamics
CG	Centre of Gravity
CS	Certification Specifications
DEF-STAN	Defence Standard
EASA	European Aviation Safety Agency
FAA	US Federal Aviation Administration
FAR	Federal Aviation Regulation
FDR	Flight Data Recorder
GPS	Global Positioning System
IAS	Indicated Air Speed
IMU	Inertial Measurement Unit
LAWR	Large Amplitude Wing Rock
LEV	Leading Edge Vortex
MAC	Mean Aerodynamic Chord
MATLAB	Matrix Laboratory
MEMS	Micro Electro Mechanical System
MPB	Multi Purpose Boom
MoI	Moment of Inertia
NACA	US National Advisory Committee for Aeronautics
NASA	National Aeronautics and Space Administration
NPL	National Physics Laboratory
NRC	National Research Council
NTPS	National Test Pilot School
OS	Operating System

PLF	Power for Level Flight
PSG	Post-stall gyration
PSS	Pitot Static System
RAF	Royal Air Force
RAE	Royal Aircraft Establishment
RAeS	Royal Aeronautical Society
SF	Stick Forward
TAS	True Air Speed
TDPF	Tail Damping Power Factor
USAF	United States Air Force
USV	Upper Surface Vortex
VBSE	Vision Based State Estimation
VLA	Very Light Aeroplanes
WP	Wing Point

Nomenclature

$\boldsymbol{a}$	Total flow acceleration vector
$\boldsymbol{a_u}$	Local flow acceleration vector
b	Wing span
C_D	Drag coefficient
C_L	Lift coefficient
C_{Lmax}	Maximum Lift coefficient
dP	Differential pressure
dP1	Differential pressure sensor no. 1
dP2	Differential pressure sensor no. 2
dt	Time step
g	Acceleration due to gravity
$\boldsymbol{H}$	Angular Momentum vector
I	Moment of inertia
I_{xx}	Moment of inertia about the the X axis
I_{yy}	Moment of inertia about the the Y axis
I_{zz}	Moment of inertia about the the Z axis
L_i	Inertia rolling moment
m	Mass
M_i	Inertia pitching moment
N_i	Inertia yawing moment

N_Z	Normal acceleration
p	Rate of roll
q	Rate of pitch
r	Rate of yaw
R	Radius
Re_c	Reynolds number based upon MAC
S	Wing area
U	Velocity
V_S	Stall speed
$\boldsymbol{v}$	Flow velocity vector
α	Angle of attack (AoA)
α_{CG}	Estimated AoA at the aeroplane CG
α_{IWP}	Estimated AoA at inside wing point
α_{OWP}	Estimated AoA at outside wing point
β	Angle of sideslip (AoS)
θ	Pitch angle
θ_y	Angle of wing tilt with reference to the horizontal plane
ρ	Air density
φ	Roll angle
ψ	Yaw angle
Ω	Rotation rate or Angular velocity vector

Acknowledgements

A project involving full-scale flight testing and research naturally involves several people whom I would like to express my sincere gratitude to. First and foremost I would like to thank my mentor and supervisor Dr Guy Gratton for encouraging support throughout, for facilitating interesting meetings and discussions in a friendly cooperative atmosphere and for being the Review Signatory on the many flight test plans necessary to conduct the research flights. I would also like to thank my supervisor Dr Cristinel Mares for guidance, support and for pointing me in the right direction as I started this journey of discovery. Dr Anthony Gee also provided encouragement and motivation in the early phases of the research and helped with weighing Glider wings for the mass properties estimation study.

A very special thank you to Håvard Finnesand at VisCo for help with the illustrations, camera and object tracking, and for operating the cockpit cameras on some of the research flights. I am also indebted to Jonny Engelsvoll for helicopter camera operation and movie production, photographers Torje Fanebust Aas and Arne Andersen, and Helicopter Pilot Kristian Elvestad for help in providing chase for the spinning Firefly. I also wish to thank Ricardo Ferreira for help with laser scanning the Firefly and the creation of the CAD model, and Valentin Buergel at Simtec for help with the pressure sensor system and the Air Data Probe.

I am grateful to Knut Lande, for initially teaching me aerobatic flight and for motivation and encouragement to join the flight test profession. I have had several encouragements from test pilots and others in industry to continue the spin research, but I would like to thank in particular Major General (ret.) Des Barker and Dr Dieter Reisinger for being supportive. Finally, and most importantly, I would like to thank a very supportive family. I am grateful beyond words for my wife Kristine who has taken care of our children at home while I spent many days and weekends at the airport conducting research flights when weather permitting.

List of Journal Papers

1. Hoff, R.I., Gratton, G.B., Gee, A.E. Estimating Sailplane Mass Properties, *Technical Soaring*, Vol. 34, No.4, October- December 2010

2. Hoff, R.I., Gratton, G.B. Camera Tracking and Qualitative Airflow Assessment of a 2-turn Erect Spin, *The Aeronautical Journal*, Vol 116, No. 1179, May 2012

3. Hoff, R.I., Gratton, G.B. Spin Induced Aerodynamic Flow Conditions on Full-scale Aeroplane Wing and Horizontal Tail Surfaces, *The Aeronautical Journal*, Vol 117, No. 1198, December 2013

4. Gratton, G.B., Hoff, R.I., Bromfield, M., Rahman, A., Harbour, C., Williams, S. Evaluating a set of stall recovery actions for single engine light aeroplanes, *The Aeronautical Journal*, Vol 118, No. 1203, May 2014

1 Research subject introduction

Stall and spin accidents have plagued aviation since the very first flights. Even today stall and spin accidents remain one of the unresolved problem areas in aviation. In particular for the single engine light aeroplanes there are several fatal accidents every year.

The problem is twofold, the pilot and the aeroplane. If the pilot finds himself in circumstances, inadvertent or deliberately, where he departs controlled flight the outcome will depend upon the pilot's ability to regain control. The pilot needs knowledge about aeroplane stall and spin characteristics and also airmanship, which is the application of knowledge, to regain control. The aeroplane on the other hand must not exhibit any undesirable or unrecoverable stall and spin characteristics that will make the pilot efforts overly difficult, or in the worst case impossible. Much effort has been put into aeroplane design to develop safe aeroplanes. However, spin test reports indicate that it is still difficult to predict spin characteristics accurately [1,2,3,4,5,6,7].

It then follows that extensive stall and spin testing is required for both new designs and also for aeroplanes that have been modified. A flight test organization is tasked to evaluate the aeroplane such that the essential knowledge of the stall and spin characteristics can be provided to the pilot. Furthermore, the flight test organization needs to evaluate the aeroplane design and if any undesirable characteristics are found, fixes or changes to the aeroplane design might be required. This testing can be hazardous and is considered to be high risk. Prototype aeroplanes have been lost during testing due to unrecoverable spins.

Due to the lack of a reliable spin prediction method, the test pilot is basically left with a careful, incremental, but nonetheless still hazardous spin testing method. A spin flight test programme of a single engine amateur-built aircraft in Norway, with the author as the Test Pilot, became the background for a spin research programme at the Brunel Flight Safety Laboratory (BFSL). While searching for a spin recovery prediction method, being relevant due to a modified tail on the amateur-built aircraft, it became clear that several spin research questions should be addressed. In particular the factors affecting spin entry and recovery characteristics and also the unsteady aerodynamic flow

over wing and tail areas should be better understood before a spin prediction method would become a future reality.

Even in recent journal papers on spinning, the aeroplane spin is labelled as mysterious [8]. A step in the right direction would be to leave mysterious behind and then advance to very complex. Spin research should endeavour to advance the knowledge of the departure from controlled flight. Both the aeroplane designer and the flight test organization would benefit if knowledge existed that enables the prediction of spin characteristics, or at least a better understanding of the governing factors. The aeroplane designer could identify problem areas early and try to enhance the aeroplane design such that the final product is as safe as possible. The flight test organization needs to reduce the risk of flight testing and also needs information about spin recovery techniques that most likely will recover the aeroplane from spin modes. The desired end result is, by improved aeroplane design and flight testing, to reduce the number of fatal accidents that so far have claimed too many lives.

Although a holistic approach to the full-scale spin research was used in this programme, and data obtained when possible from the start to final spin recovery, special emphasis was on the entry phase of the spin. This was due to the assertion that the spin entry phase is very important for the development of the spin, i.e. it is the spin entry phase that governs if the spin becomes unrecoverable or not.

2 Review of literature

2.1 Introduction

"The main object of studying the spin is to prevent it from occurring in any form from which recovery is difficult."
B. Melvill Jones, Aerodynamic Theory, 1935

To reduce the risk of spin flight testing, a flight test organization needs knowledge about spin theory and the industry 'best practice' evolved from the lessons learned in spinning evaluations of the past. Bodies of knowledge exist to support this, e.g. the FAA Flight test guide for certification of Part 23 airplanes [9], but are necessarily incomplete.

Predicting an aircrafts' spin characteristics before a flight test programme is very difficult. A case in point might be the problems Cessna had during certification testing of the Cessna 162 Skycatcher Light Sport Aircraft. One prototype aircraft was lost during spin testing after the test pilot had to bail out [1] and later there was another spin testing incident where another prototype aircraft was damaged [2]. Eventually, after design modifications had been implemented, the spin testing programme for the Cessna 162 was completed. Unfortunately, this case is probably not unique and there have been several cases of spin recovery problems encountered during spin flight testing resulting in loss of prototype aircraft (e.g. Lancair 400 [3], Gippsland GA-8 Airvan [4], Airplane Factory Sling [5,6], and a unnamed light aeroplane [7]). In some cases, costly and complex design changes have been necessary after completion of the initial spin test programme to be able to comply with spin recovery requirements such as those found in applicable certification standards, e.g. [10,11,12,13,14,15,16].

Spin behaviour of an aeroplane depend on so many variables that spin recovery prediction is very difficult. However, as we will later discuss in this Chapter there have been several attempts to provide the aeroplane designer with guidelines and predictive methods. Historically the approach to this complicated matter has been analysis complemented by the use of experimental data obtained from wind tunnel experiments of aeroplane models. As well as providing a design tool, a spin prediction method could potentially give the flight test team a heads-up regarding what they might encounter

during flight test. It could be a useful tool for risk management evaluation before the flight test. Despite being well known that such methods are based on simplified analytical methods and empirical data from wind tunnels, it is very tempting to use them in a spin flight test programme. Indeed, this has been recommended in papers presented at the European Symposium of the Society of Experimental Test Pilots [7,17]. Unfortunately, as we will conclude after reviewing available literature, use of these methods is of limited value and can give misleading results.

2.2 Prelude to spin: Departure from controlled flight

Stall is the initial condition that must be fulfilled for a spin to occur. Stall is classically defined as the angle of attack where maximum lift coefficient ($C_{L_{max}}$) is achieved. Due to wing airflow separation the drag increase and lift decrease as the angle of attack increases even further. The pilot usually has no means to know exactly where maximum C_L is achieved at a given flight condition. However, the stall from the pilot's perspective in the cockpit is defined as an uncontrollable downward pitching motion or the stick reaches the back stop (elevator at full up position) [13,14]. It is the uncommanded motion at the stall, either in the form of a motion about an axis or a high decent rate, which is the initiation of departure from controlled flight. To further investigate this uncommanded motion it is necessary to consider the stability of the aeroplane at and past the stall angle of attack. The change in aeroplane stability when transitioning from the pre-stall to the post-stall flight regime is a fundamental concept in the understanding of departure from controlled flight.

Anderson [18] discusses the aerodynamic considerations of the stall/spin problem in a historical context. Since the very first flights it has been a challenge for the aeroplane designer to provide safe stall characteristics. However, progress has been made and Anderson's view is that poorer accident rates are apparent for older aeroplanes:

"The aerodynamic features that tend to promote spin entry, i.e., low poststall roll damping, large adverse yaw due to aileron deflection, high elevator power to permit good stall penetration, and large rudder control power to induce sizable yawing moments, were all inherent in these aircraft."

Figure 1 shows typical variations of the aerodynamic parameters through stall, where it is clear that loss of stability at stall occurs. Considering the pitch stability first, the typical motion of the conventional aeroplane (monoplane with horizontal stabiliser aft) is a pitch down at the stall. It is not common for the conventional aeroplane to depart dramatically in pitch alone, e.g. pitch up or down to the vertical. However, for unconventional aeroplanes there have been some cases reported, particularly with canard (e.g. the Curtiss XP-55 [19]) and tailless designs (e.g. the General Aircraft 56/01 sailplane [20]).

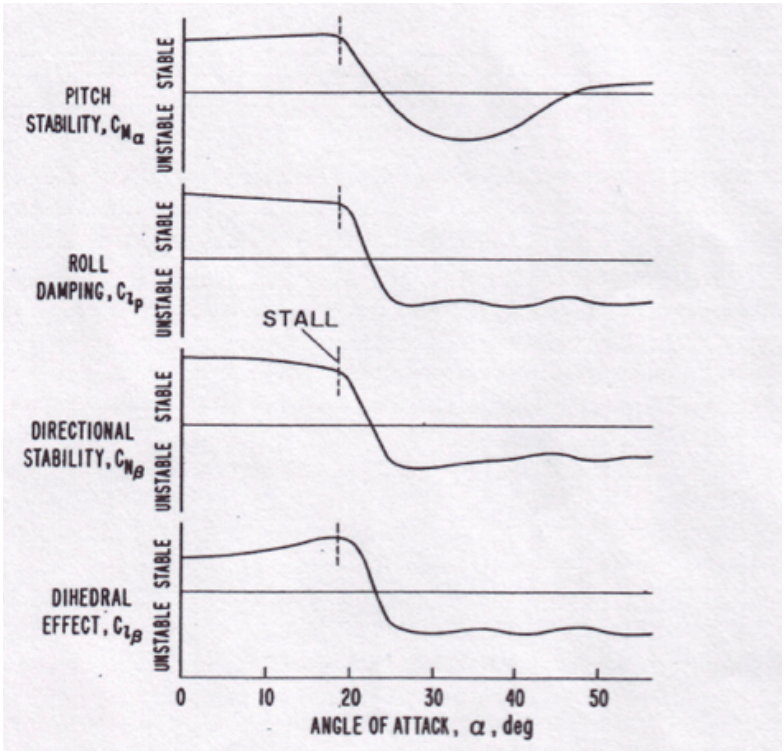

Figure 1. Typical variations of the aerodynamic parameters showing the loss of stability at the stall (figure from Ref. [18]).

The typical departure from controlled flight that results in a spin is due to a combination of the aerodynamic parameters shown in Figure 1. Consider now that a perturbation to the flight path at the stall occurs, for example caused by turbulence or the pilot mishandling the flight controls. The wing starts to roll in one direction due to the loss of roll damping. If sideslip develops and the directional stability is negative, the nose of the aeroplane yaws from the direction of flight. The lateral stability (dihedral effect) is also negative, so there will be no restoring roll due to the developed sideslip. The lack of pitch stability does not reduce the angle of attack, and if the angle of attack remains high, the wing might start to autorotate and the result is the spin.

The nature of the departure from controlled flight for a given aeroplane depends upon many variables. The effect of power for the conventional aeroplane with engine first configuration has in particular been shown to be destabilizing [21, 22]. There might be many different departure modes, depending on almost unlimited combinations of aeroplane configuration, use of the flight controls and flight conditions. Therefore, it is not uncommon for a certain departure mode to lay 'hidden' for many years and then be discovered after an incident or accident. Therefore, aeroplanes that have been in service might be sent back to the test organization for further stall and spin testing.

One such case in point is the Cessna T-37 (Figure 2), a twin engine USAF jet trainer, which was introduced in service in 1958. After thousands of hours flown in service the T-37 was the subject of a flight test programme in 2001 called HAVE SPIN [23]. The reason for the inquiry was an incident in which the T-37 departed and autorotation occurred after a formation breakout manoeuvre. The ingredients that led to the departure were high angle of attack, roll and stall. What was found peculiar with this departure was that the roll and spin was in the same direction, as opposed to an adverse yaw type of departure were the aeroplane would spin in the opposite direction of the roll. The test team found that [23]:

"…under the conditions tested with rudder fixed at neutral, aerodynamic effects governed the departures and not inertial effects."

Furthermore, two types of departures were found, the adverse yaw and the rolling departure. The rolling departure was due to a stall followed by a roll and yaw in the same direction. It is also probable that another military jet-trainer, the Aermacchi MB-326M was prone to depart in the same manner. An operational supplement to the flight manual was issued in 1985 warning against *"autorotation phenomena"* if a high roll rate was present simultaneously with the aeroplane in a *"close to the maximum lift limits"* state [24]. Interestingly, this supplement also gives some indication of how powerful these dynamic effects might be. It is warned that *"an abrupt increase of the roll rate is obtained, which exceeds the values reachable by the mere use of the lateral control"*. This indicates that the roll rate obtained in a rolling departure will be higher than what might be obtained by using the aileron control.

The motion following a departure from controlled flight is normally described as either a spin or post-stall gyration (PSG). PSG implies a gyration about one, two or even all three of the aeroplane body axes. However, PSG does not include the motion 'reserved' for the spin, which is a sustained rotation rate due to the autorotative properties of the wing. The spin motion will be described further in section 4. Usually, the departure from controlled flight will be followed by a PSG that might further develop into a spin.

Figure 2. The Cessna T-37 twin engine USAF jet trainer (courtesy of USAF).

2.3 Aeroplane spin history and the early spin investigations

Before the spin had been properly investigated, it was believed to be due to aeroplane lateral instability and a special case of side-slip [25]. The proper recovery from this condition was believed to be rudder applied in the direction of turn. In hindsight, this rudder application is in the pro-spin sense, and will thus promote the spin instead of stopping it. The first documented successful spin recovery is commonly referred to as 'Parke's Dive' after Lt. W. Parke inadvertently entered a spin from a relatively low altitude before landing at the airport. After having tried to recover the aeroplane from the spin with no result, in desperation and as a last resort, he pushed opposite rudder, which promptly recovered the aeroplane at a very low altitude. According to Berriman, this incident was debated afterwards and a description of the event, and most importantly the

use of the rudder that led to the spin recovery (*"rudder outwards"*), was reported in *Flight* magazine in August 1912 [26].

Which pilot was the one to first voluntarily enter a spin and then recover has been debated and several claims have been put forward [25]. However, the first scientific spin study was reported in a paper from March 1918 by Lindemann, Glauert and Harris [27]. Despite the 'Parke's Dive' event and subsequent article describing the spin recovery procedure of using opposite rudder, there have been reports of spin mishaps occurring during those 1st World War years where the pilots had no reliable information about the proper recovery technique [25]. In this context the study by Lindemann, Glauert and Harris was a very important milestone in the history of the spin. F.A. Lindemann (later to become Prof. Lindemann and also the Viscount of Cherwell) learnt to fly at the Central Flying School at Upavon, Wiltshire, UK during September and October 1916. After flight training, Lindemann engaged in research flying at Farnborough at the Royal Aircraft Establishment (RAE). According to his Pilot's Flying Log Book [28], he was first testing aircraft instrumentation, such as the compass and turn indicator, gyroscopic bombsight and accelerometer. His first research flight where *"Spins"* are noted as a remark was 13 June 1917 in a Royal Aircraft Factory B.E.2e aircraft. Apparently, he also flew some spin research flights in July 1917 using both an F.E.2b and a B.E.2c aircraft.

This first scientific report on the spin describes fundamental spin concepts that remain valid today. The spin was described as a spiral glide with a very steep path, with *"the wing incidence above the stalling point"*. Streamers, attached to a rod fastened in the middle of the wing struts, were used to estimate the angle of attack in the spin. Due to the high angle of attack, the drag was believed to be very large. Furthermore, the spin was described as a steady and stable motion, with low airspeed and aeroplane attitude described as wing struts horizontal and *"no appreciable sideslip"*. The report includes quantitative data from the spin experiments, such as period and radius of turn, indicated airspeed, height loss and normal loading obtained from a spring accelerometer. However, the recording of airspeed, radius of turn and height loss was noted to be uncertain due to limitations in the instrumentation used. In addition, both lateral and longitudinal levels ('bubble') were used to obtain the direction of the resultant force in the spin.

Lindemann *et al* presented equations for the aeroplane centre of gravity motion using two sets of axes, one fixed in space (i.e. global) and the other fixed in the aeroplane. Some simplifications were used, e.g. the forces on the tail sections were neglected and the sideslip was set to zero. Furthermore, data from the full-scale spin experiments were used in the analysis to obtain a theoretical solution, enabling an analysis of the variation of angle of attack during a developed spin over the wingspan (Figure 3).

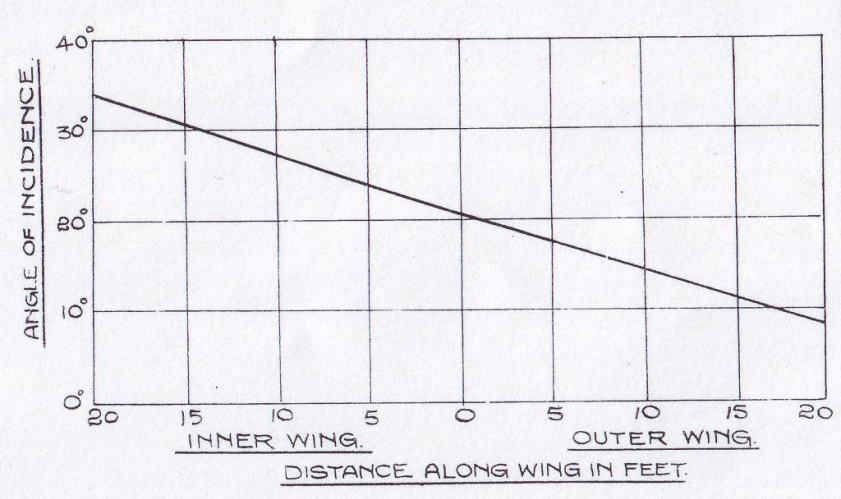

Figure 3. A result from the spin analysis published in 1918, the variation of angle of attack (termed *"angle of incidence"*) over the wingspan of a spinning aeroplane (figure from Ref. [27]).

The use of the aeroplane controls was also described, with control usage for a normal spin given as full left rudder and stick full back and to the right. From aeroplane stall, the spin entry technique recommended was to *"put on plenty of rudder while keeping the stick well back and preferably to the opposite side"*. Interestingly, the controls were also varied during the spin, and a transition to spiral mode was the result of moving the stick forward. The use of in-spin aileron resulted in increased rotation rate and airspeed. For spin recovery, it was simply stated that the reverse of the spin entry (*"rudder taken off gradually and the stick eased forward"*) could be used to transition into a spiral, or a more rapid method could be used by *"take off rudder and push the stick forward enough to flatten out in the usual way"*. However, there was a word of caution offered, that if the latter recovery technique was used it could result in a spin in the opposite direction if care was not taken when the stick was moved forward.

Glauert, an aerodynamicist at the RAE who was the second author of the first report on spinning [27], published another spin investigation report in June 1919 [29]. This report included further discussions on control usage for spin entry and recovery, more experimental data and more detailed equations for the spinning aeroplane centre of gravity motion. Glauert introduced *"strip theory"* for the spinning aeroplane, which is an estimation technique where the wing is sliced into aerofoil elements, the force estimated for each element and then finally the total aerodynamic force obtained by integrating over the wingspan. Furthermore, Glauert's report also has a section on the autorotation of the wing with reference to experimental work performed in 1918 at the National Physical Laboratory (NPL) by Relf and Lavender, where they investigated the motion of a stalled aerofoil mounted in a wind tunnel. With the wing free to rotate about a fixed axis, it was reported that the wing would autorotate at certain angles of attack beyond stall. With angles of attack below stall, any perturbations in rotation would not lead to autorotation, i.e. damping of the motion was in effect. However, at angles beyond stall, autorotation would occur. After theoretical considerations, Glauert concluded that this instability of the wing past the stall angle of attack must *"exert an important influence on the control of an aeroplane"*.

In addition, Glauert's report also included a spin test report written by Major F.W. Gooden, a Test Pilot at the Royal Aircraft Factory at Farnborough, as an Appendix. This spin testing of the F.E. 8 aeroplane was performed in August 1916, and it is probably the first spin test flight report published. Gooden described the techniques used to enter and recover from the spin and he also shared his thoughts about aeroplane controllability and the possible effects of powerful aeroplane controls. It is his view that the aeroplane in question is safe and *"perfectly stable",* but if the controls are misused they are powerful enough to change this stable aeroplane state. He further underlined this statement by explaining that he could only get the aeroplane to spin by *"the misuse of the controls"*. However, if the aeroplane departs controlled flight the controls are powerful enough to regain control if the proper recovery technique is used.

2.3.1 The simplified steady state spin

As discussed in the previous section, progress was made during those first years of spin investigations, starting with a largely unknown phenomenon to the realisation that the spin was a steady, post-stall spiral motion caused by the instability of the wing past the stall angle of attack, in effect enabling autorotation. However, despite the progress in understanding, the spin continued to be the cause of accidents due to aeroplanes failing to recover from it. Therefore, Bryant and Gates were tasked in 1924 to further investigate the spin and subsequently presented a paper on spinning in 1927 at the Royal Aeronautical Society (RAeS) [30]. They were addressing the fundamental mechanism of the spin and in particular aeroplane features that were either favourable to the development of the spin or features that were unfavourable to the recovery from the spin. It is interesting to note, that this report includes an early realisation that the spin subject is very complex and answering the appropriate research questions fully might not be possible. Furthermore, it also indicates the extent of the spin problem and the sensitivity of factors that might not be fully understood, as it reports observations of different spin characteristics on individual aeroplanes, even of the same type.

Indeed, the mathematical model of the aeroplane spin is possibly very complex, and does not lend itself well to analysis. However, to explain some of the observations from spinning, it is beneficial to start with the simplified steady state spin. It is not an accurate model of the real world spin, but it does explain some of the characteristics of the spin. We assume an aeroplane of conventional design in an erect, steady state spin with sustained yaw rate and all forces and moments are in balance. Furthermore we assume wings level, no power effects and the aeroplane symmetric about the XZ-plane. The velocity is assumed to be vertical as shown in Figure 4 below. Bryant and Gates called this simplified model of the steady state spin *"the prototype spin"* [30].

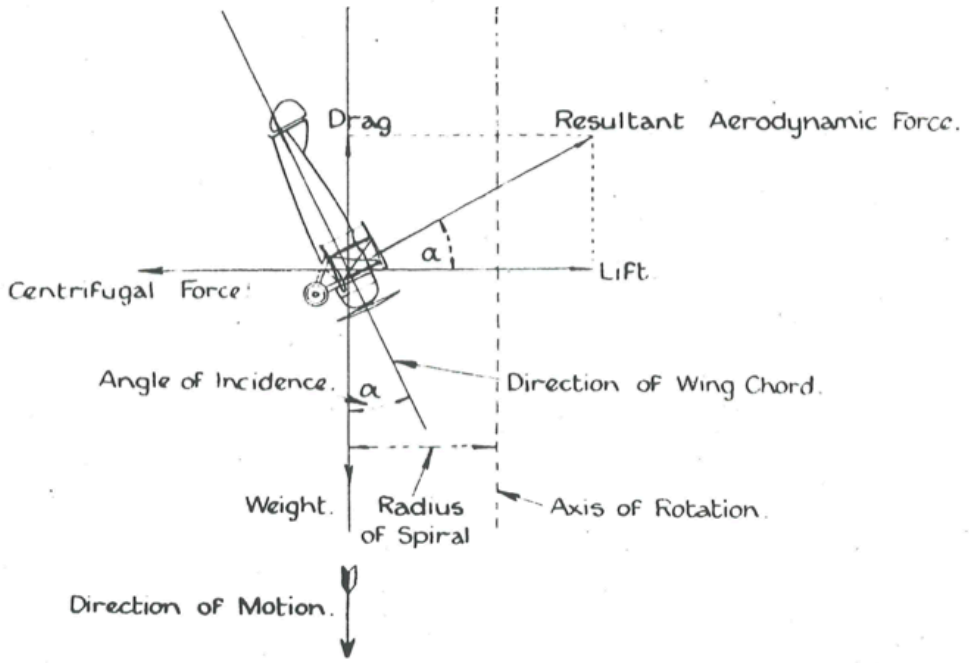

Figure 4. Illustration of *"the prototype spin"*, showing the resultant aerodynamic force and its components, lift balanced by centrifugal force and drag balanced by weight (figure from Ref. [30]).

With lift balancing centrifugal force and drag balancing weight as shown in Figure 4 we get [30]

$$\frac{1}{2}C_L\rho SU^2 = m\Omega^2 R \tag{2-1}$$

$$\frac{1}{2}C_D\rho SU^2 = mg \tag{2-2}$$

where m is aeroplane mass, g is acceleration due to gravity, U is descent velocity, S is wing area, ρ is air density , R the spin radius, Ω the rotation rate and C_L and C_D are the lift and drag coefficients respectively.

The orientation of the rigid aeroplane body-fixed axis relative to the fixed coordinate system was given by the Euler angles: pitch (θ, rotation of the X-axis in the XZ-plane), bank (ϕ, rotation of the Y-axis in the YZ-plane) and yaw (ψ, rotation about the Z-axis in the XY-plane).

The yaw was assumed to be small and disregarded, and the aeroplane angular velocity vector thus given as [30]

$$\Omega = \begin{Bmatrix} p \\ q \\ r \end{Bmatrix} = \begin{Bmatrix} \Omega \sin\theta \\ \Omega \cos\theta \sin\phi \\ \Omega \cos\theta \cos\phi \end{Bmatrix} \tag{2-3}$$

where p, q and r are the angular velocity vector components shown in Figure 5 below.

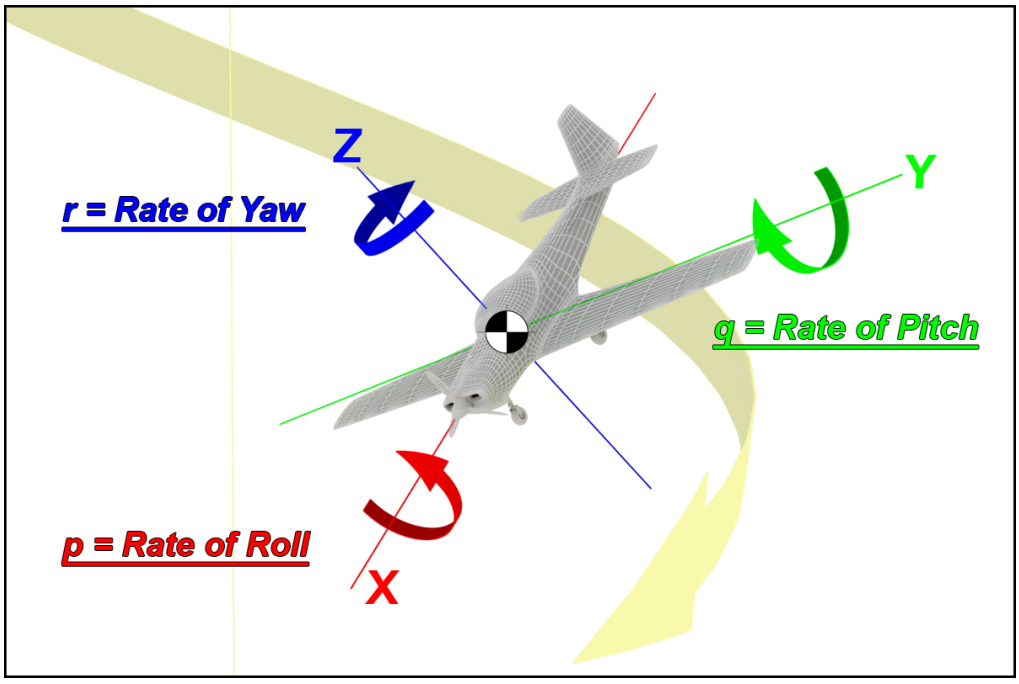

Figure 5. The components of the angular velocity vector in an erect spin to the right.

The inertia couples in a spin were then considered and the components of the inertia couples about the body axes given as [30]

$$L_i = (I_{yy} - I_{zz})qr \tag{2-4}$$

$$M_i = (I_{zz} - I_{xx})rp \tag{2-5}$$

$$N_i = (I_{xx} - I_{yy})pq \tag{2-6}$$

where L_i, M_i and N_i are the inertia rolling, pitching and yawing moments and I_{xx}, I_{yy} and I_{zz} are the moments of inertia in roll, pitch and yaw respectively. When considering the balance of inertia couples, it was the pitching moment that was believed to be of special importance due to the fact that it increased the angle of attack in the spin (i.e. pull the nose upwards towards the horizontal axis). Using the approximation of steady

state spin with wings horizontal, the following equation for the pitching inertia moment was given [30]

$$M_i = \frac{1}{2}(I_{zz} - I_{xx})\Omega^2 \sin 2\theta \qquad (2\text{-}7)$$

Although sideslip was first reported to be small and often set to zero in the derivation of the simplified steady state spin equations, it was found that the sideslip was important for the balance of the pitching moment. When introducing sideslip, it was found that it gave an additional pitching component that could be required to reach a balance of the pitching moments and thus enabling the steady spin.

The effect of the rotating propeller was also considered and it was found that the gyroscopic effect was either nose-up or –down moment depending on the spin direction and thus explaining the observed difference in rotation rate if spinning left or right. It was concluded that the use of engine might be detrimental to spin recovery since the gyroscopic effect might be pro-spin and therefore delay the recovery.

2.3.2 Autorotation explained

Glauert had earlier described autorotation and the experimental wind tunnel work performed at the NPL [29] where a stalled wing autorotated at angles above the stall angle of attack. Bryant and Gates discussed this instability in roll phenomenon further and presented the classic illustration, which have often been reproduced since then in spinning literature, showing the difference in angle of attack for the up- and down-going wing (Figure 6). With an initial angle of attack value higher than the point of stall (where C_L max is achieved) the up-going wing will have more lift and less drag and conversely the down-going wing will have less lift and more drag. Therefore, a couple exist that provides a rolling moment.

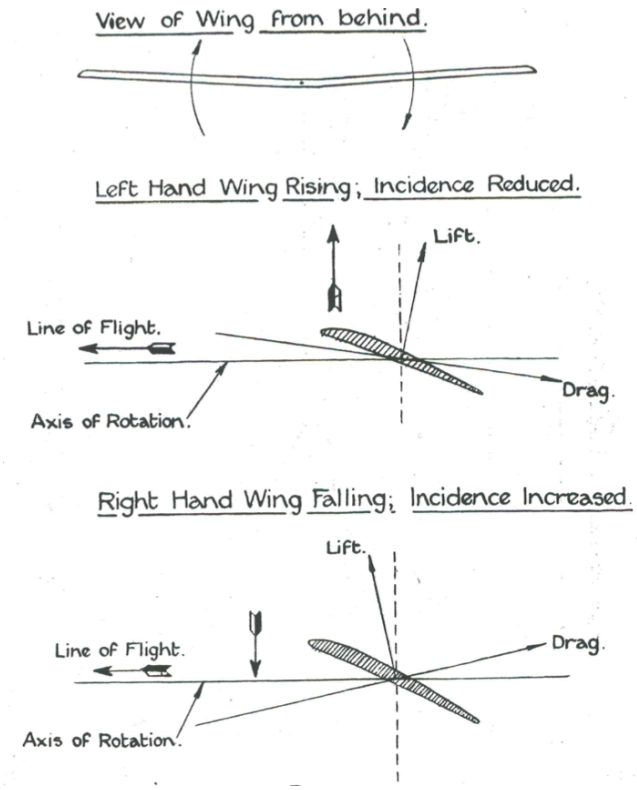

Figure 6. Illustration (from Ref. [30]) showing the difference in angle of attack for the up- and down-going wing.

Furthermore, it was observed that there were two ranges where roll instability was observed. First, from approx. 10 degrees angle of attack above the stall angle, the rate of roll increased to a steady and stable value (i.e. the autorotation speed). Then, for a range at about 30 to 40 degrees above stalling, the wing was stable in roll for small disturbances before it became unstable again. The first instability region was called *"spontaneous autorotation"* and the second was called *"latent autorotation"*. This was explained by considering the lift and drag vs. angle of attack curves, and stability in roll for small displacements depended on the sign of [30]:

$$\frac{dC_L}{d\alpha} + C_D \tag{2-8}$$

For example, the spontaneous autorotation region is after the stall angle of attack (C_{Lmax}) where the slope of the C_L vs. α curve is negative and more than equal of the drag coefficient (C_D). In Figure 7 the spontaneous region is shown on the curve between points marked A-B followed by the latent region B-C.

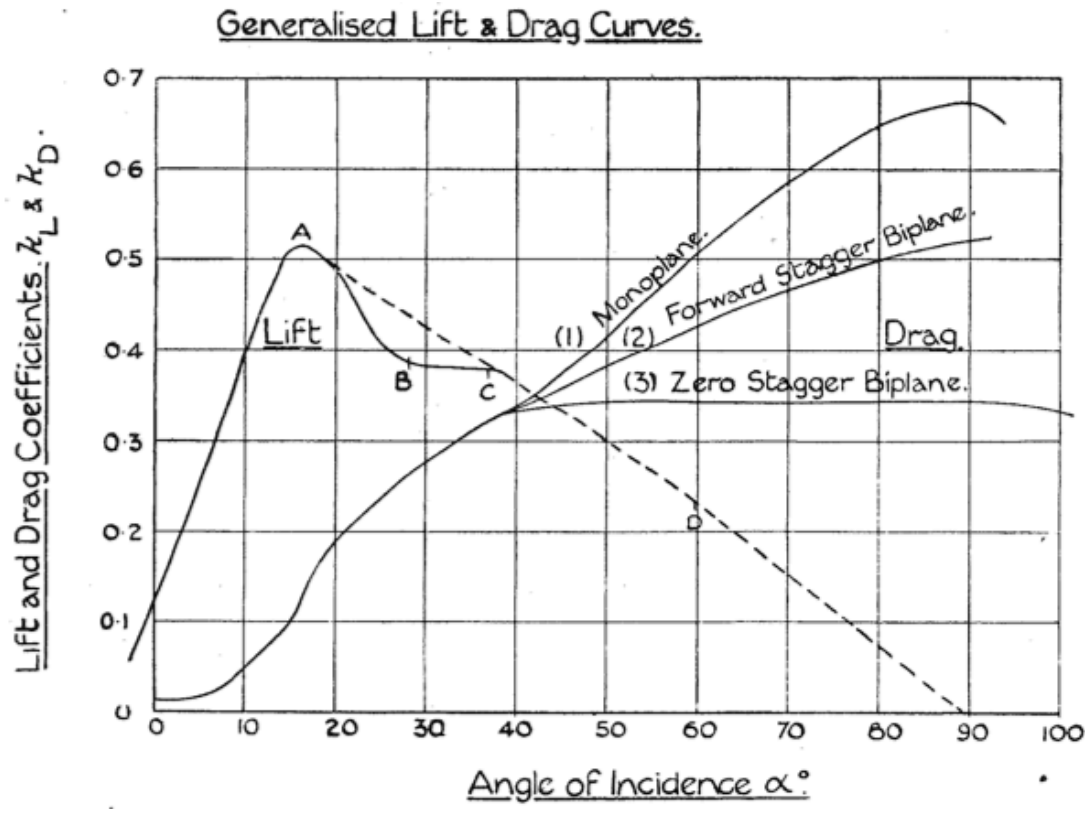

Figure 7. Illustration (from Ref. [30]) showing both the spontaneous autorotation (A-B) and the latent autorotation (B-C) regions.

2.3.3 The existence of the oscillatory spin

As we have seen in the previous sections, the fundamentals of spin including the most prominent factors affecting it were now described and a set of equations developed for the simplified steady spin. Data obtained from full-scale experiments corresponded reasonably with the estimated values obtained from the simplified steady spin equations. However, there must have been a reason for the reservations about the state of knowledge expressed in the introduction of the paper by Bryant and Gates [30]. It is likely that this reservation was due to the experimental data obtained from spin testing of the Bristol Fighter. Data traces, obtained by using instrumentation including gyroscopes used for measuring the angular velocity components, showed that the spin in this case was not steady. The yaw rate was steadily increasing to the point where recovery was started and there was an oscillation in pitch, exemplified by both oscillating pitch rate and normal acceleration values.

Records show that this oscillatory spin behaviour was debated afterwards at the Royal Aeronautical Society and several expressed opinions, but no clear conclusions explaining this behaviour were forthcoming. In the paper itself, the authors clearly stated that this was not fully understood, and therefore it is likely that the earlier held view of the spin as a steady motion was not entirely correct.

In a paper published later by Irving and Stephens [31], where the purpose was to report on the progress in spin research since the presentation by Bryant and Gates [30], the difficulty of understanding oscillatory spin modes recorded by full scale experiments was also noted. Data was presented from spinning of a *"typical landplane"* where it was shown *"...that the aeroplane alternately spins fast and steep and slow and flat"*. Furthermore, it was noted that this [31]:

"...illustrates the existence of a type of spin which is at present largely beyond the scope of model experiments or theoretical investigation"

2.4 The worst case: The flat spin

According to Jones [32], the dangerous flat spin began to occur after about 1919, and it was dangerous in the sense that the techniques described earlier used to recover from the spin was not effective. It is interesting to note that Jones comments about the flat spin being reported as a problem for aeroplanes built after 1920, not necessarily because of a certain shift in aeroplane design, but also due to the advent of parachutes there were now survivors that could explain what they had experienced.

Jones explain that two types of spins were encountered, the slow-steep and the fast-flat. In the first case, the rotation rate was about one turn every 3 seconds and with an angle of about 35-45 degrees to the vertical. Conversely, the dangerous fast-flat spin had a rotation rate of one turn per second and the aeroplane attitude was within 10-20 degrees of the horizontal. Furthermore, it was not uncommon for an aeroplane to first spin in the slow-steep mode and then transition to the dangerous fast-flat mode with a rather rapid transition between them.

Jones discussed the balance of pitching moments in the steady state spin, with the pitching inertia moment given by equation (2-7) being balanced by the negative aerodynamic pitching moment, and the role of this balance to increase the angle of attack to the very high values. In addition, the role of the aerodynamic yawing moment was discussed and in particular the importance of opposing the inertia yawing moment so that the rotation rate remained low. From the spin motion of the steady state spin it is clear that for the flat spin, it is the yaw component of the angular velocity vector that dominates. For the completely flat spin the rotation is all yaw, and conversely for the steep spin where the nose is pointing straight down the rotation is all roll. Jones suggests the use of fins, *"or their equivalent in body depth near the tail"* [32], to provide anti-yaw moment and thus reduce the spin rotation rate.

There have also been more recent reports of flat spins as a result of unconventional use of controls. There have been at least two accidents in the UK where the use of controls at spin entry might have caused the flat spin to develop. The first was in 1976 when an Avions Pierre Robin HR200/100 entered a flat spin during spin training and continued spinning into the ground [33]. Although the reason that this particular aeroplane spun at a much flatter angle is not clear, the use of power and opposite aileron (right aileron in a left spin) during spin entry might have been contributing factors. The second accident was in 2007 when a Tipsy Nipper T.66 entered a flat spin during aerobatic sequence practice [34]. Again opposite aileron was used for the spin entry and the pilot realised that the spin *"had gone flat"* after the first turn. After several recovery attempts the aeroplane eventually recovered after 26 turns.

It should be emphasized that whilst the fast-flat spin described by Jones [32] does correlate well with many reports (e.g. as described in References [7, 34]), there have been reports of the exact opposite occurring. Patton, a former FAA and NASA test pilot, reports that one time during certification flight testing of the Mooney M-20B, the spin became flat and slow when he exceeded the required one turn spin [35]. In addition, during flight testing of the Pilatus PC-7 Turbo Trainer, the spin became flatter and slower when the moment of inertia was increased [36]. This underlines that the spin might not be amenable to simple theoretical analysis.

2.5 Successful spin recovery defined

Certified aeroplanes must comply with spin recovery requirements such as may be found in applicable certification standards. We can define a spin recovery as successful if it conforms to the certification standard. The general requirement is that it must be impossible to obtain unrecoverable spins with any use of the controls. However, aeroplanes are certified in different categories and we have to look closer at the applicable requirements.

2.5.1 The spin recovery requirements

Aeroplanes certified in the part 23 [13, 14] normal category must be able to recover from a one-turn or three second spin, whichever takes longer, after one additional turn using normal recovery controls.

After one turn most aeroplanes have not yet stabilized in the spin. This is called the incipient or entry phase of the spin. There is no guarantee that an aeroplane certified in normal category will recover from a spin if it is allowed to continue spinning past this one turn. In a spin, the angle of attack might increase after the first turn. This can be seen when examining time histories of spinning aeroplanes (e.g. two NASA general aviation, single engine, low wing, spin research aeroplanes, one with a conventional tail [37] and one with a T-tail [38]). The FAA Flight test guide for certification of Part 23 airplanes states that the objective of the one turn spin requirement is to provide a *"margin of safety"* [9] if the spin is encountered inadvertently.

This also corresponds with the British Defence Standard [15] requirement for inadvertent spins. If a spin is encountered during manoeuvres it is desirable to assume some time delay between loss of control and initiation of recovery action. The appropriate recovery technique is to be applied after 5 seconds or 1 turn whichever is the shorter.

The Federal Aviation Regulation [14] has alternative certification requirements for normal category; the optional spin resistance requirements. The aeroplane must demonstrate very good stall, post-stall and spin characteristics and immediate recovery

from spin must be possible. If the aeroplane is to be certified as spin resistant the spin recovery is naturally not an issue, because it should not spin. But to this date there exists no aeroplane of conventional design that has reached full certification as spin resistant. Some aeroplanes have been certified using spin resistant criteria (e.g. the Lancair LC-40 [39] and Cirrus SR20 [40]) but have used equivalent level of safety findings to be able to reach final certification [41]. The European Certification Specifications [13] does not by default recognise the optional spin resistance requirements.

On the other hand aeroplanes certified in the aerobatic category, or utility category seeking spin approval will be intentionally spun in service and they therefore require more extensive spin testing to comply. The requirement is that the recovery be within one and one-half turns after six turns or three seconds, whichever takes longer. After six turns it can be assumed that most aeroplanes have stabilized in the spin. However, some aeroplanes do not reach a stable condition but remain oscillatory or develop a spiral dive. Either way the spin recovery is considered successful if it is within one and one-half turns after six turns in the spin. A summary of quantitative spin requirements for light aeroplanes and sailplanes is shown in Table 1.

It is important to note that in addition to the quantitative requirements, qualitative handling qualities requirements are also often specified for the post-stall and spin flight regime. For example, the US military standard [16] requires that the proper recovery technique must be readily ascertainable by the pilot, and simple and easy to apply under the motions encountered.

Furthermore, it is essential that all possible configurations are tested under conditions that might be encountered when operating the aeroplane (e.g. effect of altitude, abnormal control usage, spins with flaps down and power on). Configurations assumed to be critical for spinning, for example, control deflections in the critical end of the allowable tolerances range, must be explored. This results in many different aeroplane configurations that must conform to the spin recovery standard and is referred to as the spin matrix [9].

The British and US military standards also require testing of spin entries from both the erect and inverted attitude and from dynamic flight conditions. Finally, for the Military

trainer type aeroplane, the inverted and flat spin must also be evaluated. The British Defence Standard [15] quantitative recovery requirement for these cases is a maximum of 2 turns after recovery action is initiated for the inverted and flat spin respectively.

2.5.2 Spinning trial conduct

Normally, the spinning trials in a flight test programme for a prototype aeroplane are conducted towards the end of the certification programme with the aeroplane in the final aerodynamic configuration. A spin trial programme might also be required for aeroplanes in service if they are subjected to modifications that might affect the spin characteristics [17]. In addition, spinning trials have also been conducted after spin problems have been encountered in service, either due to reported incidences [23] or because of more frequent spin accidents than compared with other similar aeroplanes in service.

A spin test programme is considered to be hazardous, so a significant amount of effort is directed towards mitigating risk in the pre-flight stage. The engineering part of the risk mitigating process has historically been by using scale models of the applicable aeroplane configuration and spinning them in a vertical wind tunnel [1,7]. Unfortunately, the predictive capability of the spin tunnel has been unreliable in identifying unrecoverable spin modes and this will be further discussed in section 2.8.

The test pilot is usually prepared by spinning other similar aeroplanes as a personal build-up of flying skill and training for spin characteristics observations. The prototype aeroplane that will be subjected to flight testing is prepared for emergency spin recovery in case unrecoverable spin modes are encountered, usually by installing a spin chute in the tail section of the aeroplane [3,4,7,17] or a ballistic recovery system might be used for the lighter aeroplanes [2]. In addition, test pilot egress is critical as there have been several cases of spin chutes failing to successfully recover the aeroplane from the spin [3,4,7], so personal pilot safety equipment such as parachute and helmet are worn and arrangement for quick cockpit egress is provided (e.g. door ejection or canopy removal).

Since the spin testing is considered high risk, normal practice is to start with the least risk conditions and work towards the more critical cases which have historically been

shown to be problematic, such as spins with an aft CG and with power. If problems are encountered which require a redesign of the airframe, additional iterations through the spin matrix might be required which result in a significant number of total spin test flights. For final certification, modifications made for conducting a spinning trial (for example a spin chute installation) must be removed before full compliance with the applicable certification specification are shown.

Certification standard	Spin requirement	Recovery requirement	Remarks (weight categories)
General Aviation			
FAR and CS 23.221 Normal Category	1 turn or 3 seconds (whichever takes longer)	1 turn	(max 5700 kg)
FAR and CS 23.221 Aerobatic Category	6 turns or 3 seconds (whichever takes longer)	1.5 turns	Must recover from any point in a spin
Military Aviation			
DEF STAN 00-970 Part 1/5 Section 2.12.26 Class I Spins from manoeuvres	1 turn or 5 seconds (whichever is the shorter)	Not specified	Class I : Small Light Aeroplanes
DEF STAN 00-970 Part 1/5 Section 2.12.21 Class I Types of Spin	8 turns*	2 turns	* or as defined by the Aeroplane Specification
MIL-F-8785C* 3.4.2.2.2 Class I Post-stall gyrations and spins	All modes of spin that can occur	1.5	* no longer in use, but used as a historical reference by the current US Military standard
Microlight and Very Light Aeroplanes			
BCAR Section S 221 Spinning	1 turn or 3 seconds (whichever takes longer)	1 turn	For any aeroplane not controlled by weight shift (max 450 kg)
CS-VLA 221 Spinning	1 turn or 3 seconds (whichever takes longer)	1 turn	Very Light Aeroplanes (max 750 kg)
Sailplanes			
CS 22.221 Spinning	1 turn	1 turn	Sailplanes (max 750 kg) and Powered Sailplanes (max 850 kg)
CS 22.221 Not cert. for intentional spinning	5 turns	1.5 turns	
CS 22.221 Intentional spinning certified	5 turns	1 turn	Must recover from any point in a spin

Table 1. A summary of quantitative spin requirements for aeroplanes and sailplanes

2.5.3 Non-compliance

Although the requirements are quite specific, there have been cases where aeroplanes that do not comply with the certification standard have entered service. As already mentioned the manufacturer might have used equivalent level of safety findings to be able to reach final certification. In other cases specific guidelines or limitations might have been imposed limiting the operation of the aeroplane.

In the case of the current Royal Air Force (RAF) trainer, the Short Tucano T Mk. 1 (Figure 8), the spinning assessment [42] concluded that the erect spin had oscillations in roll that were not within the limits set by the British Defence Standard [15]. Furthermore, the rotation rate was greater than the permitted value. It was therefore concluded that the spin is unsatisfactory for a training aeroplane but is acceptable for dual spinning demonstrations. The recommendation was that the Tucano should be cleared for intentional spinning despite these shortcomings. However, limitations were imposed, e.g. the aeroplane must be captained by an experienced Service pilot.

Figure 8. The Short Tucano T Mk.1 RAF turboprop trainer (courtesy of G. Gratton).

In other cases, aerodynamic ‘fixes’ might be tried when undesirable spin characteristics are encountered. For example, predecessor of the Tucano in the RAF trainer role, the BAC Jet Provost T Mk. 5, has a set of nose strakes (Figure 9) on the forward fuselage. The Jet Provost spinning characteristics was not satisfactory for a trainer due to large oscillations in pitch and roll. It was believed that these oscillations were due to the outside wing tip and canopy becoming *“partially unstalled at the end of each turn, and giving rise to pitching and rolling moments”* [43]. Installing a set of nose strakes on the lower forward fuselage increased the yaw rate and thus the angle of attack. In addition, ‘Camrex’ walkway paint was applied to the outer wing leading edge to enhance flow separation. The desired end result, a stable spin, was thus achieved by reducing unstable pitching and rolling moments.

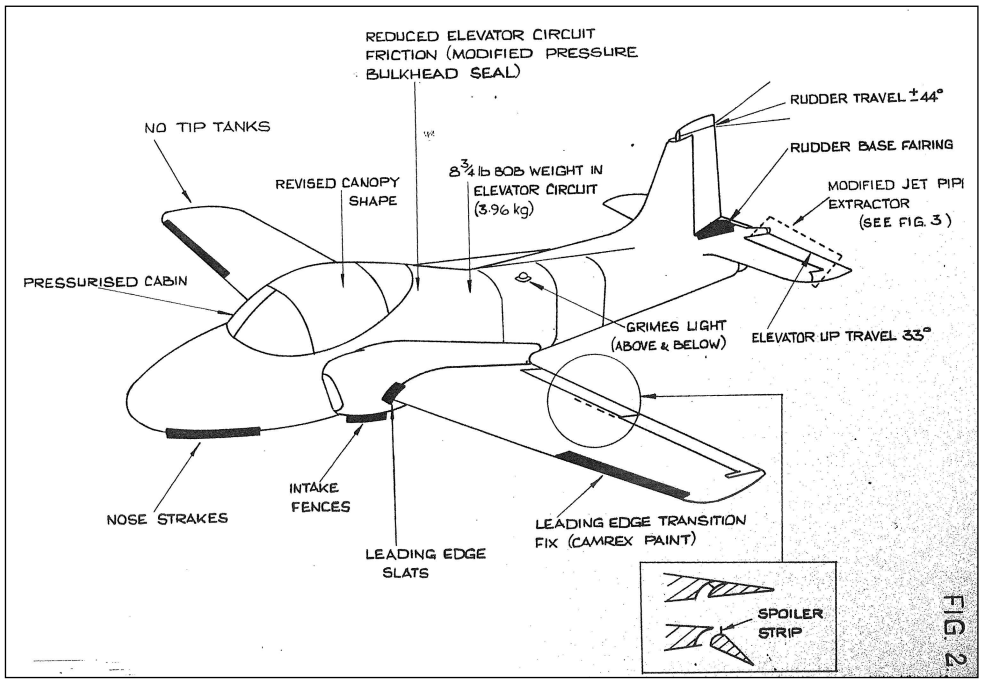

Figure 9. Sketch of the BAC Jet Provost T Mk. 5 RAF jet trainer. Note the nose strakes and Camrex paint applied to the outer wing leading edge (illustration from Ref. [43]).

2.5.4 Aeroplanes that are not certified

In some countries (e.g. UK, France, Norway and the USA) aeroplanes are flown that are not certified and thus do not necessarily conform to any known certification standard. These aeroplanes might have experimental category status due to modifications for a certain research purpose, or more typically they are amateur built aeroplanes. The

environments under which experimental aeroplanes operate varies from country to country and they might be deregulated. Quantitative requirements as listed in Table 1 might not exist for this category of aeroplanes and spin flight testing might not be required at all. If there is no requirement it will be the owner or test pilot who decides if spin testing is to be performed and to which standard.

Certified or not, the reason for the spinning evaluation is the same, to provide the pilot with information about the aeroplane stall and spin characteristics and to ensure that the aeroplane will recover from a spin. In the case of amateur built aeroplanes there might be limited resources and time available for a spinning evaluation. In addition expensive safety equipment such as a spin chute might be out of reach and thus the risk mitigation will be limited. The result is typically that the full spin matrix is not explored and the limited spin testing is not to the standard that would be required for a fully certified aeroplane.

2.6 Spin recovery technique

Lindemann *et al* [27] broke new ground in spin understanding when they wrote in 1918:

"The methods of starting a spin and of coming out of it are obvious once its nature is realised."

For spin recovery the desired result is to reduce the yaw rate and the angle of attack. The yaw rate must be stopped to regain directional control. The angle of attack must be reduced to stop the autorotation of the wings and recover to the pre-stall flight regime. The best generic technique for spin recovery has been considered for a long time. The recommended use of controls for recovery described below was the result of a National Advisory Committee for Aeronautics (NACA) research program in the 1930s [44]:

> *"The recommended operation of the controls for recovery from a spin, which presupposes that the ailerons are held in neutral throughout the recovery, is as follows:*
> *1) Briskly move the rudder to a position full against the spin.*

2) After the lapse of appreciable time, say after at lest [sic] one-half additional turn has been made, briskly move the elevator to approximately the full down position.
3) Hold these positions of the controls until recovery is effected."

It has been reconfirmed as the most effective spin recovery technique in later spin research programmes by the National Aeronautics and Space Administration (NASA) and variants of this technique has been developed and published, for example by Stowell [35]. This technique is referred to as the NASA Standard Spin Recovery or simply the Standard Recovery.

It should be emphasised that this is a generic technique that should be used as a starting point for initial flight testing. For a given aeroplane model there might be very important variations in this technique that will greatly influence the spin recovery. Consider again the jet trainers T-37 (Figure 2) and Jet Provost T Mk. 5 (Figure 9), which are similar in configuration (with the main exception that the Jet Provost is a single, and the T-37 is a twin engine jet) and designed for a similar training role. Flight testing of the T-37 concluded that the stick should be abruptly put full forward (elevator full down) one turn after applying rudder [45]. Conversely, the Jet Provost T Mk. 5 Pilot's Notes warns the readers that if the stick is moved harshly to the fully forward position this could lead to an inverted spin, which clearly is not a desirable spin recovery result. The recommended technique for the Jet Provost T Mk. 5 is to move the stick smoothly and centrally forward until the spin stops, but not further than just ahead of neutral [46].

Furthermore, it is important to note that the order of opposite rudder first and then elevator is of great importance for typical light single engine aeroplanes. If the elevator leads the rudder a higher rotation rate might develop and this could lead to a delayed recovery. This undesirable effect of forward elevator use in an established spin was noted as a warning to pilots in the paper from 1932 by Irving and Stephens [31], and there have been more recent reports of accelerated spin mode cases [37, 47] when elevator is put forward, or not held fully back, while maintaining pro-spin rudder.

2.7 Effect of controls

Research by NACA [48] on the effect of control usage on the recovery from a spin found that $(I_{xx} - I_{yy})$ was an important parameter. NACA spun 65 models in the free-spinning wind tunnel and found separation of control effects when considering the inertia yawing moment parameter

$$\frac{(I_{xx} - I_{yy})}{mb^2} \tag{2-9}$$

where m is aeroplane mass and b is wing span. When the mass of the aeroplane is distributed mainly along the fuselage, the moment of inertia in pitch is greater than the moment of inertia in roll, and then the value of (2-9) will be negative. This is called a fuselage-loaded aeroplane and will be the case for a single engine aeroplane with light loading along the wings. With piston twin-engine designs, or single engine aeroplane designs with mass distributed along the wings (e.g. fuel stored in tip tanks), the opposite is true and are then called a wing-loaded aeroplane. The effects of controls for the two different mass distribution cases are shown in Table 2. Regarding the aileron setting, aileron with the spin is defined as aileron control set in the same direction as the spin rotation direction (for example left stick in a left turn spin) and conversely for aileron against the spin.

Mass distribution	**Favourable effect on the recovery**	**Unfavourable effect on the recovery**	**Predominant control for recovery**
Fuselage-loaded	Aileron with	Aileron against	Rudder
Wing-loaded	Aileron against	Aileron with	Elevator

Table 2. Effect of controls on the recovery from the spin.

For fuselage loaded aeroplanes it was summarised that for the spin recovery, full rudder reversal before moving the elevator down is imperative and moving the elevator down after the rudder reversal is desirable. This is in agreement with the NASA Standard Spin Recovery technique. For wing loaded aeroplanes moving the elevator down is imperative and full rudder reversal desirable.

A possible explanation for this effect of controls on the recovery was given by Neihouse [48] based on observations of spinning models in the wind tunnel. The inertia yawing moment, given by Equation (2-6), is proportional to the product of $(I_{xx} - I_{yy})$ and the wing tilt θ_y (defined as the angle between the Y-axis and the horizontal axis). The algebraic sign of the inertia yawing moment depends only on the algebraic signs of $(I_{xx} - I_{yy})$ and θ_y. The wing tilt θ_y is positive when the right wing is down in a right turn spin. When the models spun in the wind tunnel with the aileron set with the spin in a right turn spin, they spun with the right wing down. If the aeroplane is fuselage-loaded, the value of (2-9) is negative, and the result is a negative (anti-spin) inertia yawing moment. This is obviously a favorable condition as the inertia yawing moment opposes the spin motion. With the aileron set against the spin a negative wing tilt was observed and the result is an unfavorable pro-spin inertia yawing moment.

Later observations, from full-scale flight research at NASA, was an increased rotation rate and steeper spin attitude when spinning with aileron set with the spin direction [22]. Other observations were increased oscillations in roll and pitch rates [37, 38]. Even if the effect of aileron with the spin might be favourable for the recovery, the recommended spin recovery technique is usually that the ailerons are held neutral as described in the NASA Standard Spin Recovery in the section above.

2.8 Problems with wind tunnel results

Wind tunnel experiments and data have clearly advanced the knowledge of the aeroplane spin. However, evidence suggests that wind tunnel spin prediction has not reached the required level of accuracy needed for prediction of spin characteristics. There have been cases where discrepancies between wind tunnel results and full-scale flight test have been found [7, 36, 49, 50, 51]. Table 3 lists some examples of discrepancies observed when flight testing prototype aeroplanes that spans from the US Navy jet trainer T-45A to the Beech Model 77, a light single engine general aviation trainer.

Aeroplane model	Wind tunnel result	Flight test result	Remarks
McDonnell Douglas T-45 A	Two stable inverted spin modes (at -25 and -60 degrees alpha) found.	A third stable inverted spin mode found (at -40 degrees alpha)	Rotary balance wind tunnel data and six degree-of-freedom simulation used
Pilatus PC-7	Spin steeper and faster when increasing the moment of inertia.	Spin flatter and slower when increasing the moment of inertia	There were also other discrepancies believed to be caused by power effects and aileron position
Percival Prentice	Model tests indicated satisfactory spin recovery	Spin became flat (alpha estimated: 70 deg.) and unrecoverable	Anti-spin parachute used for recovery
Unnamed light aeroplane	Spin at a pitch angle of 40 degrees and capable of recovery	Spin became flat and unrecoverable	Test pilot had to bale out
Beech Model 77 “Skipper”	Spin only attainable with aileron set with the spin	Aeroplane would only spin with ailerons held against the spin	

Table 3. Examples of discrepancies observed when flight testing 5 prototype aeroplane models.

For three of the prototype aeroplanes presented in Table 3, in particular the effect of ailerons in the wind tunnel seems to be the opposite of the expected. For the fuselage-loaded aeroplanes, which these represent, aileron against the spin should produce an unfavorable pro-spin inertia yawing moment. For the unnamed light aeroplane [7] the wind tunnel tests recorded the best recovery result when aileron was set against the spin. Also, for the Beech Model 77 the recorded wind tunnel effect of aileron position was the opposite of the flight test result. Finally, the Pilatus PC-7 wind tunnel test showed the effect of ailerons to be weak and flight test results showed delayed recovery when aileron against the spin direction was used. In summary, the flight test results correspond with the discussion in Section 2.7 regarding the effect of ailerons, but the wind tunnel results for these three aeroplanes do not.

The difference in Reynolds number might be the reason for the wind tunnel discrepancies. In the spinning tests of the Percival Prentice reported by Harper in 1948

[49], the discrepancy was believed to be due to scale effects on the damping in yaw of the fuselage. At full-scale Reynolds number the damping was not sufficient and the result was an unrecoverable 'fast and flat' spin (α estimated to be 70 deg.). More damping was achieved by installing strakes on the aft fuselage and the Prentice then spun with a lower rotation rate and a reduced angle of attack (α estimated to be 45 deg.).

Another source of error might be the effect of power, in particular for high performance propeller aeroplanes (e.g. the Pilatus PC-7). There are also practical limitations with the use of small aeroplane models in the wind tunnels. For example, regarding the spin recovery technique, the delayed elevator movement after rudder is applied was not implemented due to limitations on the small spin tunnel models used by NASA [52]. Furthermore, the models are hand launched into the wind tunnel, so nothing can be learned about the stall, departure from controlled flight or spin entry characteristics. Apparently, the predictive capability of the wind tunnels in the post-stall flight regime is limited.

2.9 The very important tail

"The most effective protection against catastrophic spin is a well-considered tail design that keeps the control surfaces in action in all conditions that may occur in actual flight."

Richard von Mises, Theory of Flight, 1945.

The tail is believed to be the most important aerodynamic contribution to termination of a developed spin in light aeroplanes since the rudder is the primary control for reducing the pro-spin yawing moment. Therefore, it is not surprising that many researchers and aeroplane designers have tried to develop theories and general guidelines for tail design. There are many factors regarding tail design that could possibly influence spin characteristics, such as the shape, size and relative positions of vertical and horizontal tail, rudder, elevator, fins and fences. The shape of the fuselage, tail position relative to aeroplane CG and the influence from the wing could also be contributing factors.

The first systematic investigation of different tail designs was probably the studies conducted at RAE in the first years of the 1930's. Irving and Stephens described, in their

paper from 1932 [31], about spinning experiments where they spun scale models (free flight) inside a balloon shed at Farnborough. Using 1/15 and 1/20-scale models of the Bristol Fighter aeroplane, seven different tail designs were tried to investigate design features that were favourable for spin recovery. In the subsequent discussion at the Royal Aeronautical Society, it was the Chairman of the session (Mr. Wimperis) who eloquently expressed that the *"tail was the villain of the piece"*. It was believed that if the tail was not designed properly, it could lead to *"dangerous spinning"* [31]. In particular the relative position of the horizontal tail to the vertical fin and rudder was believed to be important. In the aforementioned discussion at the RAeS, Bryant credited Irving with the discovery of the blanking effect the horizontal tail could have on the fin and rudder during the spin [31]:

"Mr. Irving's discovery of the blanking of the fin and rudder by the tailplane had shed the first streak of daylight on to the mystery of the flat spin"

Later in the 1970's, NASA also did a study with spinning scale models in a wind tunnel where they investigated the effects of different tail designs [52]. Unfortunately, this has not yet resulted in a design process or accepted design standard that has been shown to consistently result in acceptable spin characteristics. The quest to keep *"…the control surfaces in action in all conditions",* as stated in the quote above by Richard von Mises, is still a formidable challenge for the aeroplane designer.

2.9.1 The Tail Damping Power Factor (TDPF)

The first attempt to create a design guideline based on experimental data from a wind tunnel was done by RAE in the period 1934 to 1937 [53]. This design guideline was further developed by NACA after accumulating a significant amount of empirical data from wind tunnels. The relative density of the aeroplane and the distribution of mass were also considered in addition to the tail geometry. The geometric properties of the vertical tail surfaces were believed to be of special importance since the horizontal tail was assumed to cause a wake that shielded parts of the vertical tail (i.e. blanking of the vertical tail). Only the vertical tail surfaces in the free air stream were believed to be effective for spin recovery. This guideline was called the Tail Damping Power Factor

(TDPF) and was used as a guide for the design of the tail to ensure good spin recovery [54].

However, NASA later discounted the TDPF criterion. NASA performed an investigation in the Langley spin tunnel on a 1/11-scale model of a research aeroplane, which represented a typical low-wing single engine, light general aviation aeroplane [52]. The tail assembly of the model was removable and nine different tail configurations were used. When correlating the results with the predictions from the tail design criterion, discrepancies were found. The paper concluded that TDPF cannot be used to predict spin recovery characteristics, but certain principles implicit in the criterion may still be valid and should be considered.

One could say that the TDPF related research went through several cycles with a gradual decline in acceptability, from suggested use as a tail design criterion for safe spin recovery [54], to ‘use with caution’ due to the limited considerations from other effects (e.g. the wing) on the spin [52], and finally ‘do not use’ because the assumptions used initially were wrong [55].

In this final discounting of the TDPF in the NASA study from 1989 [55], they measured the empennage and aft fuselage surface pressure on a 1/7-scale model in the wind tunnel. While investigating aeroplane spin dynamics, isolating the aerodynamic effects from the inertia effects is a real challenge. Measuring pressures on lifting surfaces is clearly a very direct method for investigating aerodynamic force. In the wind tunnel they tried several configurations, e.g. taking alternately the wing and horizontal tail off the complete aeroplane configuration, and they concluded that both the wing and horizontal tail influence the pressure distribution on the tail in an adverse sense, i.e. reduced damping of yawing moment. Furthermore, they measured negative pressure on top of the horizontal tail and suggested that this negative pressure influences the pressure on both sides of the vertical tail. The results from this study showed that the assumptions made when the TDPF criterion was first conceived were wrong.

There have also been signs of the TDPF failure to reliably predict successful spin recovery in the aeroplane industry. Cessna did a considerable amount of research and testing to improve the spin characteristics of the Cessna 150 series [56]:

"Several vertical tail geometries were tested, including a grossly disproportionate rudder, none of which produced the desired results, and all of which helped discredit the historic criterion developed by NACA for predicting spin recovery – tail damping power factor (TDPF) – which also fell out of favor at NASA at about the same time."

2.10 Spin problems encountered due to minor modifications

There have been reports suggesting that even small modifications to the wing or tail design can result in dramatic changes in spin behaviour. During a spin wind tunnel investigation, NASA found that a certain low wing model had a very sensitive airflow phenomenon at the trailing edge of the wing at its juncture with the fuselage. Changing the cross sectional shape of the wing fillet was a very important factor in determining how the model spun [52]. Furthermore, regarding wing modifications it is interesting to note Patton's report from spin research at NASA [35]:

"…we found leading edge wing modifications that would put us into a flat spin regardless of the tail design used. And we could repeat this flat spin behaviour on all the test airplanes. On the other hand, we also found that a variation of the same wing modification that promoted flat spinning could be used to make all the test airplanes highly resistant to spinning."

During spin test trials of the Grumman F11F-1 fighter aircraft, Grumman test pilot 'Corky' Meier encountered *"massive oscillations about all three control axes"* [57] after the thickness of the trailing edge of the rudder was changed. Previously, using a thinner rudder trailing edge, the test aircraft had successfully passed the applicable US Navy spin requirements. Since the rudder modification was so small, it was suggested by the engineers that the spin re-testing could proceed without the emergency spin chute installation. Luckily, the test pilot disagreed and the spin chute was installed and was then used by the pilot for spin recovery. After subsequent test flights and further investigation it was revealed that this slight change in rudder trailing edge design *"had made the rudder twice as powerful as the original rudder"* [57].

In another case, an unrecoverable spin was encountered while spin testing the Cessna C-195. Thompson reported that they were *"evaluating the effects of a minor aerodynamic change on spin recoveries"* [56]. Although it is not stated exactly what the minor aerodynamic change was, they were apparently not expecting any problems since the usual spin test safety precautions (e.g. emergency spin chute and movable ballast) were not used. Furthermore, there were also two test pilots on-board and they even had their parachutes in the back seats. The spin was started at 10 000 feet and the spin recovery test point was the reverse recovery (elevator put forward before opposite rudder). Luckily, the aeroplane recovered at 600 feet after they were able to jettison one door at 1000 feet. Subsequent spins were flown with the safety equipment installed, but it was not possible to recreate the unrecoverable spin [56].

2.11 Spin resistant aeroplanes

When a very large rudder is used, excessive yaw might be generated when full rudder application is used, either to enter a deliberate spin or by mishandling the controls. The result might be a yaw rate high enough to induce a flat spin. Therefore, reducing the size of the rudder instead of enlarging it might make an aeroplane resistant to spin. Another form of control limiting is to limit the elevator travel. The angle of attack attainable by the use of elevator will have influence on both the departure from controlled flight characteristics, or more specifically the magnitude of stability loss as discussed in section 2.2, and the autorotative characteristics of the wing. For example, Meier reports that rudder and elevator limiting was indeed used as a design policy at Grumman [57]:

"It was Grumman policy to restrict rudder and elevator angles to the minimum necessary for all air maneuvers in order to keep the spin as docile as possible and to have rapid recovery characteristics."

In particular for general aviation aeroplanes, spin resistance could be an excellent safety feature since many accidents occur due to inadvertent spins at such low altitudes where spin recovery might be impossible anyway. Preventing the inadvertent spin from occurring at all is the natural approach for reducing accidents. However, such aeroplanes might be found to be spin resistant during flight testing, but with different flight conditions and mishandling of the controls by the pilot the danger is that the aeroplane

enters a spin during service. Then these ‘limited’ controls might not be effective enough to recover the aeroplane from the spin. This is consistent with the views expressed by Stinton [58] who believes that an aircraft that displays reluctance to enter a spin is likely to also show reluctance to recover.

Recent thought, particularly in the USA has seen tendency towards the certification of aircraft as spin resistant. This has been related to research by NASA [41], which has shown that drooped leading edges (referred to as ‘cuffs’) are very effective for spin resistance. However, problems have occurred when aeroplanes with cuffs have been subject to spin testing [17,59]. The problem might be that the cuffs develop lift at a higher angle of attack than the rest of the wing. The variation of angle of attack over the span of a spinning wing with cuffs is probably not linear as shown in Figure 3. The effect on the autorotation of the wings might be of such a nature that spin recovery is very difficult. The flight testing of the Lancair Columbia 400 prototype gives some insights in the problems encountered when spin resistant aeroplane required spin recovery testing [59]. After many fixes had been tried without success to satisfy the spin recovery requirements, the effect of the wing cuffs was reduced by adding stall strips on the cuff leading edges. It thereafter passed all the required tests. Furthermore, one of the conclusions in this flight test report was that the wing leading edge aerofoil shape has a lot of influence on the stall/spin behaviour.

2.12 Nose length to tail length ratio and scaling effects

The nose length/tail length ratio criterion was a result of an empirical study by Kimberlin after a test aeroplane that met the TDPF criteria *(“…off the chart in the good direction”*) was lost during testing [60]. This aeroplane had a longer nose than its predecessor, which led to the assertion that there might be a problem with aeroplane designs that have a higher nose length to tail length ratio.

To further investigate this on several aeroplane designs, in which Kimberlin had knowledge about the individual spin flight test programmes, the nose length to tail length ratios were obtained. Lengths were measured first from the wing 25% MAC point to the propeller hub for the nose length, and then from the same point on the wing to the 25% MAC point of the vertical tail for the tail length. The result was then plotted against

wingspan. Reference [60] shows the results for 32 general aviation aeroplanes, although the specific types are not identified. Three categories were identified; no spin problems for ratios 0.4 or less, mixed results for ratios of 0.4 to 0.5 and spin problems were encountered for all the aeroplanes with ratios above 0.5.

The Micco MAC-145B single engine prototype aeroplane could not meet the FAR 23.221 aerobatic category spin recovery criteria for multiple turn spins during the initial spin flight test programme [61]. The Micco MAC-145B had a nose/tail length ratio of 0.65 putting it well into the 'spin problems' category in the study described above. However, after modifications the Micco MAC-145B met the multiple turn spin requirement and was certified despite this nose to tail length ratio. The modifications are described in the spin test report [62]:

"..by installing two inner wing near-fuselage fuel tanks plus eliminating fuel in the large outer wing tanks for spins, a significant reduction in the Yawing and Pitching Moments of Inertia was realized. Also, nose cowl strakes were added for consistent spin recovery results."

Although the nose to tail length ratio might be a factor that have influence on spinning characteristics, e.g. due to possible aerodynamic effects of the forward fuselage or the resulting change in moment of inertia when increasing nose length, it is believed that it was the mass distribution of the wings that were the major factor causing the problems the Micco had during initial certification. This underlines the importance of estimating the moment of inertia of an aeroplane before spin flight testing. In particular, when an aeroplane is scaled upwards (e.g. nose length or wingspan increased) the change in moment of inertia should be investigated. Research by NACA [63] concluded that uniformly decreasing the moment of inertia led to steeper spins and higher angular and vertical velocities, and faster recoveries. This corresponds with the flight test results of the Pilatus PC-7 [36] that spun flatter and slower when increasing the moment of inertia.

2.13 Moving wall and accelerated flow effects

Further to Kimberlins recommendation to *"...avoid long noses during design of airplanes that must be certified for spins"* [60], long slender noses are believed to be

problematic for fighter aircraft susceptible to flat spinning. For example Ericsson and Beyers [64] notes that the long forward fuselage of the Grumman F-14 Tomcat fighter was possibly part of the flat spin mode problem causing several accidents during its time in service. They argued that moving wall effect [64] dominate as the slender body (i.e. the nose of the aircraft) rotates and this result in a pro-spin yawing moment.

The moving wall effect has also been discussed by Ericsson in the context of the enhanced flow separation of a plunging wing and the corresponding delay in flow separation for a pitching wing [65]. According to Ericsson, the dynamic overshoot of the stall angle of attack for a pitching wing can be explained by two components, the first being a time lag effect due to the acceleration of the flow. The second component is the moving wall effect, described by Ericsson as a *"leading-edge jet effect"* [65], which modify the boundary layer and results in a promotion of the stall for the plunging wing and conversely a delayed flow separation for a pitching wing.

Furthermore, Beyers and Brown from NRC in Canada [66], discusses the dynamic stall phenomenon and in particular the delay of stall-onset due to increased wing pitch rate. They presented experimental stall data from full-scale flight research using the single-engine North American T-6G aeroplane, where they found that the stall angle of attack varied directly with the pitch rate used during stall entry. This is an example of full-scale flight research (at $Re_c = 3.3x10^6$) results that supports both the analytical work and other experimental results discussed by Ericsson [65].

2.14 Discussion and conclusions

The historical development of spin theory, from the departure from controlled flight to the flat spin, has been discussed in this chapter together with the requirements, recovery technique, effect of controls and some lessons learned from spinning evaluations. Despite many years of spinning research and evaluation, spin testing is high risk and apparently there is more work to be done in advancing our knowledge of high angle of attack aerodynamics.

Empirical estimation methods for spin prediction, such as the TDPF, have been shown to be unreliable. It is interesting to note that both the TDPF and the nose length/tail length

ratio criteria do not consider the aerodynamic effect from the wing. Predicting the aerodynamic effect from the wing is at present very challenging due to the non-linear nature of the post-stall environment. This might be one of the primary causes for the failure of these criteria to reliably predict spin characteristics.

Furthermore, whilst spin tunnels are very useful for identifying problem areas early in the engineering process and give insight into the spin of a given aeroplane model, there have been discrepancies between wind tunnel and flight test results. Therefore there is absolutely no substitute for taking utter care with spinning preparations, applying risk mitigation and using incremental methods of approaching the spin during flight testing.

Clearly, the Moment of Inertia (MoI) is very important to consider for the recovery to be successful after rotation has commenced. Equally important is the effect of the controls to affect a recovery. Apparently, it is difficult to predict the aerodynamic effect of a particular control shape, size and effect of varying deflection angles when an aeroplane is spinning.

3 Methodologies for evaluating spinning characteristics

3.1 Introduction

To be able to study the spin motion of the aeroplane in adequate detail, quantitative data is required. Of particular interest are the angles between the aeroplane body axes and the relative wind such as the angle of attack and sideslip. Furthermore, the components of the angular velocity vector, rate of roll, pitch and yaw, are essential data. The classic approach to capture the spin motion of a given aeroplane is by measurement of several parameters using on-board instrumentation. The aeroplane instrumentation will typically be air-data sensors mounted on a boom to measure flow angles and true airspeed ahead of the wing and a solid-state gyro package to measure accelerations along the body axes. In addition the control surface positions and forces might be recorded. The key parameters describing the spin motion are then plotted as time histories. For example, during a comprehensive stall/spin research programme in the 1980's, NASA conducted several full-scale spin investigations using single-engine general aviation aeroplanes and published detailed time histories of several parameters [22, 37, 38].

However, this classic approach will necessarily require a properly instrumented aeroplane. Instrumenting an aeroplane is expensive and it will also alter the aeroplane modification state. There might be airworthiness implications when instrumenting a certified aeroplane. Furthermore, the well known challenge in experimental physics; how to measure a system without influencing it, is also applicable for the aeroplane spin. When instrumenting a light general aviation aeroplane, the modification might change both of the 'spin fundamentals'; inertia and aerodynamic flow. While flight testing the Lancair Columbia 400 [59], the aerodynamic effect of the boom was found to be equivalent to a slight rudder deflection. Furthermore, it was found that the boom degraded the spin recovery characteristics.

In this research programme an alternative method has been used to capture the spin motion. Finding an alternative approach was partly motivated due to cost involved in instrumenting the research aeroplane. In addition, the aeroplane chosen for the research programme was a certified aeroplane and changing the airworthiness status was challenging, although this was actually performed later in the research programme. This

method (as outlined below) is a Vision Based State Estimation (VBSE). The main resources in this method are a complete aeroplane CAD model and high quality video imagery of the spinning motion. The CAD model was required to go from the 2D video imagery to a 3D model of the spin motion.

3.2 The research aeroplanes and spin entry and recovery technique

The main research aeroplane chosen for the spin research programme was the Slingsby T67M200 Firefly. This particular aeroplane is certified according to the European Certification Specification, CS-23 [13], and is an aerobatic category aeroplane. It is representative of the typical single-engine military type trainer with fixed gear and a 200 horsepower engine. A 3-view of the Firefly used is shown in Figure 10 and more details are listed in Table 4 (data from the Slingsby T67M200 Pilots Notes [67]). The Slingsby Firefly is based on an earlier French design, the Fournier RF6B, which first flew in 1974 and was built using wood. Slingsby first license-built the French design and gave it the designation T67A. Later, the aeroplanes were built using glass-reinforced plastic and the designation became T67M [68]. The Firefly used in this research project was flown with sensors and a Multi Purpose Boom (MPB), and in this modified form was designated T67MX.

Full-scale research spin flights were also flown using another military trainer type aeroplane, the Saab Safir model SB 91 B2. The Saab Safir is also a low-wing, aerobatic category aeroplane, but with retractable undercarriage and it is from an older generation (first model flown in 1945). The general layout of the Safir is shown in Figure 11 and design details are also listed in Table 4 (data from the Saab Safir Airplane Manual [69]).

Interestingly, both the Firefly and Safir have had aerodynamic ‘fixes’ installed to modify spin characteristics. The Firefly has anti-spin strakes on aft fuselage to increase the damping contribution in a spin [58]. The T67A and the very first T67M aeroplane made did not have these strakes, but they were from then on added to all the models and even enlarged on the T67M200 model [70]. It is also interesting to note that the higher-powered model, the T67M260, has an enlarged rudder that was *“introduced to improve spinning”* [70]. Regarding the Safir, information from former Saab employees [71]

indicate that a dorsal fin and a small ‘spin strip’ just below the rudder were added to reduce the time to recover after anti-spin controls were applied.

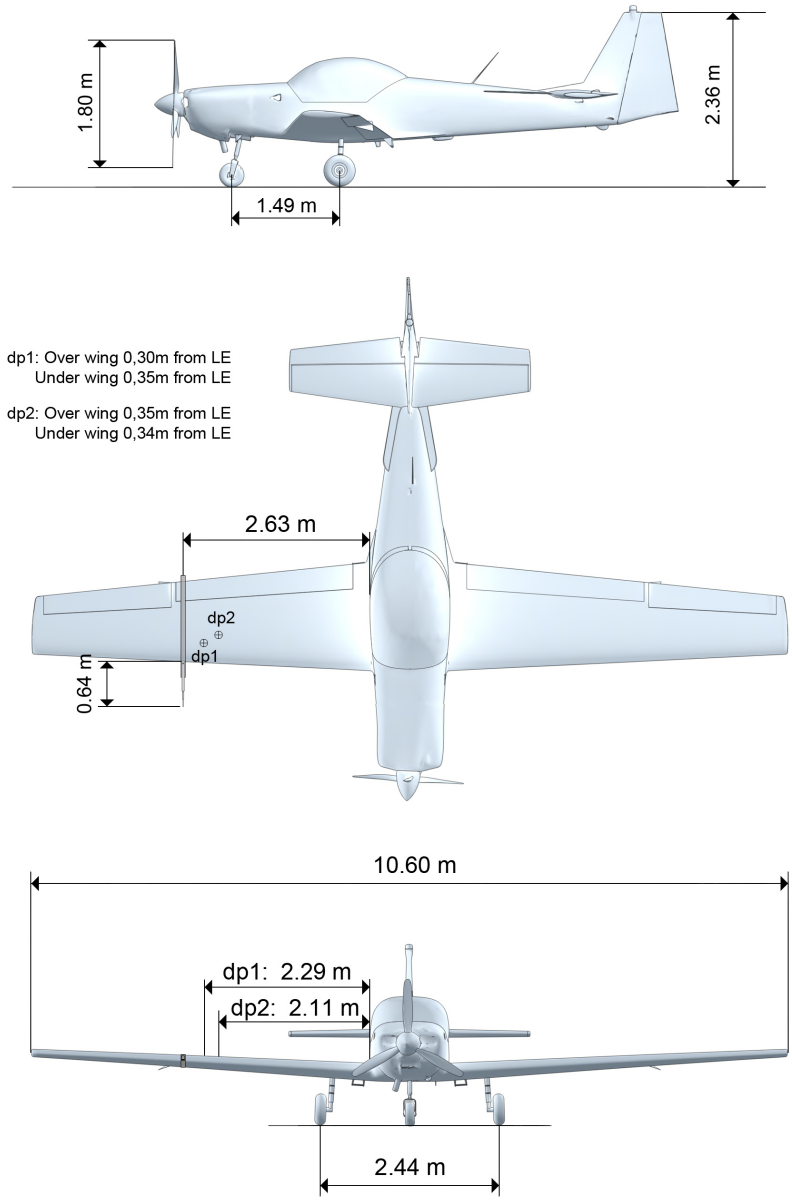

Figure 10. A 3-view of the Slingsby T67MX Firefly. The position of the Multi Purpose Boom with the Air Data Probe attached is shown together with the position of the static ports used for differential pressure measurements (dp1 and dp2).

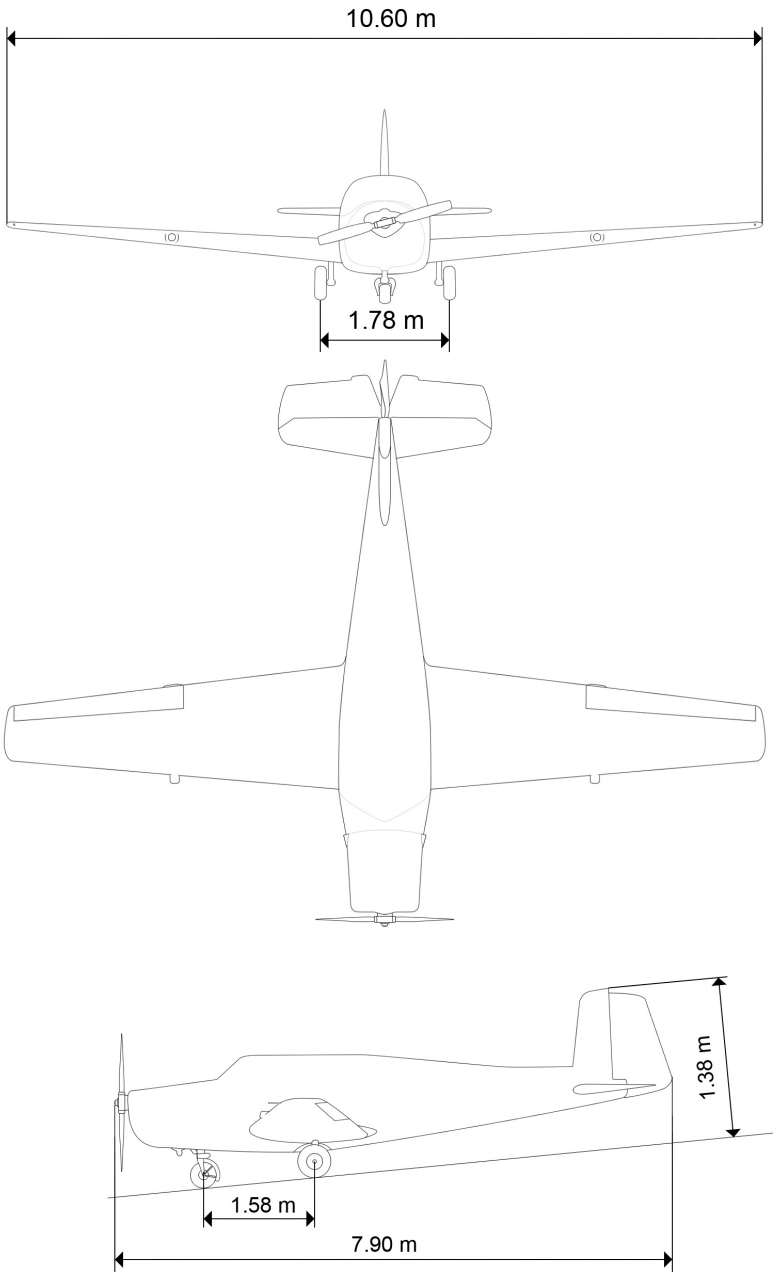

Figure 11. A 3-view of the Saab Safir (model SB91B2) used in the BFSL spin research programme.

Fuselage:	**T67M200**	**SB91B2**
Overall length (m)	7.323	7.9
Overall height (m)	2.36	2.2
Wing:		
Span (m)	10.6	10.6
Surface area (m^2)	12.6	13.6
Dihedral	3°30′	
Incidence at root	3°	4°
Incidence at tip	0°20′	-1.2°
Root section	NACA 23 015	NACA 23 018
Tip section	NACA 23 013	NACA 4412
Area of one aileron (m^2)	0.62	0.825
Horizontal tail:		
Fixed surface area (m^2)	1.65	2.55 (total, both fixed
Elevator surface area (m^2)	0.99	and elevator)
Vertical tail:		
Fin surface area (m^2)	0.8	1.53 (total, both fin
Rudder surface area (m^2)	0.81	And rudder)

Table 4. Slingsby T67M200 [67] and Saab SB91B2 [69] general data.

The primary aim of this research was to study the aeroplane spin at full scale. Research flights in the atmosphere are more challenging due to the non-controlled environment, as compared to a controlled environment typical of a laboratory or wind tunnel. It was essential that the exact same spin entry and recovery procedure be used consistently. Furthermore, since the aim was to study the aeroplane spin, post-stall gyrations (PSG) should be kept to a minimum. The spin entry technique used was the low-energy type, i.e. not accelerated, where spin entry controls are applied just before (1 knot) the stall. However, when using this spin entry technique, which compares to typical entry techniques used in a flight-training environment, PSG will most likely be evident during the entry and initial phase of the spin (2-3 turns). It is possible that other spin entry techniques could be used to minimise PSG even more, but such trials are beyond the scope of the present study. Engine was kept at flight idle from before spin entry and throughout all the spins flown for this study to minimise any gyroscopic or aerodynamic effects from the propeller. The stalling speed, from level flight, engine idle, using 1 knot/second deceleration rate and cruise configuration was 58 IAS (55 CAS) for the Slingsby Firefly and 54 IAS (54 CAS) for the Saab Safir.

The detailed spin entry procedure used is described below:

1) A visual reference was chosen on the ground and in front of the aeroplane. This reference was used to count the number of turns.
2) The stall was entered from level flight, trim set in the range 1.4 - 1.5 V_S and engine set to idle power.
3) Speed was reduced towards stall speed (deceleration rate 1 knot/sec.). At just before (1 knot) the indicated stall speed, spin controls were set simultaneously. If spinning to the left, spin controls were full left rudder and full aft stick with ailerons centred.
4) The aeroplane entered the spin, and turns counted when passing the reference mark chosen on the ground. At the required number of spin turns, the spin recovery controls were set. For a left turn spin, the rudder was set from full left to full right (rudder reversed). After the rudder was set full opposite the turn direction, the stick was centrally moved forward until the spin stopped.
6) Depending on the actual mass properties, atmospheric conditions and turns spun, the spin will stop after additional turns (e.g. after ¾ turn). The controls are then centralised and the aeroplane was pulled out of the resulting dive.

The spin recovery technique used corresponds well with the NASA Standard Spin Recovery discussed in section 2.6. Due to the relative high rotation rate (according to the Slingsby Pilots Notes [67] it is 2.5 seconds per turn), the aeroplane has rotated about half a turn while the rudder has been reversed (plus a very brief pause) before the stick is moved forward. At this point there is a slight deviation in technique. The original Standard Recovery [44] states that the stick should be ‘briskly’ moved to the approximately full down position. The Slingsby Pilots Notes includes a slightly different description:

“Holding the ailerons neutral, progressively and firmly move the control column forward until the spin stops. It may be necessary to move it all the way forward to the front stop. The rate of control column movement should be such that it would move from fully back to fully forward in about 3 seconds.”

3.3 The creation of a Firefly CAD model

A complete and accurate CAD model was required for camera tracking. Targets on the spinning aeroplane, as shown on the video imagery, were mapped onto the 3D model. The approach chosen to create this model was laser scanning using a Leica HDS scanner [72]. The laser scanning process resulted in an 'as-built' digital 3D model of the actual aeroplane used in this spin research programme.

The Slingsby was scanned in the hangar, using 9 different laser scanner positions around, above and under the aeroplane. Laser scan targets, used to merge the scans, were placed on the walls and on various stands in the hangar. In addition, colour photos were taken from each scan position. These colour photos were used to overlay colour on the 3D point-cloud. A total of 29.9 million data points were collected on the aeroplane. The 9 scans were merged into one point-cloud. Figure 12 shows this point-cloud from one of the nine scan positions.

Figure 12. The coloured point-cloud of the Firefly. Note the laser scan targets on the walls.

After post-scan data processing using Leica Cyclone [73] software, a meshing procedure was applied to go from a point-cloud to a usable 3D CAD model. The point-cloud was then imported into the 3Dreshaper [74] software application. The aim of the meshing procedure was to eliminate incoherent points, filter and smooth to reduce the model [75].

It was a challenge to find the right meshing properties and most of the meshing had to be edited manually [75]. Figure 13 shows the point-cloud before the meshing procedure and Figure 14 shows the CAD model after the meshing procedure.

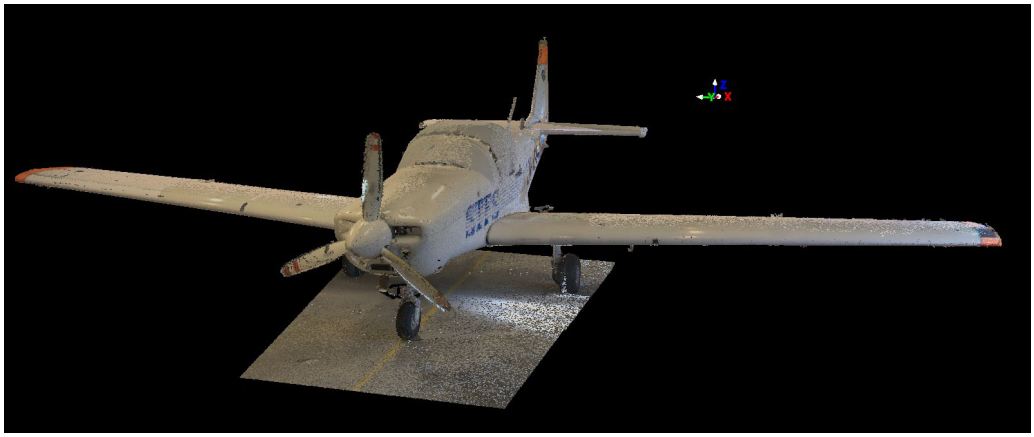

Figure 13. The point-cloud before the cleaning and meshing procedure.

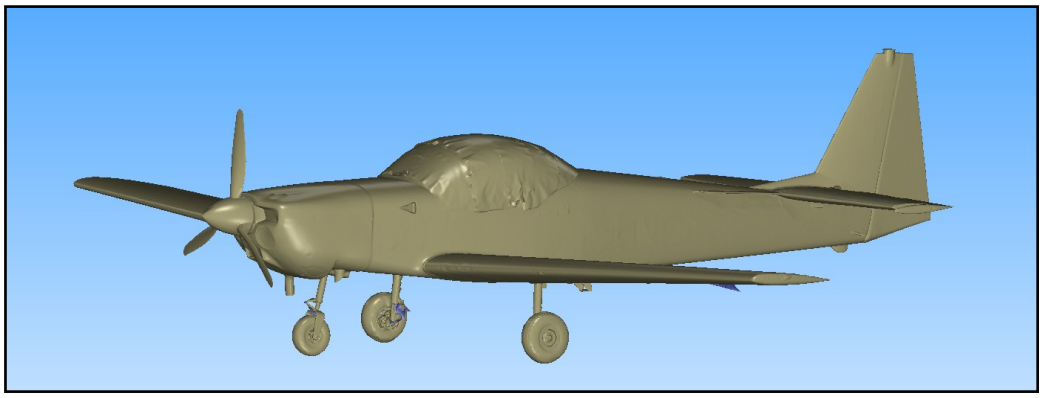

Figure 14. The Firefly after the meshing procedure.

3.4 Obtaining high quality video imagery of the 2-turn Firefly spin

Having created a CAD model of the research aeroplane, the next step was to obtain high quality video imagery of the 2-turn spin. Due to the near vertical high-rate descent, it was difficult to capture the spin from a chase aircraft. In the Slingsby Pilot Notes [67], the height loss is given as 250 feet per turn, plus 500 feet for recovery. The approach chosen was to use a helicopter as chase aircraft. The helicopter is a stable camera platform and high-end camera rig installations are available. In addition, the helicopter can enter an autorotation with a resulting high-rate of descent (approx. 1500 – 1800

feet/min). However, even if the helicopter is autorotating, it cannot match the rate of descent of a spinning aeroplane (estimated to be twice the rate of the helicopter from entry to 2nd turn, increasing as the spin develops).

The helicopter type used as a chase aircraft was a Eurocopter AS350 BA. The left door was removed and a Panasonic AG-HPX500 [76] camera was mounted in a special purpose rig. The camera was gyro stabilized using three Kenyon Labs KS-8 [77] gyros. This camera installation enabled the camera operator a clear view of the spinning aeroplane at all times. The camera installation is shown in Figure 15 and the flight position of the camera operator is shown in Figure 16. In addition, a Pentax K20D [78] (with a 50-135mm f/2.8 lens) still photo camera was used with a photographer taking photos from the left front seat.

Figure 15. The camera installation in the helicopter.

Figure 16. The flight position of the camera operator.

Due to the elevated risk of formation flight a detailed formation procedure was used. A pre-flight briefing was held with all crewmembers present and the applicable Air Traffic Control unit was contacted and briefed on the flight and formation procedure. The helicopter entered holding at a pre-determined rendezvous point in the designated block of airspace. The Slingsby intercepted the helicopter and joined up in line abreast formation. A beachline was used as the ground reference for the spin. When the helicopter was safely in position and the camera operator confirmed an acceptable camera angle, a radio call was made from the helicopter to continue as planned.

The aeroplane was put into a 2-turn spin to the left, with the helicopter positioned to the right, behind and slightly below the aeroplane at spin entry position. As the aeroplane reduced speed to enter the spin, the helicopter reduced speed towards 40 knots indicated airspeed. When the Slingsby entered the left spin, the helicopter pilot initiated autorotation. It was apparent immediately that the rate of decent of the Slingsby in the spin was greater than that of the helicopter in autorotation.

When the aeroplane had completed one turn, the helicopter pilot turned slightly left to enable the camera operator to follow the aeroplane in the spin. The indicated airspeed in

the helicopter during autorotation was approx. 40 knots. As the aeroplane recovered from the spin, the helicopter recovered from the autorotation.

High quality video and still imagery of the left 2-turn erect spin were obtained. Examples of the very high quality images ‘shot’ from the helicopter are shown in Figure 17 and Figure 18. In Figure 17 the aeroplane has entered the left turn spin, completed just over ½ turn over the beach line, and full left rudder and full elevator up (aft stick) is set. The aeroplane was just about to complete the 1-turn in Figure 18 and will in the next split second roll and yaw further to the left.

Figure 17. Left spin entry (just over ½ turn) ‘shot’ from the helicopter.

Figure 18. Aeroplane about to complete 1-turn in the spin.

3.5 Vision Based State Estimation: Capturing the spin motion

The next step in the spin motion capture process was, using the video imagery 'shot' from the helicopter, to match targets on the spinning aeroplane to the CAD model using SynthEyes [79] tracking software. Several targets were selected on the airframe, e.g. the tip and bottom of the vertical tail, wing- and horizontal tail tips and the centre of the wheels. As the aeroplane rotates in view, new additional points are established. The raw 3D animation from SynthEyes, describing the motion of the aeroplane in 3D, was then imported into Autodesk 3ds Max [80] software package for further processing.

The result from this first object tracking test was promising. The CAD model spinning in a digital 3 dimensional space could replace the Firefly spinning in the movie. The spin motion can be frozen at any time and the view rotated 360 degrees in any direction. A screenshot from the spin animation is shown in Figure 19. The spin position frozen is the same as shown in Figure 18 (just before 1-turn in the spin), but the view angle is rotated and the aeroplane shown from a different angle.

Looking at the movie first and then the animated Firefly spin second, it appeared to be the same motion. For illustration purposes this object tracking seemed to be a good match. However, when trying to quantify the data (e.g. estimating angle of attack and sideslip), it became clear that the animated motion was not perfect. The rotational motion of the aeroplane seemed to be reasonable; however, the translational motion was erratic. The reason for this lack of quality was believed to be due to the motion of the camera in the helicopter. Thus, another formation flight was flown where the aim was to track both the object (the spinning aeroplane) and the camera motion. To be able to track the camera motion, the Firefly was spinning over the beach line, but this time in the other direction with land instead of sea in the background. In addition to points on the aeroplane, tracking points were established on the terrain in the background. A screenshot from SynthEyes [79], showing points on aeroplane with geometry overlay from the CAD model and points in the background, is shown in Figure 20. Ideally, a dual tracking of both aeroplane and camera will result in the 'true' spin motion. However, tracking the camera turned out to be a real challenge. Firstly, the helicopter itself was not in steady motion during the autorotation. Secondly, the camera operator was adjusting the gyro stabilized camera angle in order to capture the spinning Firefly.

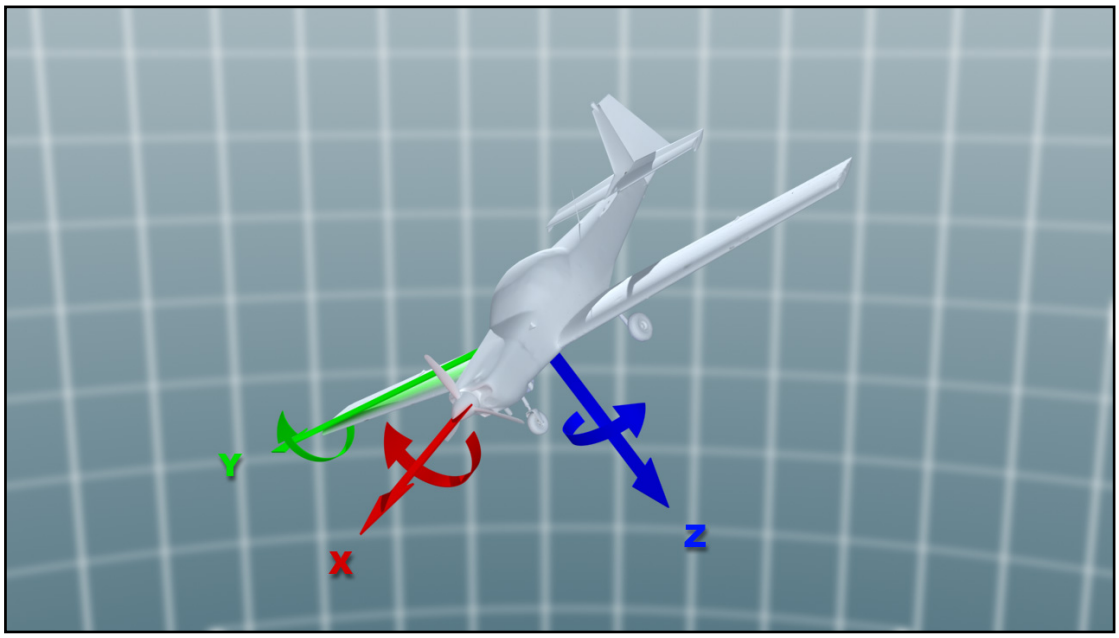

Figure 19. Spin motion frozen in 3D space and view rotated.

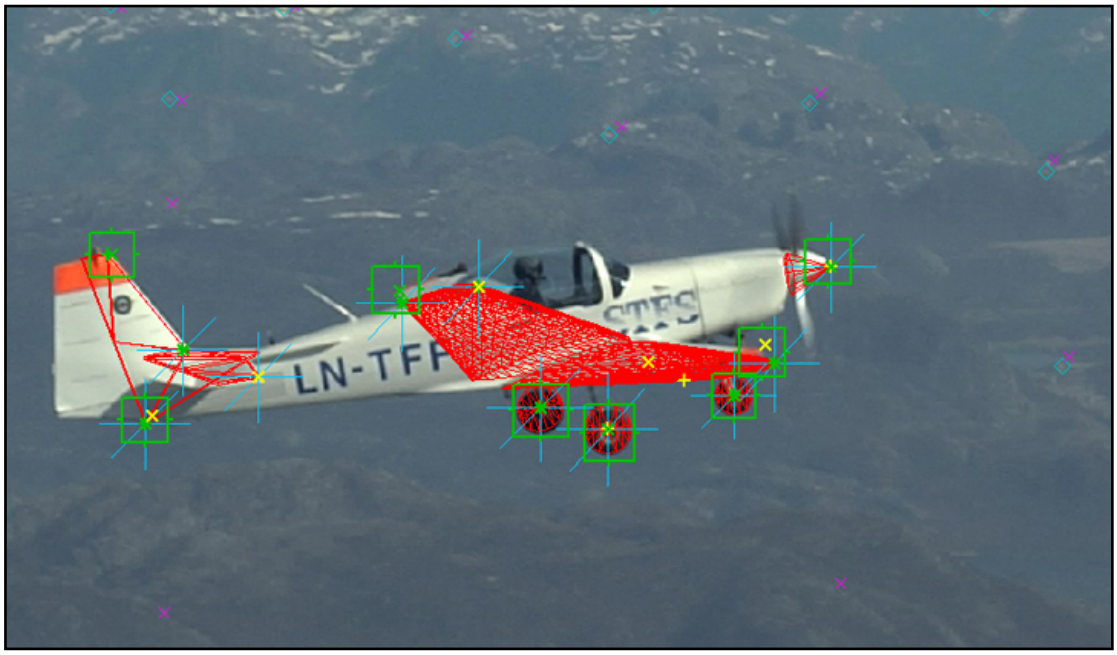

Figure 20. A screenshot from SynthEyes [79] showing points on aeroplane with geometry overlay from the CAD model and points in the background.

The result from the second flight was successful in the sense that the aeroplane trackline (the path of the aeroplane CG in the 3D space) was established. However, due to the complex helicopter and camera motion the initial conditions were not established and post processing of data was required.

The camera and object tracking in SynthEyes assumes a fixed camera position. Therefore, motion had to be added to the camera in the 3ds Max Visual Studio. A speed reduction scheme in the initial direction of flight (i.e. global X-axis), from an initial speed of 59 kn to 14 kn at end of tracking was imposed for the camera motion. In addition, the trackline had to be aligned to the direction of flight due to the helicopter manoeuvring relative to the aeroplane in the formation flight. The rotational motion was kept unaltered. Finally, the trackline was smoothed by removing 66 of 259 points. The process for smoothing the trackline can be explained as follows: a tube with a diameter of 20 cm was pulled over the smoothed trackline, and using this as the standard deviation, the points that fell outside of this tube were removed (Figure 21).

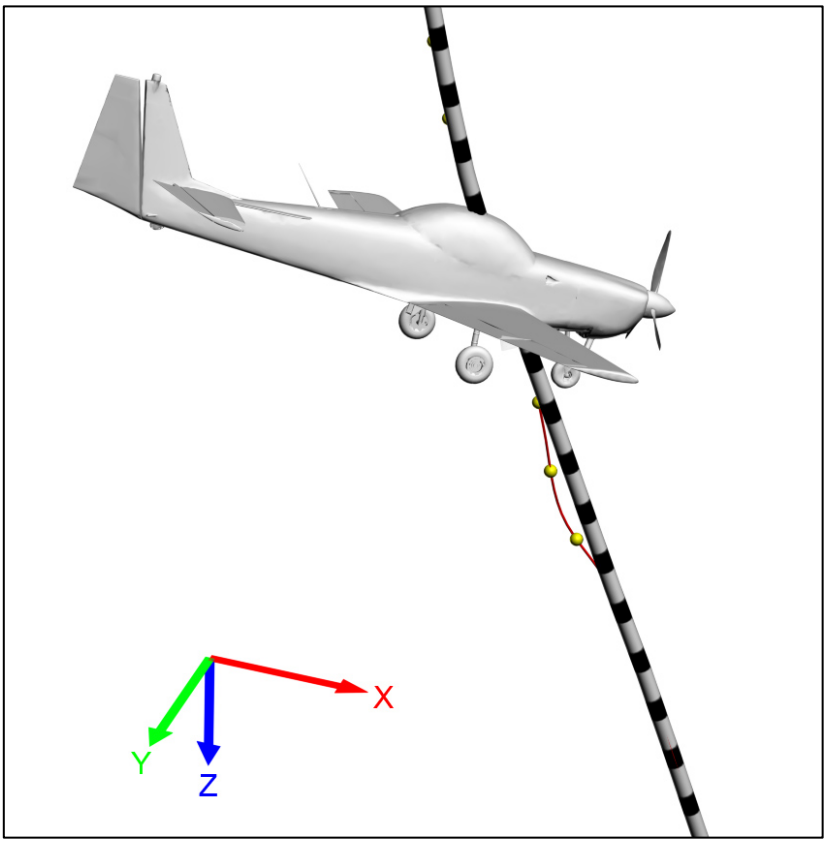

Figure 21. The smoothing of the aeroplane CG trackline. The red line is the original trackline and the yellow dots are the points that were outside the standard deviation tube and were therefore removed.

In summary, the following steps were performed to obtain the VBSE:

1) Camera motion tracking in SynthEyes (camera 'pan and tilt', i.e. yaw and pitch motion) using background points in the video imagery.
2) Object tracking in SynthEyes, i.e. the mapping of points on the video imagery (2D) to the aeroplane CAD model (3D).
3) Data was imported from SynthEyes into the visual 3D studio and camera motion was added.
4) The aeroplane CG trackline was aligned to the direction of flight to cancel the motion of the helicopter relative to the aeroplane in the formation flight.
5) The aeroplane CG trackline was smoothed by removing 66 of 259 points.

The initial angle of attack (α) just before spin entry was estimated at 15 degrees. Having established the trackline in 3D, estimated α and ß was recorded every 5th frame (Figure 22). α was estimated to be the angle between the X-axis and the trackline component in

the XZ-plane, and likewise ß the angle between the X-axis and the trackline component in the XY-plane.

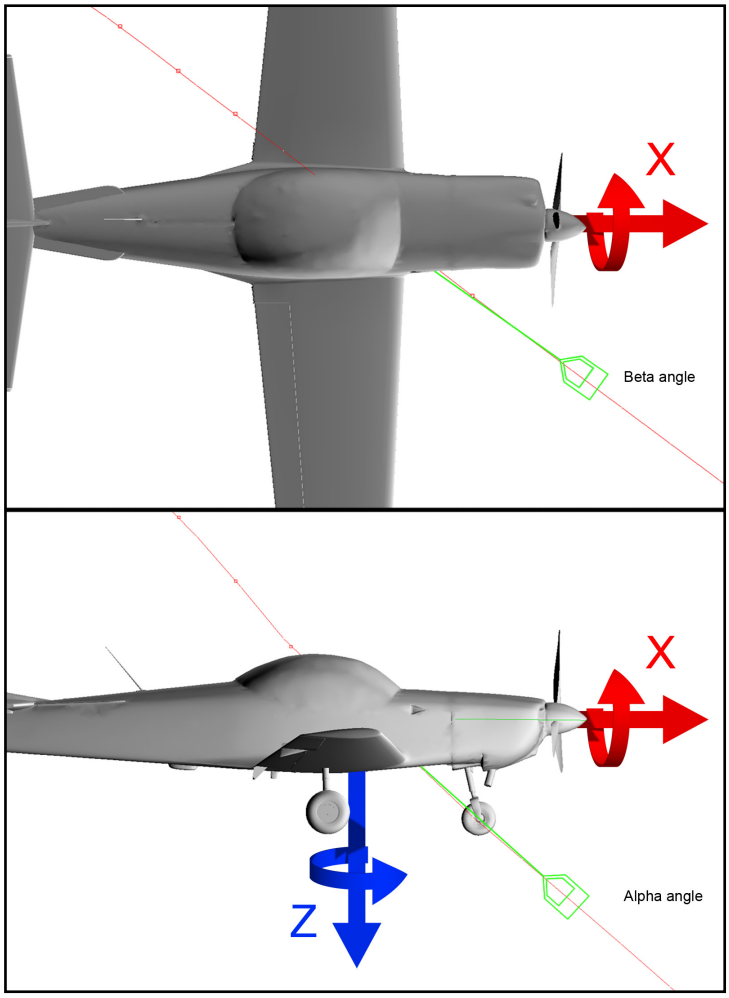

Figure 22. Estimated Angle of attack (α) and sideslip (ß) were measured every 5th frame.

The advantage of using this method to create illustrations for flight training or academic use is clear. The spin motion, which is truly the most complex of the aeroplane motions, can be frozen at any time and the view angle rotated 360 degrees around any axis. The angles and how they relate in 3D space can be studied from all sides. Figure 23 shows the final result of an illustration created to visualize the spin motion. Three spin positions, where the second position is the same as shown in Figure 18 and Figure 19 above, are frozen on the trackline.

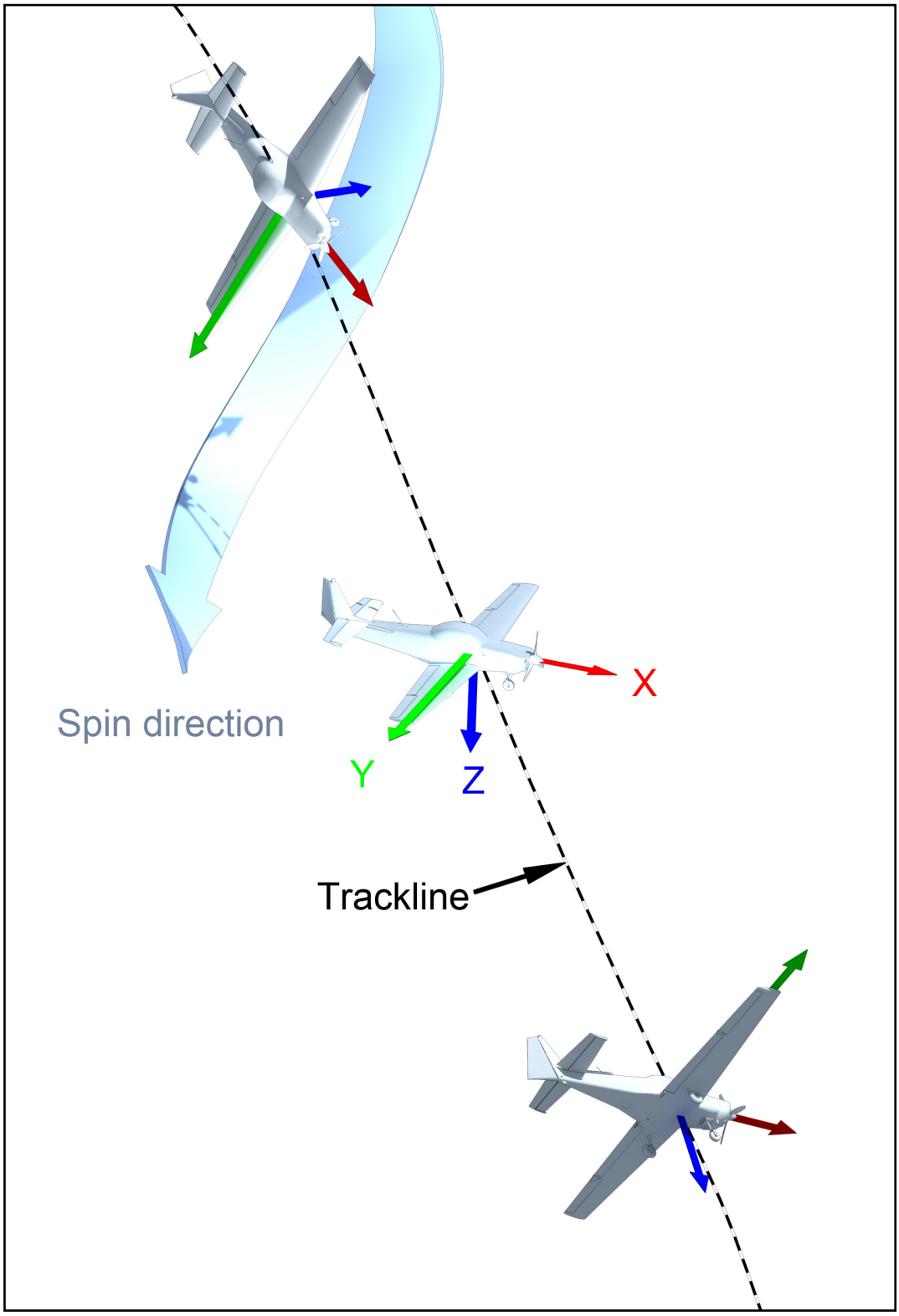

Figure 23. An illustration showing three spin positions frozen on the trackline. The second position is the same as shown in Figure 18 and Figure 19.

Ideally, VBSE is a 'what-you-see-is-what-it-is' approach to flight testing. If this alternative method is successful, advantages are that there will be no calibrating issues with complex on-board instruments. In a university environment, having access to

special purpose full-scale aeroplanes is not common. Therefore, the cost and time involved for instrumentation can be a hindrance for full scale aeroplane flight testing. With the use of VBSE, data can be obtained by using aeroplanes available for rent for a limited time. The cost driving factors will be the creation of a CAD model, the chase aircraft and the required camera equipment. For this research programme a helicopter was used, which is a rather expensive solution for chase aircraft. However, the cost involved with helicopter hire for a day or two, is small compared to the costs involved with having a special purpose and instrumented aeroplane available. When studying other motions than the spin, not involving such a high rate of descent, less expensive chase aircraft might be used.

3.6 Video imagery of tufts on wings and tail surfaces

Wool tufts of approx. 15 cm length were placed along the wings and both horizontal and vertical tail. A symmetric and structured grid pattern, as opposed to a random tuft distribution normally used to indicate areas of separated flow, was used on the wings to enable a study of the turbulent flow structure during spinning conditions. A grid spacing of 24 cm was used both spanwise and chordwise (except between the first rows of tufts where the fuel cap is positioned in-between). A total of 15 rows of tufts were used on each wing and 7 rows of tufts were used on the horizontal tail surfaces (see Figure 24 below). In addition, tufts were placed on the left aft fuselage side.

Figure 24. The Firefly research aeroplane with the symmetric and structured tuft grids on wings and horizontal tail surfaces.

Several on-board cameras were used to capture the tufts on the spinning Firefly. The principal camera positions were on the left wingtip, inside the cockpit shooting movie of the tufts on the wing through the transparent Perspex canopy and on top of the aft fuselage. The mounting arrangement on the wing tip was inspired by sport parachute equipment, using Velcro fastener, a special purpose remote control and safety wire. The camcorder used on the wing tip was a Sony HDR-CX105 [81] and a JVC Everio G [82] was used inside the cockpit. On the aft fuselage a Muvi Micro Camcorder [83] (mass approx. 50 g and dimensions 55x28x22 mm) was used to capture the tufts on the horizontal tail. This camera was mounted using a double set of mounts for redundancy.

In addition to the on-board cameras, the helicopter had both a high-end movie camera rig and a still photo camera operator in the front seat, as described in section 3.4. The video and still imagery obtained from the helicopter were high quality and well suited for post-flight analysis.

To aid the analysis, four movies were synchronised and shown together in the same image. When entering the spin, the controls are set to their full positions simultaneously.

This setting of spin control positions was used to synchronize the movies. In addition, it was possible to crosscheck the synchronization by using the fact that momentarily one of the cameras was shooting another camera. For example, the helicopter was shown in some frames from the wing tip camera. When the helicopter disappears from view, the wing tip camera itself should at the same instant disappear from view in the helicopter camera frame. The camera frame rate was 25 frames per second. The exception was the micro camera, which had a rate of 20 frames per second. Therefore, it was a challenge to synchronize the movie from the micro camera. The first frame in one second is synchronized and then the remaining 19 frames are slightly out of sync (+/- 15 ms).

For a 2-turn spin, flown as described in Section 3.2 (2-turns + 1-turn in recovery), approx. 320 images are generated. One of these synchronized images is shown in Figure 25. The 'time code' shown in the middle of the image is: spin number (several 2-turn spins were flown during each flight) : minute : second : frame number (25 frames per second).

Figure 25. Four movies synchronised and shown together in the same image. The Firefly has completed 1-turn in the spin at 4 seconds and 10 frames (the spin entry was at 0 second 20 frames).

3.7 The MTi-G Flight Data Recorder

An MTi-G [84] Flight Data Recorder (FDR) was used to measure the angular velocity components; roll, pitch and yaw rates (p, q, r). The MTi-G is an integrated GPS and Inertial Measurement Unit (IMU) with a Navigation, Attitude and Heading Reference System (AHRS) processor. The rate of turn sensor is a Micro Electro Mechanical System (MEMS) solid-state type. The rotation rate (Ω) was estimated using the following equation:

$$\Omega = \sqrt{(p^2 + q^2 + r^2)} \tag{3-1}$$

To be able to determine the start and end of the spin from the recorded data only, without recording the position of the flight controls, the following spin criteria were used (when recording data at 25 Hz):

- Start of spin at time where |p| > 1, minus 35 time steps (1.4 sec)
- End of spin at time where |p| < 0.1, plus 25 time steps (1 sec)

These start and end of spin criteria were crosschecked and confirmed valid by studying the Euler angles, e.g. the start time correspond with pitch angle increase due to full back stick.

Furthermore, to establish the turn completions from recorded data, a technique was used where rotation rate is integrated with respect to time and then divided by the circumference:

$$\text{No. of turns} = \frac{\int \Omega \, dt}{2\pi} \tag{3-2}$$

This technique of integrating Ω has earlier been used in other spin flight test programmes (e.g. as reported by Muller and Pommera [85]). A MATLAB program was written for this research project, where estimated omega from equation (3-1) was integrated using trapezoidal integration for every time step as the spin developed. For every consecutive natural number, the time step was saved and the number of turns

shown as a vertical line together with the plotted parameter. Figure 26 below shows the Saab Safir yaw rate for a right hand 6-turn spin. The turn completions are shown as vertical lines.

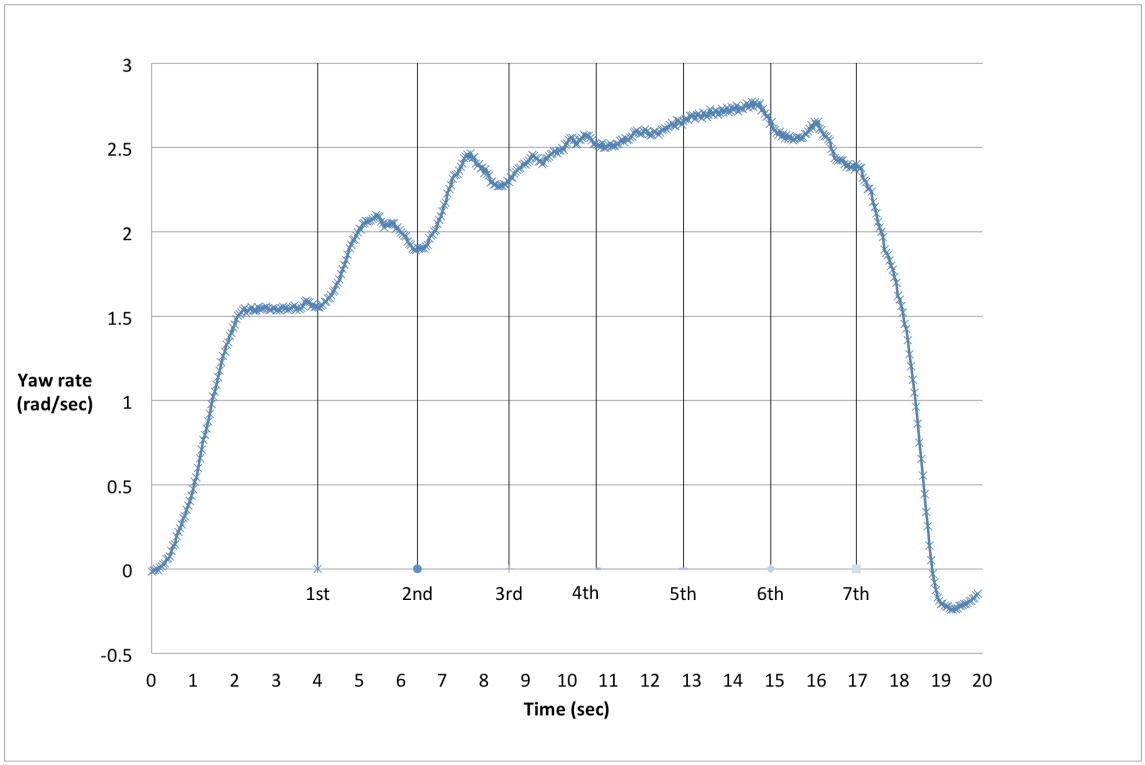

Figure 26. Saab Safir yaw rate for a right hand 6-turn spin. The turn completions are shown as vertical lines (which are numbered 1st, 2nd etc.).

3.8 The PSS-8 Pressure Sensor System

A modified electronic Pitot-static system, the PSS-8/WT [86], was used to measure the difference in pressure between the upper and lower horizontal tail surface. The electronic circuit board has two differential pressure sensors and the pressure differential was measured on the lifting surface using plastic tubes connected to the circuit board. The pressure ports are 2 mm in diameter and one is defined as a '+' port and the other as a ´-´port. The sign convention is only a definition, for example if pressure is higher at the ´+´port the differential pressure is positive, and conversely if the pressure is higher on the ´-´port the result is a negative differential.

Aerodynamically, the optimal approach for measuring static pressure on a lifting surface would be to drill holes in the surface and connect the pressure measurement tubes from the inside. However, drilling holes in the surfaces of the research aeroplane would

modify the structure and was not considered to be an acceptable modification from an airworthiness perspective. Therefore, small (2 mm internal diameter) plastic tubes were routed from the circuit board installed in the aft fuselage to the desired points on the surface as shown in Figure 27. The tube marked dP1 was connected to the first, and dP2 was connected to the second differential pressure sensor.

The risk when using this technique for surface pressure measurements is ‘pollution’ of data if a dynamic pressure component is measured in addition to the static pressure. For the present spin research application this scenario is possible if any net reverse flow is present on the lifting surface. While performing preliminary testing of this pressure measurement technique on a point on the upper Safir wing, reverse flow was indeed observed in the data traces as ‘spikes’, e.g. the differential pressure suddenly shifting sign due to the sudden increase in total pressure. Therefore, to be able to use this pressure measurement technique, a detailed knowledge of flow direction (e.g. by using tufts on the surface) is required to identify time frames where the flow direction is aligned with the tube inlets.

Figure 27. The modified Pitot-Static system circuit board was installed in the aft Saab Safir fuselage and the plastic tubes were routed on upper and lower surface to the desired points used for measurement.

When using this technique later on the Firefly research aeroplane, a rubber O-ring was used around the end-point of the tube to create a static sink (22 mm in diameter) and thus protect the tube inlet. This arrangement can be seen in Figure 28 and Figure 29, with the latter figure showing static sinks on the upper side and underside of the wing. The differential pressure data obtained using these static sink ports showed no indication of ‘spikes’ or sudden sign reversals.

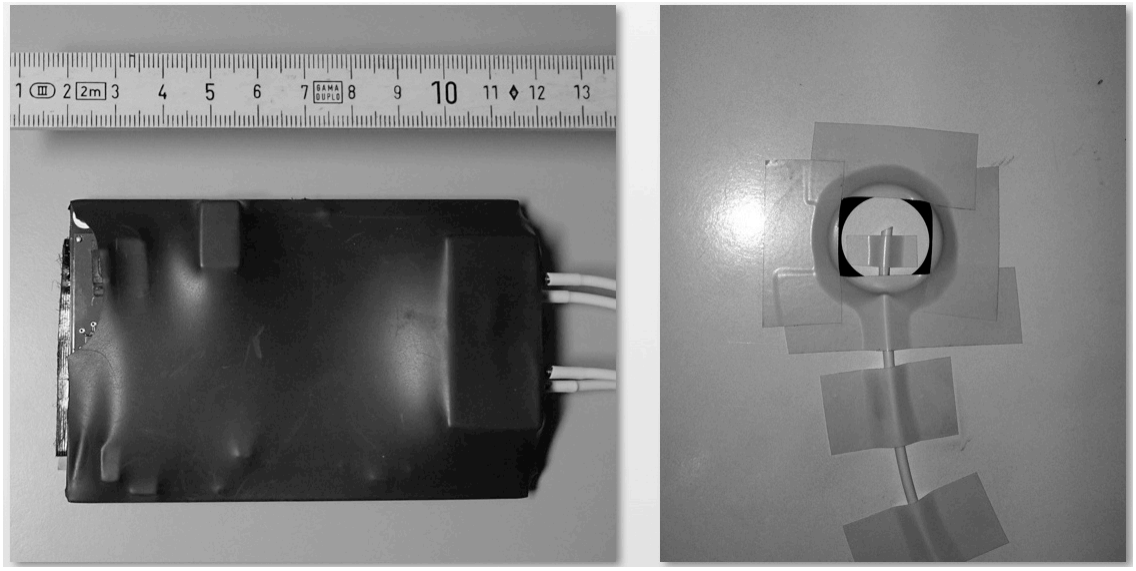

Figure 28. The modified Pitot-static system circuit board with two differential pressure sensors is shown to the left and the static sink port is shown in the image to the right.

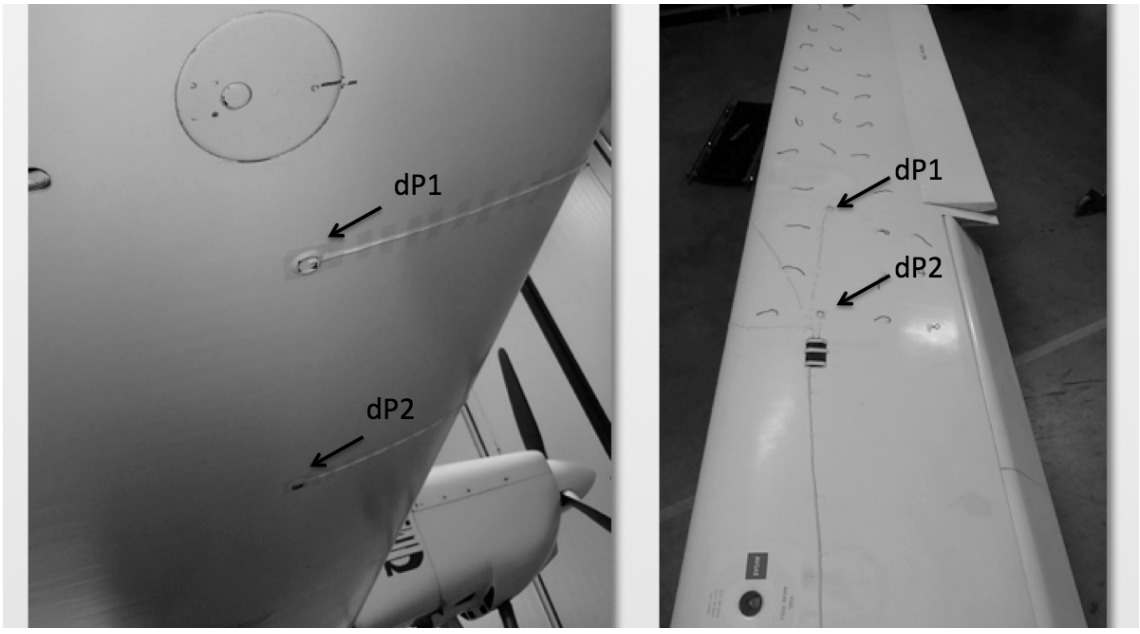

Figure 29. The static sink ports on the right Firefly wing. The small electronic circuit board can also be seen just in front of (towards the fuselage) the dP2 port on the upper side of the wing.

3.9 The Multi Purpose Boom

The Multi Purpose Boom (MPB), designed to carry research equipment such as a smoke source or an Air Data Probe (ADP), was designed and built specifically for this research project. When used with a smoke source attached it was referred to as the ‘smoke boom’ (see Figure 30 below). The primary aim of the smoke boom was to use the smoke source

to visualise the flow on the upper wing surface in addition to observing the smoke trail as it left the trailing edge of the wing. Therefore the smoke source was positioned ahead of and slightly above the wing leading edge. The smoke canister used was the 'Comet' [87], made for use as smoke signal for sport parachuting. This is of the cold smoke class, and as the name suggest no heat is generated and was therefore believed to be the safest option.

The ADP used was a 5-hole probe with integrated pressure and temperature sensors [88]. Angle of attack (α), angle of sideslip (ß), CAS, TAS, air temperature and pressure altitude data was logged via a real time measurement computer at 25 Hz. The ADP was calibrated in a wind tunnel before it was used in this project. Both angle of attack and sideslip measurements are limited to a range of +/- 20 degrees. Due to the limited α range, the ADP was mounted with a negative incidence relative to the wing chord on the Firefly wing to enable measurements of the higher stall angles. The measured α angles had to be corrected for up-wash effects (see Appendix 1 for details regarding mounting of the ADP and flight calibration).

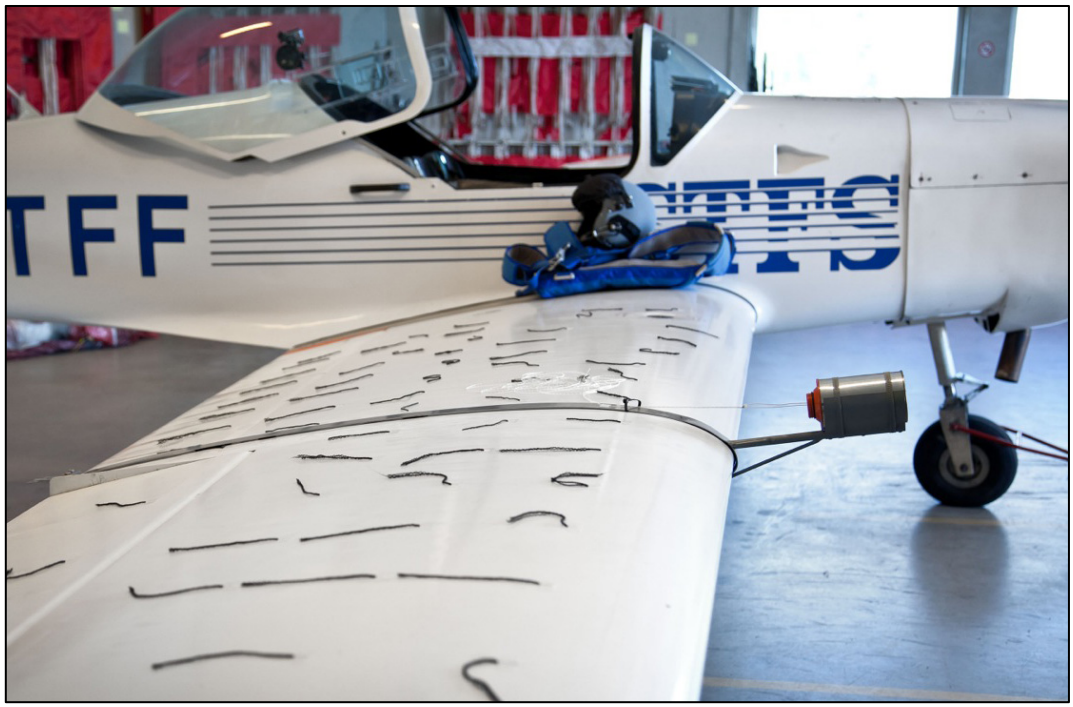

Figure 30. The 'smoke boom' attached to the right wing of the Firefly research aeroplane.

Figure 31. The ADP attached to the right wing of the Firefly research aeroplane. Note the negative incidence of the ADP relative to the wing chord.

The airworthiness of the MPB installation and the safety issues were of paramount importance in the design process and fail-safe design principles were applied throughout. Before commencing data gathering research flights, the MPB system had to be ground and flight tested to ensure safe operation. Approval of flight conditions for developmental flight testing was obtained from EASA after a lengthy approval process including a statement of technical satisfaction from the UK CAA. Eventually, a Norwegian Permit to fly was issued based on the EASA approval, with appropriate operational restrictions to enable flights with the MPB attached on the right wing of the Firefly research aeroplane (T67MX).

3.10 Data accuracy, synchronisation problems and integrity of measured data

During this research programme, many challenges were encountered related to data calibration and synchronisation of sensor systems. Two of the sensor systems (the MTi-G and ADP) had measurement capabilities that were limited due to the dynamic motions of the aeroplane and the high angles of α and ß reached during spinning. As described above the ADP has a limited range of measurements and was only usable for obtaining data up to the point of stall. The MTi-G limitations will be further discussed below.

Data from the three sensor systems (MTi-G, PSS-8 and ADP) were synchronised post-flight by matching the timestamps (milliseconds since midnight). The MTi-G manual lists an orientation worst case acquisition and computation time of 5.38 ms for the aerospace scenario and output mode [84]. For the PSS-8/WT, a delay in the system of 10 ms could be expected if a 3 metre tube length was used [89]. The longest pair of tubes used for measurements was 1.38 metre for differential pressure sensor 1 (dP1). For the present research application these delays were considered to be well within the accuracy required.

However, problems were encountered during the data reduction process related to the synchronisation of timestamps. The time source for the PSS-8 and ADP was the laptop operating system (OS), and the MTi-G used GPS time. When examining the data traces post-flight, a lag between the systems using the OS time and the MTi-G was suspected. Therefore, a synchronisation manoeuvre was flown to enable matching of milliseconds between the sensors using the OS as a time reference and the MTi-G using the GPS time. The aeroplane was trimmed at powered level flight (PLF) and then a pull-up was performed. The time when the air data measurements (α from the ADP) indicated a pull-up was matched with pull-up indications from the FDR. Usually, a time correction factor had to be added before matching the milliseconds for synchronisation. Below in Figure 32, a time history of α (AoA), pitch rate (q) and normal acceleration (Nz) during the pull-up manoeuvre from PLF is shown after a time correction factor was added, and thus the sensors synchronised.

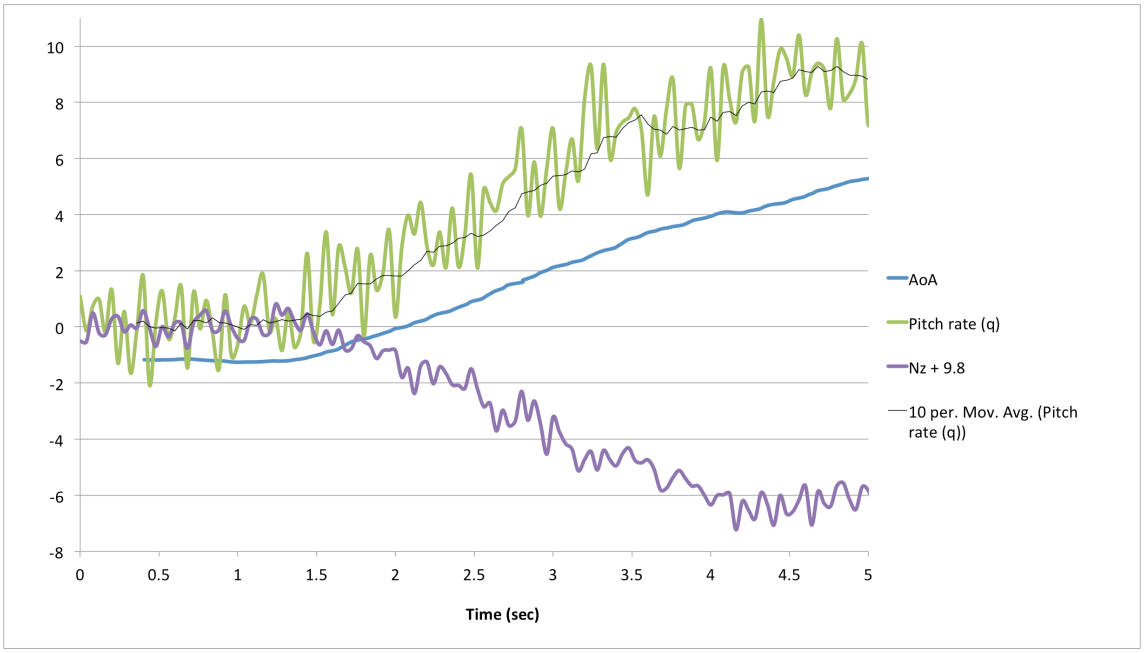

Figure 32. Time history of the pull-up maneuver used for sensor time synchronization.

The MTi-G is a motion-tracking device, which uses GPS for position and orientation correction [84], and as the name implies it uses the history to perform its real-time state estimation. Since the aeroplane spin motions of interest in this research project were highly dynamic with relatively large angular rates, the MTi-G derived parameters were believed to be of limited value for studying the spin. Although data from the FDR rate of turn sensor (angular rates) were used consistently throughout the project, the derived parameters (e.g. the Euler angles) were not used for analysing the spin motions. However, the Euler angles were used in a few cases related to sensor calibration where dynamic aeroplane motions were limited (e.g. ADP calibration for up-wash effects).

GPS altitude data from the MTi-G was used to compare with results obtained from the VBSE. There are several error sources influencing the accuracy of a GPS position, e.g. atmospheric effects and available satellites, and the MTi-G manual specifies a standard positioning service accuracy of 2.5 meter CEP (Circular Error Probable) [84]. However, the most important factor for the GPS position estimation is obtaining a good GPS fix. Earlier spin tests with GPS systems revealed time frames with loss of GPS signal as the aeroplane rotated in the spin and therefore there was a concern that the GPS fix could momentarily be lost during spin entry. Fortunately, the MTi-G also logged GPS status, which enabled a review of status post-flight. The satellite status for the spin showed a loss of satellites during entry, however not to the extent that a GPS fix wasn't obtained.

For example, before one 6-turn spin entry 10 satellites were used by the FDR and during spin entry 7 satellites were used, indicating a loss of only 3 satellites as the aeroplane rotated to the inverted attitude. Apparently, the position of the GPS antenna at the very top of the Firefly Perspex canopy enables a GPS fix even when the aeroplane is momentarily in the inverted attitude. Unfortunately, an enhanced GPS service such as Differential GPS where a network of ground stations are used to increase the location accuracy was not available for this project, but this would improve the GPS performance and is recommended for future research projects.

Density altitude at spin entries was determined by using the pressure altitude from the aeroplane altitude instrument set to standard pressure and temperature was obtained from published upper wind and temperature (Flight Level 50) charts. Corrections were applied based on the International Standard Atmosphere lapse rates. For the research flights with the ADP, which measured both air temperature and pressure altitude continuously, more accurate data were available and enabled a comparison of these two techniques. Using an example from a 6-turn spin entry at 6000 feet indicated altitude (based on a sea level pressure setting), the first estimation technique resulted in a density altitude of 5200 feet compared with a density altitude of 5300 feet using data from the ADP. This difference of 100 feet, or about 2%, was believed to be well within the accuracy required for reporting density altitude.

For the PSS-8 sensor system, data did not exist that enabled a direct comparison of measured values. Therefore, a gradual build-up approach was used. Before the differential pressure (dP) measurement on the Safir horizontal tail in the spin, the variation in dP was obtained during pre-stall flight where the dP values varied as a function of airspeed, which was a reasonable and expected result (lift varying with the square of airspeed). Before measuring dP on the Firefly wing points during spins, several manoeuvres were flown with a gradual build-up, from minimal flow separation (as indicated by the tufts) at the stall to the more dramatic flow separation observed during a post-stall Large Amplitude Wing Rock (LAWR) mode. At each step the differential pressure data was compared to other sources of data if possible, for example ADP data for the stalls and visual observations of tufts. The data obtained from the PSS-8 measurements will be shown and discussed in chapter 6.

3.10.1 VBSE accuracy considerations

Considering first the accuracy of the object tracking in SynthEyes [79], the software reported the root-mean-square error in distance between the 2D tracking point's position and the solved 3D positions. For the object tracking performed this error was reported to be 3 pixels. To find the equivalent error distance in real space the demagnification factor and the size of the CCD image sensor used in the camera are required. The Panasonic AG-HPX500 camera uses a 2/3 inch sensor with an aspect ratio of 16:9 (14.8 mm x 8.3 mm) and a pixel size of 7.7 microns [76, 90]. Using an object size of 10 m and the object spanning half the digital image, the demagnification was 1350:1. However, it should be noted that due to the dynamic motion of both the object (the spinning aeroplane) and the camera platform (the autorotating helicopter) this demagnification factor was not constant throughout the recording. Using these data, we get an estimated error in real space of 31 mm (7.7 microns x 3 pixels x 1350). Extending this to an error in angle measurement if a point is displaced 31 mm in each direction from one frame to the next, we get an estimated error of 2.5 degrees.

The errors due to steps 3 to 5 of the VBSE method as described in section 3.5 was difficult to quantify due to limited data that could be used for comparison. The approach used to establish a reasonable accuracy of the VBSE method was to compare with three different sources of data, first a qualitative comparison of the estimated ß angle with the smoke trail from the 'smoke boom', then comparing the vertical altitude loss with GPS altitude data and finally comparing the rotational motion (time per turn) with data from the FDR rate sensors (angular velocities). Thereby the angular position of the aeroplane in the spin, and both the rotational and translational motion would be compared to other data sources. The results from these comparisons will be discussed in the next chapter (section 4.6).

4 The spin motion

4.1 Introduction

The spin motion was introduced and described in section 2 in a historical context. The nature of the spin motion will now be studied and discussed further. Firstly, 4 qualitative descriptions of the spin motion as perceived by the pilot in the cockpit will be presented. In addition to the two research aeroplanes introduced in the previous chapter, two additional aeroplanes have been used for these qualitative descriptions. Although both of these aeroplanes are also military type trainers, the NDN 1 Firecracker [91] has a low aspect ratio wing design and the Aermacchi MB-326M Impala [24] is a jet trainer, and thus both have some unique characteristics that add breadth to the discussion. Additional spin data and spin characteristic descriptions, from earlier spinning trials for both the BAC Jet Provost and the Short Tucano, have also been included for comparison. Both of these aeroplanes were introduced in Section 2. The reason for the particular emphasis on the military type trainers is the requirement for spin training usually found in a typical military pilot training syllabus. Therefore, this type of aeroplane has spinning as a part of its mission requirement and the spin characteristics do have an operational significance beyond just satisfying a certification requirement.

Any study of the spin motion would be incomplete without considering the gyroscopic effects. When rotation has started, angular momentum is in effect and is very important for the understanding of how the spin motion develops. Angular momentum was estimated using data obtained from the Firefly research aeroplane spins.

Anecdotally, from the author's 13 years of experience as an aerobatic flight instructor, the spin motion apparently varies from one spin to another even if the exact same spin entry and recovery technique is used. To further investigate this lack of consistency, several spins have been flown in the Firefly research aeroplane and data obtained for comparison and analysis.

Finally, the Vision Based State Estimation (VBSE) method introduced in the previous chapter was used to obtain data to gain further insight into the spin motion. The VBSE method was used to obtain data that would be challenging to acquire using

instrumentation on the research aeroplane itself. The accuracy of the VBSE has been discussed and data obtained compared, both qualitatively and quantitatively, with other sources of data. The utility of the VBSE method for use in studying the spin motion was demonstrated using two examples.

4.2 Qualitative descriptions of the spin motion as perceived by the pilot

The spin entry (1st turn) will be dependent on the spin entry technique used and also the energy state of the aeroplane as the controls are set for spin entry. As earlier explained in Section 3.2, the spin entry technique and the timing (just before or at the onset of stall) have been kept constant throughout this research programme. This type of spin entry technique, which is comparable to the technique used in a typical pilot training syllabus, usually result in a 1st turn where the rolling motion is significant, i.e. the aeroplane will typically roll 360 degrees during the 1st turn.

The general specifications for the 4 military trainer type aeroplanes and the mass properties conditions used in the tests are shown in Table 5 below.

	Firecracker	**Impala**	**Firefly**	**Safir**
Engine	Lycoming AEIO-540 (260 HP)	Rolls-Royce Viper MK22-1 (2500 lb thrust)	Lycoming AEIO-360 (200 HP)	Lycoming O-435-A (190 HP)
Dimensions				
Wingspan	7.92 m	10.57 m	10.6 m	10.6 m
Length	7.7 m	10.66 m	7.3 m	7.9 m
Wing area	11.9 m^2	19 m^2	12.6 m^2	13.6 m^2
Aspect ratio	5.3	5.8	8.9	8.3
Mass properties				
Weight empty	949 kg	2,598 kg	730 kg	833 kg
MTOW	1,288 kg	4,350 kg	975 kg	1050 kg
TOW	1,220 kg	3,643 kg	895 kg	1005 kg
CG Range (%MAC)	24 – 29	22 – 30	21 – 26	5 – 27.1
CG (%MAC)	25.6	28.1	21	13

Table 5. General data for 4 military training aircraft

An aircraft's spin characteristics may vary depending on many factors, e.g. atmospheric conditions, mass properties and pilot technique. Although these test flights were flown using configurations and weights used for a typical training flight, these descriptions

should be considered ‘snap shots’ of these aircrafts’ spin characteristics. Data and descriptions of the spin motion are from the test pilot notes taken during these flights and from video imagery obtained during the same flights.

4.2.1 Norman Aeroplane Co. Firecracker

The Firecracker (Figure 33) is a one-of-a-kind prototype aircraft that never made it into production. Interestingly, it has a low aspect ratio wing design, apparently to imitate handling characteristics of operational fast jets.

Figure 33. The NDN-1 Firecracker prototype aeroplane.

A right hand 3-turn spin was entered from 9,000 feet. At entry, the nose initially raised above the horizon, followed by a roll to the inverted attitude and a pitch down below the horizon. After the ½-turn point as the aeroplane continued rolling towards a wings level attitude again, the nose pitched up towards the horizon, reaching a maximum at the 1-turn point before pitching down again. In addition to the pitch oscillation, roll and yaw hesitation, followed by acceleration, was clearly apparent. The first turn was completed in about 4 seconds, then an increase in rotation rate, 2 seconds for the 2nd and 3 seconds for the 3rd turn. After 3-turns, recovery controls were set and rotation ceased after an additional ½ -turn.

A left hand 3-turn spin was similar to the right hand spin, with a few exceptions. First, the left hand spin was flatter (higher angle of attack) at the 1-turn point compared to the right hand spin. At the 2- and 3-turn points the nose attitude seemed to be the same for the left and right hand spins. Also, when the stick was moved forward for the recovery, there was a noticeable acceleration in roll. The rotation rate increased before it stopped 1¼ turn after recovery controls were set at the 3-turn point. Screenshots from cockpit video imagery is shown in Figure 34.

The last spin flown in the Firecracker was a left 6-turn. Elapsed time from entry to 1-turn was 4 seconds and then 3 seconds per turn for the remaining turns. There were oscillations in both pitch and roll throughout. The rotation rate increased in the recovery phase. Rotation ceased 1½ turn after recovery controls were set at the 6-turn point.

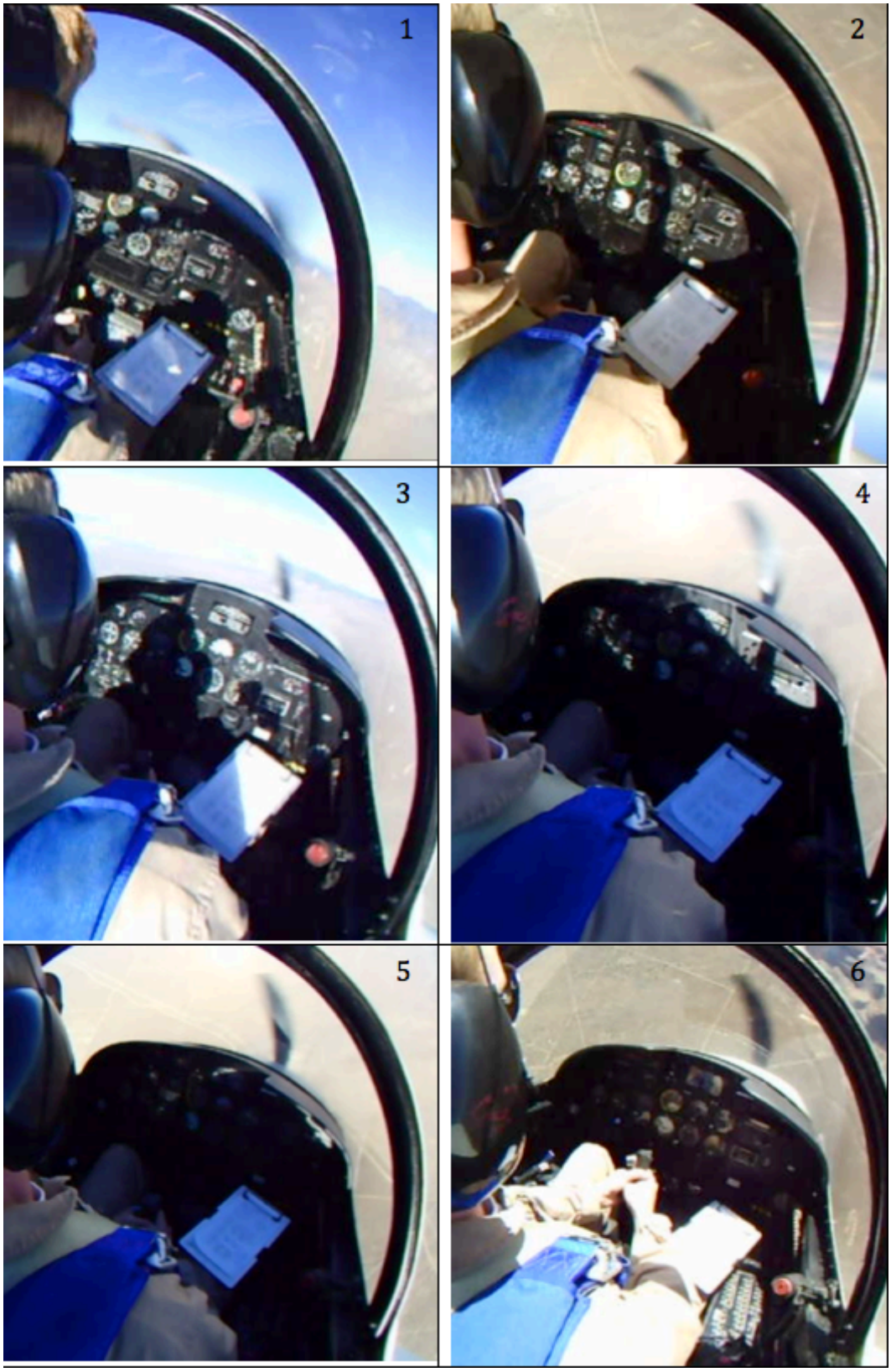

Figure 34. Left, 3-turn Firecracker spin 1) Entry 2) ½-turn point with horizon visible in the lower right corner 3) 1-turn point 4) 2-turn 5) 3-turn and finally 6) Recovery

4.2.2 Aermacchi Impala

The Impala (Figure 35) is a jet trainer used for more advanced military training and the example flown for this research project is residing at the National Test Pilot School (NTPS). This military trainer is also different in the sense of being in the medium weight category. The other three military trainers discussed in this section are in the lightweight category.

Figure 35. The Aermacchi MB-326M Impala used at the National Test Pilot School (Photo from NTPS).

A left hand 3-turn spin was then entered from 19,000 feet. There was minimal pitch-up at entry. As the aeroplane rolled in the direction of applied rudder, the aeroplane pitched down and the nose was well below the horizon at the ½ turn point. The nose came up slightly at the 1-turn point, before pitching down again and the spin became steeper for the 2nd and 3rd turns. The rotation rate was described as smooth, however a slight roll hesitation followed by acceleration could be observed at the 2-turn point. Elapsed time for 1st turn was 5 seconds and then 3 seconds per turn for the remaining turns. After recovery controls were set, rotation ceased after an additional ½ turn. Screenshots from a camera mounted in the tail is shown in Figure 36.

A right hand 6-turn spin entry was similar as for the 3-turn spin described above and the nose came up at the 1-turn point before pitching down for a steep spin. However, there was marked roll and yaw hesitation at each turn completion point. Recovery was complete after an additional ¾ turn.

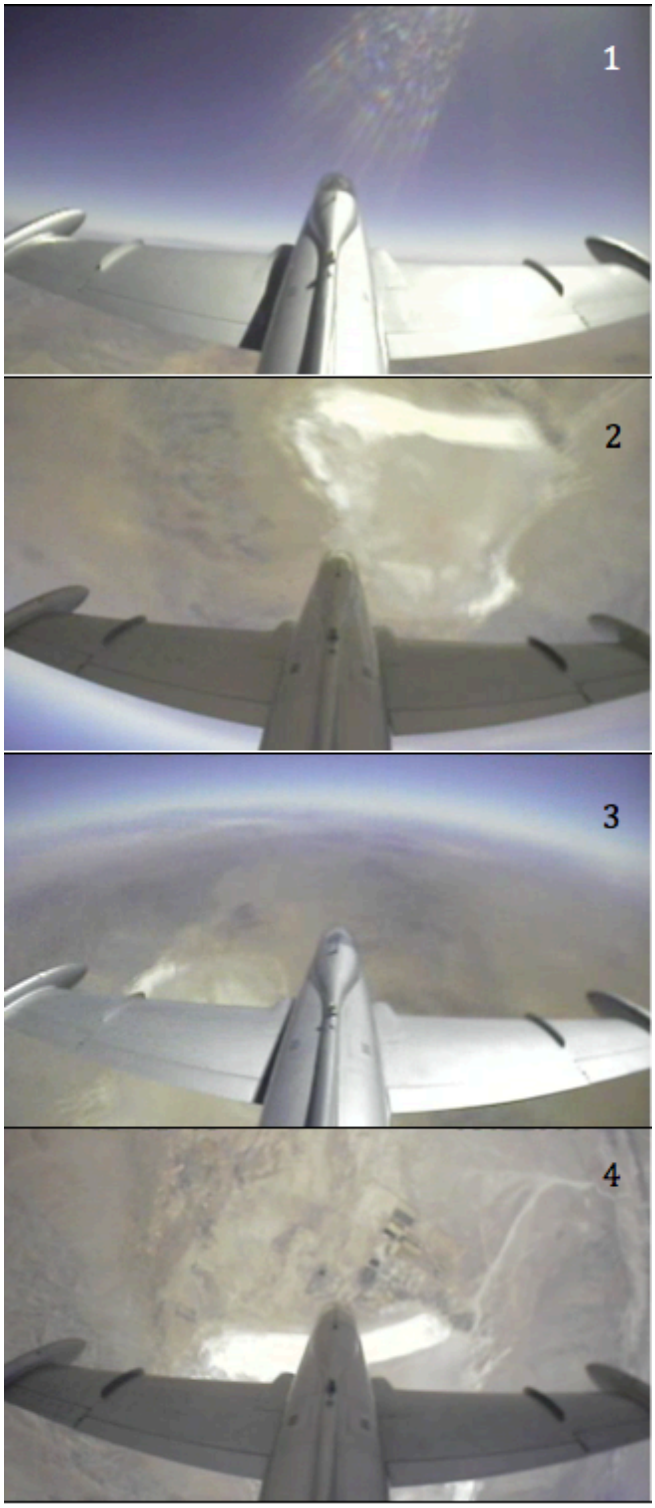

Figure 36. Left hand Impala spin 1) Entry 2) ½-turn point 3) 1-turn point 4) Recovery

4.2.3 Slingsby Firefly

The spins were flown from 5,000 feet. The Firefly pitched up initially before yawing, rolling and pitching to a steep nose down attitude at the ½ turn point. The nose pitched up from the ½-turn point, reaching a maximum nose high attitude at the 1-turn point before pitching down again. There was noticeable increase in rotation rate as the stick was moved forward for the recovery and turns in recovery was ⅘ turn for the 3-turn spin and 1½ turns for the 6-turn spin.

The pilot perceived the rotation rate as mostly smooth and steady. However, some oscillations in roll, yaw and pitch could be observed. A Firefly left spin, photographed from a helicopter, is shown in Figure 37. The Firefly spins will be covered in much more detail in the following sections in this chapter.

4.2.4 Saab Safir

Qualitatively, the Safir spins to the right were similar to the Firefly. At entry, the nose pitched up as the aeroplane yawed and rolled in the direction of applied rudder. A steep nose down attitude was reached at the ½-turn point before pitching up to a nose high attitude at the 1-turn point. From the 1-turn point the nose pitched down and spun thereafter at a steeper nose down attitude.

Oscillations about all three axes were observed, but did not have the same magnitude as observed in the Firecracker. After the 3rd turn, the spin seemed to stabilise at a higher rotation rate, however subtle oscillations in pitch could still be observed.

Spin entries to the left resulted in a spiral mode. The Safir spin entry to the left, as perceived from the cockpit, was similar to the right spin entry. However, after the 1st turn the nose pitched down to a steep attitude and there was a transition to a spiral, with speed and load factor build-up. Recovery from the spiral was instant as soon as the stick was put forward.

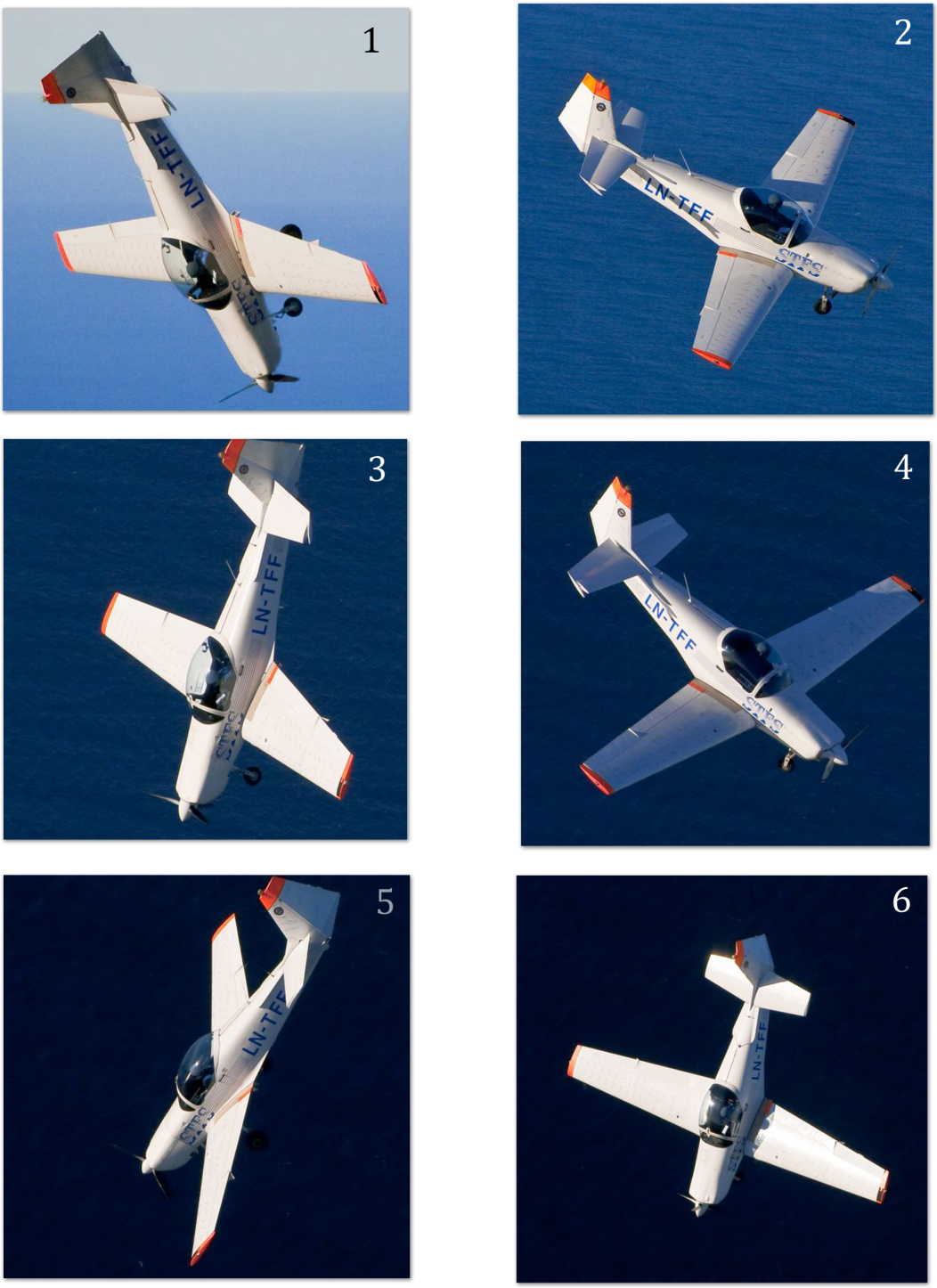

Figure 37. Left, 2-turn Firefly spin 1) Just passed ½-turn point 2) Before 1-turn point 3) 1½ -turn point 4) Before 2-turn 5) ½-turn in recovery 6) Recovery continued

4.2.4 Summary of qualitative descriptions of the spin motion

Four military trainer type aircraft have been spun and their spin characteristics have been observed and noted. Table 6 lists a summary of these aircrafts' spin characteristics as perceived by the pilot in the cockpit. However, note that these spins in the 4 aeroplanes were not flown under the same atmospheric conditions, so they should not be directly compared, but the table shows data that are representative of what might be reported by a test pilot using written notes and cockpit video imagery.

	Firecracker	**Impala**	**Firefly**	**Safir**
3-turn spins				
Time 1-turn (rotation rate)	4 sec	5 sec	4 sec	4 sec
Time 2-turn	2 sec	3 sec	2.5 sec	2.5 sec
Time 3-turn	3 sec	3 sec	2.5 sec	2 sec
Turns in recovery	½	½	⅘	¾
Altitude consumed (incl. recovery)	2,000 feet	4,000 feet	1,400 feet	1,500 feet
6-turn spins				
Turns in recovery	1½	¾	1½	1½
Altitude consumed (incl. recovery from the dive)	3,600 feet	6,000 feet	2,000 feet	2,500 feet

Table 6. Summary of spin characteristics as observed from the cockpit.

There were varying degrees of oscillations about all three axes (roll, pitch and yaw). These aircraft did not rotate and descend with a steady attitude downwards in the 'text book' spin helix. The spin motion seemed to reach a semi-steady state, evidenced by the perceived normalisation of a spin mode after 2-3 turns, but there were clearly more or less subtle variations in motion in all cases.

Apparently, the nature of these oscillations was peculiar to aircraft type. However, there were also some similarities worth noting. All 4 aircraft had a 'twin peak' in estimated α (angle of attack) during spin entry. The first peak was just after spin entry control application, with the nose pitching up initially before rolling and yawing towards the inverted attitude. The angle of attack was then apparently decreasing and seemed to be at

a minimum at the ½-turn point before reaching a maximum at the 1-turn point (the second peak in α). This twin peak in estimated α seemed to be the footprint of the spin entry when using the spin entry technique described in section 3.2.

4.3 Additional data from the Tucano and the Jet Provost spinning trials

Data from spinning trials of two additional military trainer type aeroplanes will also be presented to give further insight into spinning motions that can be encountered in a military trainer. These two aeroplanes, the Tucano T Mk. 1 and the Jet Provost T Mk. 5, were introduced in section 2.4.2. Data and information is from the Tucano spinning assessment performed in 1989 [42], and the Jet Provost Mk. 5 handling and performance assessment for service release trials from 1968 to 1969 [43]. Both of these aeroplanes are in the medium weight trainer category, comparable to the Impala described above.

A data comparison of two left hand 6-turn spins are shown in Table 7. It is clear that the Tucano has an oscillatory spin mode. In the spinning assessment report [42], the oscillations for erect spins (with idle power, for the 5^{th} or 6^{th} turn) was reported as +/- 100 and +/- 30 degrees per second for roll rate and yaw rate respectively. It was suggested that oscillations were related to aileron position in the spin, and when using aileron set with the spin direction a very oscillatory spin was noted (especially when spinning to the left). The Jet Provost reportedly also had more oscillations when aileron with the spin was used, e.g. mild oscillations with half aileron and moderately large variations in roll rate with ¾ aileron used. However, the resulting motion when using aileron with the spin were not believed to cause pilot disorientation in the Jet Provost.

	Jet Provost T Mk. 5	**Tucano T Mk. 1**
Entry speed, IAS (kn)	90	80
Entry altitude (feet)	25,000	15,100
Min. altitude recorded (feet)	19,200	10,100
Time from entry to exit (sec)	23	25
Developed spin:		
Mean pitch rate (deg/sec)	10	20
Mean roll rate (deg/sec)	80	87
Mean yaw rate (deg/sec)	50	80
Oscillation in pitch rate (deg/sec)	Approx. +/- 20	Approx. +/- 75
Oscillation in roll rate (deg/sec)	Approx. +/- 10	Approx. +/- 100
Oscillation in yaw rate (deg/sec)	Nil	Approx. +/- 15
Recovery:		
Increase in roll rate during recovery (deg/sec)	Approx. + 100	Approx. + 100
Push force on stick required for recovery (N)	222	302
Data for the Jet Provost from time history plot in Fig. 18 in Ref. [43] and likewise data for the Tucano from Annex C, flight 149/1.5 in Ref. [42]. Mass range for the Tucano was given as 2300-2900 kg and Jet Provost mass was stated as 2780 kg.		

Table 7. Comparison of left hand 6-turn spins in the Jet Provost and the Tucano.

4.4 Gyroscopic effects

As the aeroplane starts to rotate in the spin, angular momentum is in effect. The angular momentum vector is given by

$$H = I\Omega = \begin{Bmatrix} I_{xx}p \\ I_{yy}q \\ I_{zz}r \end{Bmatrix} \tag{4-1}$$

where I_{xx}, I_{yy} and I_{zz} are the principal moments of inertia and (p, q, r) are the angular velocity vector components. The angular momentum vector components can be considered as three gyroscopes, and will be abbreviated to roll, pitch and yaw 'gyro' respectively. The principal moments of inertia were estimated for the Firefly by using the representative figures method [92]. In this discussion, symmetrical loading about the X-axis is assumed (e.g. the exact same load in both wing fuel cells). Estimated angular momentum components were then plotted in Figure 38 below by using angular rates from a 6-turn left Firefly spin.

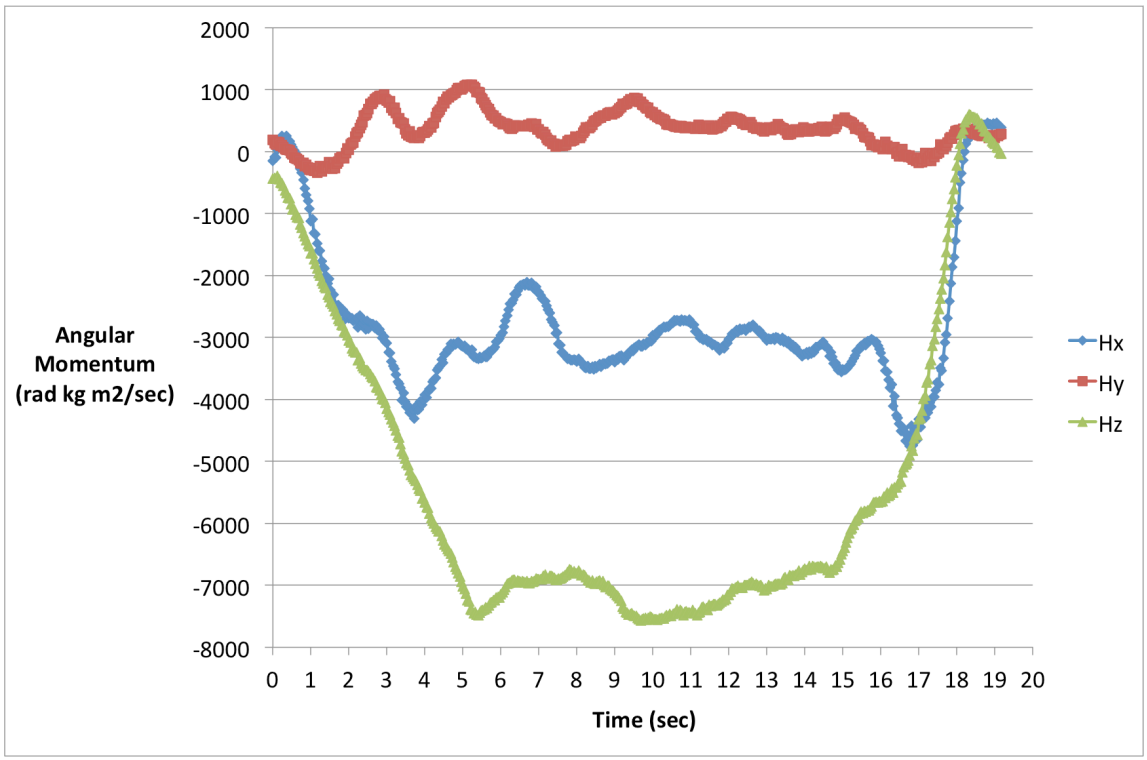

Figure 38. Estimated angular momentum components (H_x, H_y and H_z) were plotted using estimated MoI and angular rates from a Firefly 6-turn left spin (CG at 21% MAC, takeoff mass was 900 kg and spin entry was at approx. 5900 feet density altitude).

A gyroscope has a fascinating characteristic, which is rigidity in space. If disturbed by an applied moment in an axis perpendicular to its spinning direction, it will resist this movement by precessing the moment 90 degrees. Furthermore, this precessed moment results in a moment opposing the initial disturbance. This natural stability characteristic, i.e. inherent resistance to movement, has many practical applications in aerospace engineering. For example, in inertial navigation systems (INS) two gyros spinning in opposite directions are used for increased stability. However, in a spin the roll and yaw gyros are spinning in the same direction, and as we will see, this arrangement promotes the spinning motion.

In the spin, we have observed rotation about all three axes (rolling, pitching and yawing). Usually, in literature the gyroscopic effects are described after considering one axis after another (e.g. by Stinton [58]). However, the three gyros should not be considered in isolation. They are literarily in this together, spinning about the same CG. As shown in Figure 38, particular the roll and yaw gyros have significant angular momentum. When considering an imposed angular moment, there will always be two

precessed moments. However, when considering the angular momentum, the corresponding value of each one is of interest. For the light aeroplane, the angular momentum about the Z-axis is often highlighted as the dominant due to the typical higher MoI value about the Z-axis ($I_{zz} \sim I_{xx} + I_{yy}$). However, as can be seen in Figure 38, the roll gyro must also be considered during the spin entry (peak value at 3.6 seconds).

Below in Table 8 the effects of imposing a moment on the gyros are shown, e.g. a pitch down into the roll gyro. The roll and yaw gyros will spin in the same direction during an upright aeroplane spin. However, the aeroplane pitches up or down so there are two possible directions for the pitch gyro. The term 'Anti' is used to describe a direction opposite to the spin direction and conversely 'Pro' is the same as spin direction.

Imposed moment (or torque)	**Angular momentum**	**Torque-induced precession**
Pitch Down	Roll gyro	Anti yaw
	Yaw gyro	Pro roll
Pitch Up	Roll gyro	Pro yaw
	Yaw gyro	Anti roll
Roll	Pitch-up gyro	Anti yaw
	Pitch-down gyro	Pro yaw
	Yaw gyro	Pitch-up
Anti roll	Pitch-up gyro	Pro yaw
	Pitch-down gyro	Anti yaw
	Yaw gyro	Pitch-down
Yaw	Roll gyro	Pitch-down
	Pitch-up gyro	Pro roll
	Pitch-down gyro	Anti roll
Anti yaw	Roll gyro	Pitch-up
	Pitch-up gyro	Anti roll
	Pitch-down gyro	Pro roll

Table 8. Effects of the possible imposed moments on the angular momentums for the spinning aeroplane.

The gyroscopic effects in the spin should not be considered to be ideal in the sense that the imposed moments are not necessarily applied as impulses, but rather imposed over a certain time period and the applied moment might be nonlinear. In addition, the level of stability (i.e. the resistance to movement) is not necessarily of such a nature that an imposed moment by using the flight controls is not effective in moving the aeroplane in the desired direction (e.g. stick forward result in a nose down movement). In this discussion, assume that the elevator and the ailerons will induce an aerodynamic moment when the controls are moved. To further investigate the gyroscopic effects in a spin induced by moving the aeroplane controls while spinning, the following experiments were performed in the Firefly research aeroplane. First a left 6-turn spin was flown as a baseline for comparison, i.e. controls were not moved during the spin. Thereafter, a spin was flown where the stick was moved off its backstop after the 3-turn point in the spin and moved to a position in-between the backstop and neutral (i.e. stick moved forward) for an additional turn before it was moved back against the stop and kept there until the recovery procedure started at the 6-turn point. Finally, another left 6-turn spin was flown where the aileron was moved to the full left position (i.e. stick kept fully aft and to the full left position) and kept there until the recovery procedure started. Since both of these control applications during the spin is not considered to be normal, in the sense that they are not normally used during training or described in the Firefly Pilot Notes [67], they can be considered to be mishandling of flight controls.

The rotation rates (Ω) for these three spins are plotted in Figure 39. According to the integration of omega technique, the 3-turn point was at 8.4 sec for the baseline spin. Accounting for a short delay due to the research pilot setting the applicable control position, a response was expected from about 9 seconds in the time history. As can be seen in Figure 39, both of these mishandled control usage examples resulted in an increased Ω in a period from 9 to 11 seconds as compared to the baseline 6-turn spin. To further explain the effects, the time history of the respective angular velocity components has been plotted in Figure 40.

Considering the stick forward (SF) case first, the pitch rate was reduced from the 9 second point compared to the baseline spin (Figure 40), indicating elevator effectiveness. According to Table 8, the gyroscopic effect of a pitch-down imposed on the yaw gyro is pro-roll. Indeed, it can be observed in Figure 40 that the roll rate

increases from the 9 second point and reaches a maximum at the 10 second point. For comparison, the baseline spin has a reduction in roll rate during this period.

For the aileron in (AI) case (i.e. aileron with the spin), there was initially a slight increase in roll rate, which might indicate that the aileron act in the normal sense (i.e. left aileron result in a left rolling moment). Again, using Table 8 the gyroscopic effect of an imposed rolling moment on the yaw gyro is a pitch-up. It can be observed in Figure 40 that the pitch rate did increase in the period from 9 to 10 seconds. Furthermore, the pitch rate for the baseline spin had a reduction in pitch rate for most of this period.

Apparently, the observed motion during the spin resulting from the use of controls, as revealed by the angular velocity components, can be explained by using Table 8. Interestingly, it can also be observed in Figure 40 that there was also an increase in yaw rate for both these cases during the same time period with maximum values at approx. the 10 second point. To be able to explain this increase in yaw rates resulting from gyroscopic effects (i.e. neglecting any aerodynamic effects), it is necessary to have an additional iteration through Table 8. For example, for the AI case the description above ended with a pitch-up due to the imposed rolling moment on the yaw gyro. Starting again with a pitch-up moment imposed on the roll gyro, the result is pro yaw (i.e. increase in yaw rate).

For the SF case, it is necessary to have two iterations through Table 8 to arrive at a pro yaw result, namely from the pro roll (resulting from the pitch-down into the yaw gyro) into the yaw gyro leading to pitch-up, then finally pitch-up into the roll gyro resulting in a pro yaw. However, it should be noted that there might be another gyroscopic effect resulting in increased yaw rate in the SF case. The propeller on the Firefly has a clockwise rotation (viewed from the cockpit) and an aeroplane pitch-down moment into the rotating propeller result in pro yaw. As explained in Section 3.2, all spins were flown with the engine at flight idle to minimise any gyroscopic or aerodynamic effects from the propeller. Investigating the gyroscopic effect of an idling propeller was beyond the scope of this research project.

Note also for the AI case, a pitch-up moment imposed on the yaw gyro results in anti roll, which might explain why there was a reduction in roll rate despite the fact that the

aileron was kept in the full left position until the spin recovery was started. Apparently, both these cases of mishandling the flight controls during the spin aggravated the spin in the sense that the rotation rate increased, although it was only temporarily for the application of aileron with the spin (AI) case. In particular, moving the stick forward seems to have the greatest potential for increasing the rotation rate to a higher level. From the pilots viewpoint, moving the stick gradually forward during the spin (i.e. while keeping the rudder fully applied in the direction of spin) might be described as 'feeding the gyros' since the nose down moment exerted by the elevator result in enhanced roll and yaw rates due to the gyroscopic effects. This is clearly unfortunate if the desired result is to limit the spin rotation rate so that it doesn't reach the very high values where spin recovery might be difficult.

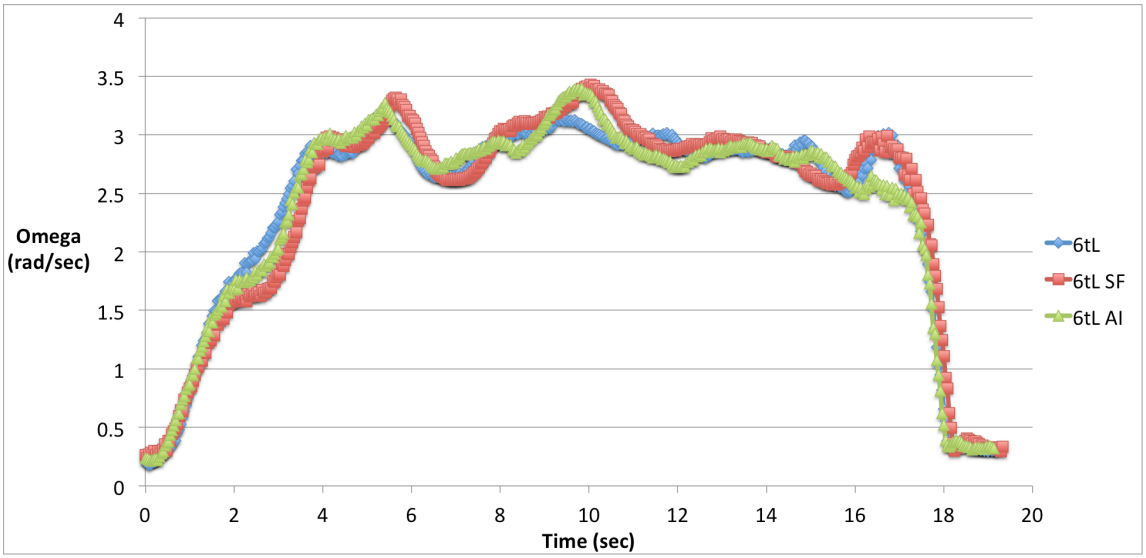

Figure 39. Comparison of Ω for three 6-turn left spins in the Firefly where two of these spins were mishandled control cases.

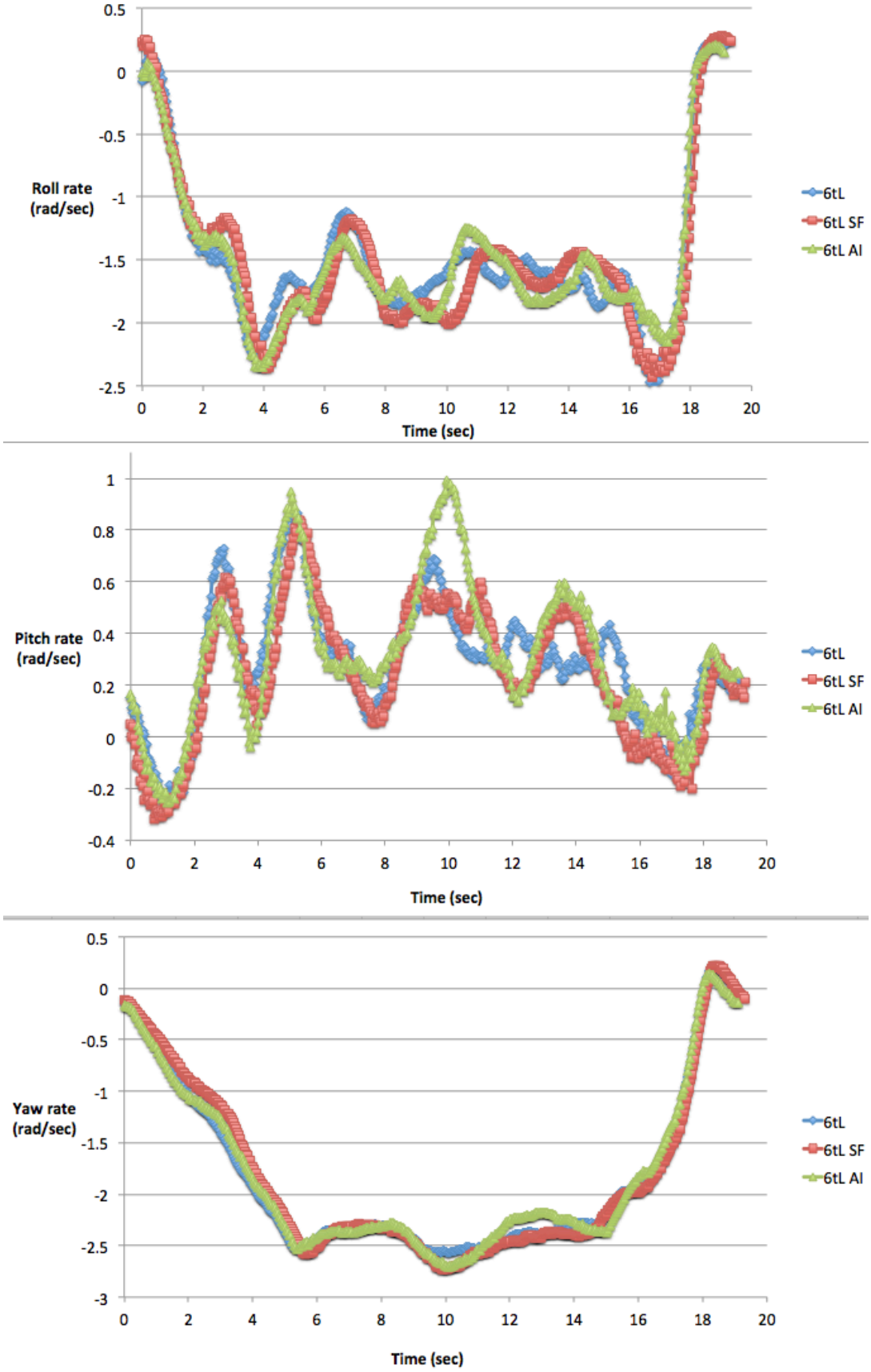

Figure 40. Comparison of roll, pitch and yaw rates for the same spins as shown above in Figure 39.

4.4.1 Historical note: ‘The cornfield bomber’

The ‘cornfield bomber’ is the nickname given to a Convair F-106 Delta Dart interceptor aeroplane after it landed by itself, i.e. without the pilot [93]. The pilot got into an uncontrollable flat spin and had to eject since he was not able to recover by using the controls. After the pilot ejected the aeroplane recovered from the spin and glided to a landing in a field.

Many were surprised by the aeroplane’s apparent automatic spin recovery after the pilot ejected as a last resort of saving himself from the uncontrollable spin. However, there might be several reasons why this is so. First, an ejection involves a significant push upwards when the ejection seat clears the aeroplane. Due to Newton’s third law, there must be an equal and opposite force acting downward, in effect a pitch down moment reducing the alpha and thus aiding the recovery. Secondly, the sudden 'removal' of the pilot and ejection seat reduces the pitching and yawing MoI, which again reduces the angular momentum. Third, it is possible that the sudden removal of the forward fuselage top section (cockpit canopy) changes the aerodynamics of the rotating fuselage in front of the CG, and this might dampen the autorotational forces of the forward fuselage.

4.5 The variation in spin motion

Anecdotally, it is often claimed that no two spins are the same. For some aeroplanes, it might seem that the only thing constant in the spin motion is the lack of consistency. In particular the number of turns after recovery controls are set seem to differ from one day to the other. The notion is usually that the slight difference in atmospheric conditions or slight differences in pilot technique are the reasons for this variation in spin motion. To further investigate this, data was obtained from several spins in the Firefly research aeroplane for comparison and analysis. This data set includes 3 left and 4 right 6-turn spins and an additional 2 6-turn spins with the MPB installed. The aim was to keep the conditions as similar as possible for these flights (e.g. aeroplane take-off mass within 5 kg and CG position at 21% MAC) and the same test pilot, using the spin entry and recovery techniques described in Section 3.2, flew all flights. Research flights were flown when the weather conditions were favourable for aerobatic flight, i.e. atmospheric high-pressure system (sea level pressure was in the range 1010 – 1027 milibar), good

visibility and light winds (wind velocity range from calm to 9 knots recorded at the departure airport) and no reported turbulence.

Below in Figure 41 and Figure 42 are the omega time histories for the spins in the data set. From these figures, three phases of the spin can be identified. The first phase, from 0 to 6 seconds, is the entry or initial phase and the last phase, the spin recovery, starts at about 14 seconds for the right spins and about 15 seconds for the left spins.

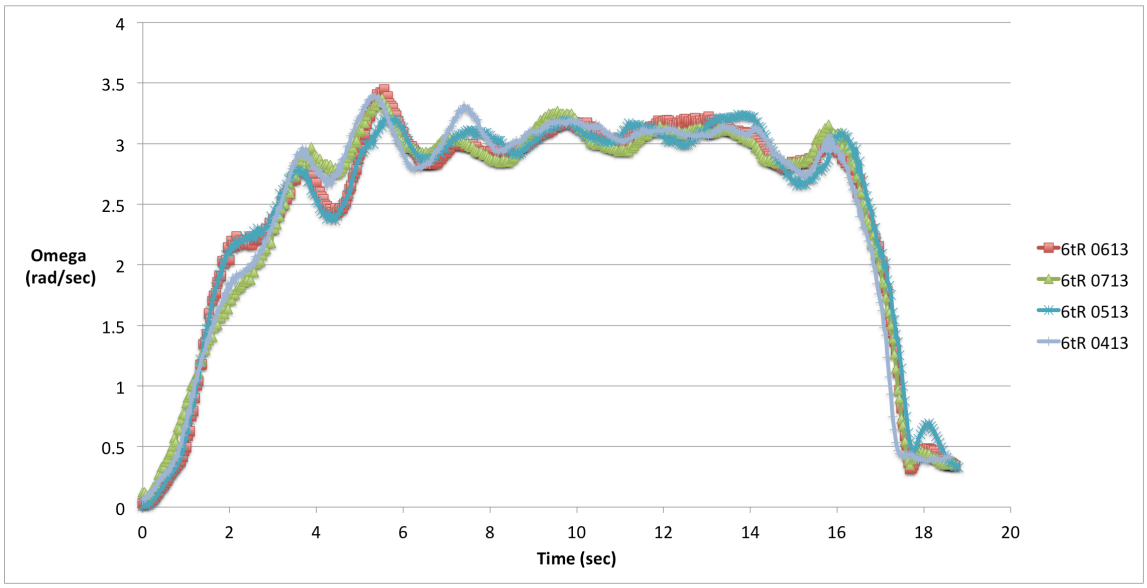

Figure 41. Omega (Ω) time history for 4 right 6-turn spins.

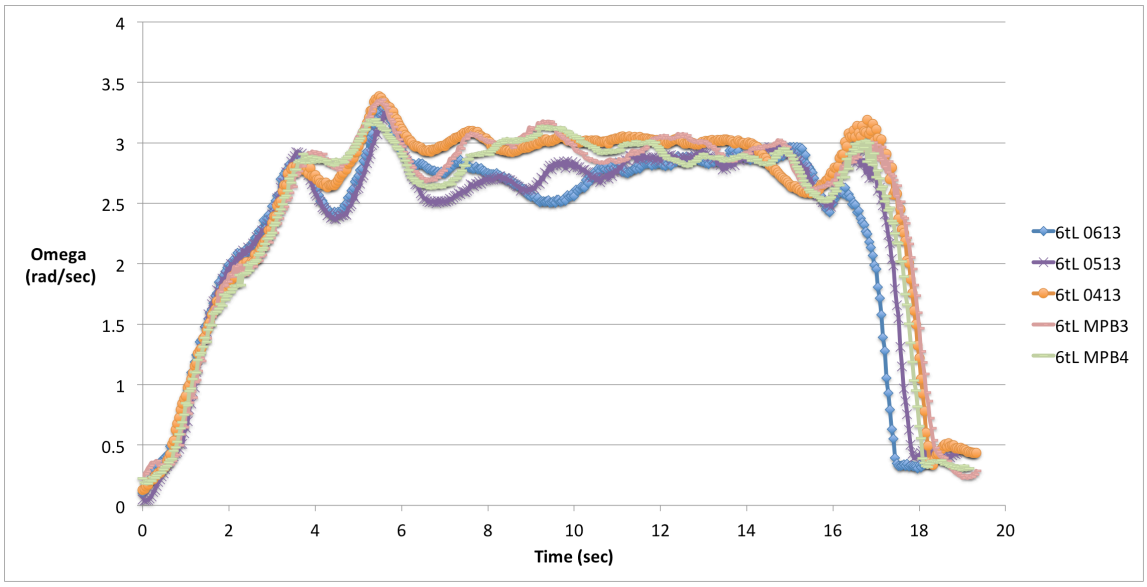

Figure 42. Omega (Ω) time history for 5 left 6-turn spins, two of them with the MPB installed.

The spin phase from about the 2nd turn (6 seconds) to the point where recovery starts is the developed phase. Developed in the sense of the spin motion having reached a state where Ω is oscillating at a certain level, and the oscillations in Ω have been reduced compared to the spin entry phase. For the developed phase, the right 6-turn spins oscillated about a slightly higher Ω level than the left spins.

The Ω time histories in Figure 41 for the right turn spins were consistent for the 4 different flights in this group. The correlation coefficients between these 4 flights were in the range 0.98 – 0.99, where the correlation coefficient is a measure of linear relationship between two measured sets of data and a coefficient value of 1 indicates a perfect positive correlation. However, for the left turn spins in Figure 42 the time histories were not as consistent, although the correlation coefficients were still in the range 0.87 – 0.98 (see Table 9 below).

Spin research flights	**Correlation coefficient**
0413 - 0513	0.95
0413 - 0613	0.87
0513 - 0613	0.94
MPB3 - MPB4	0.98

Table 9. The correlation coefficients for the left 6-turn spin omega histories.

Table 10 below shows data obtained from the 9 spins in the data set using the MTi-G FDR, both time per turn obtained from the integration of Ω technique (see Section 3.7) and GPS altitude loss per turn. Data is grouped according to type of spin (left or right turn) and in addition a 3rd group for spins with the MPB installed.

6-turn left	Time per turn (sec)			Alt loss per turn (feet)			
(3 spins)	Min	Max	Average	Min	Max	Diff in %	Average
1	3.8	3.9	3.9	110.6	132.8	20	124.0
2	2.1	2.3	2.2	144.8	178.8	23	160.9
3	2.1	2.4	2.2	182.2	221.4	22	199.7
4	2.1	2.4	2.3	198.8	281.9	42	241.4
5	2.1	2.2	2.2	204.2	270.1	32	240.9
6	2.1	2.2	2.1	209.2	250.6	20	235.7
***7**	2.2	2.7	2.5	237.2	357.0	50	297.1

* Only data from 2 spins in turn no.7

6-turn right	Time per turn (sec)			Alt loss per turn (feet)			
(4 spins)	Min	Max	Average	Min	Max	Diff in %	Average
1	3.9	4.0	4.0	106.4	149.5	41	127.1
2	2.1	2.2	2.1	143.5	162.8	13	157.5
3	2.1	2.1	2.1	177.0	194.9	10	185.9
4	2.0	2.0	2.0	194.6	223.2	15	204.9
5	2.0	2.1	2.1	196.7	236.1	20	212.5
6	2.0	2.0	2.0	196.5	215.1	10	205.9
7	2.2	2.2	2.2	228.5	241.0	5	233.3

With MPB on right wing:

6-turn left	Time per turn (sec)			Alt loss per turn (feet)			
(2 spins)	Min	Max	Average	Min	Max	Diff in %	Average
1	4.0	4.0	4.0	133.4	138.7	4	136.1
2	2.1	2.1	2.1	139.6	157.9	13	148.7
3	2.2	2.3	2.2	192.7	202.8	5	197.7
4	2.0	2.1	2.1	205.0	228.4	11	216.7
5	2.2	2.2	2.2	224.3	243.4	9	233.9
6	2.1	2.2	2.1	220.3	226.0	3	223.1
7	2.2	2.3	2.3	243.3	255.2	5	249.2

Table 10. Data obtained from 9 spins showing the variation in time and altitude loss per turn for three groups of spin (all 6-turn, right, left and left with MPB installed).

Table 10 shows little variation in time per turn, only 0.1 second difference between the minimum and maximum values for the right turn and also for the left turn spins with the MPB installed. For the left turn spins, without the MPB installed, the variation was greater with 0.1 to 0.3 seconds difference from 1st to the 6th turn. For the 7th turn (after spin recovery was started) the difference was up to 0.5 second. Overall, the difference was greater for the altitude loss recorded by the GPS. For the 6-turn left spins the

difference in % was in the range 20 to 42, and even 50% for the 7th turn. The difference in altitude loss for the right spins was 41% for the 1st turn and thereafter in the range of 5 to 20% for the remaining turns. For the 2 left turn spins with the MPB installed, the difference in altitude loss per turn in % was in the range 3 to 13.

Difference in pilot technique could possibly be the reason for variation in spin motion. Unfortunately, the positions of the aeroplane controls were not recorded in this investigation and thus the time when controls were set for entry or recovery could not be determined with precision. An inadvertent aileron input during spin entry or in the developed phase could possibly either increase or reduce the rotation rate. Furthermore, if the pilot fails to keep the stick in the full aft position, i.e. inadvertently moves the stick forward, the result would be an increased rotation rate. During the spin recovery, if the stick is put forward before the application of opposite rudder, an increased rotation rate with a subsequent prolonged recovery could possibly be the result. Also, a delay in setting recovery controls after the 6th turn would result in an error if estimating the turns in recovery using the present technique for analysing the data (integration of Ω). However, for the majority of spins in the data set and in particular for the right turn spins, the consistent rise in Ω in the entry phase and the reduction in Ω during recovery do not indicate large variations in pilot technique.

For the narrow density altitude range (from 5200 to 6000 feet) recorded at spin entry in this data set, it was not possible to establish a relation between density altitude and time per turn or accumulated altitude loss.

To further investigate the variation in spin motion, the average altitude loss per second (i.e. the average vertical velocity) for the three groups of spins was determined from the data shown in Table 10 and shown in Figure 43 below.

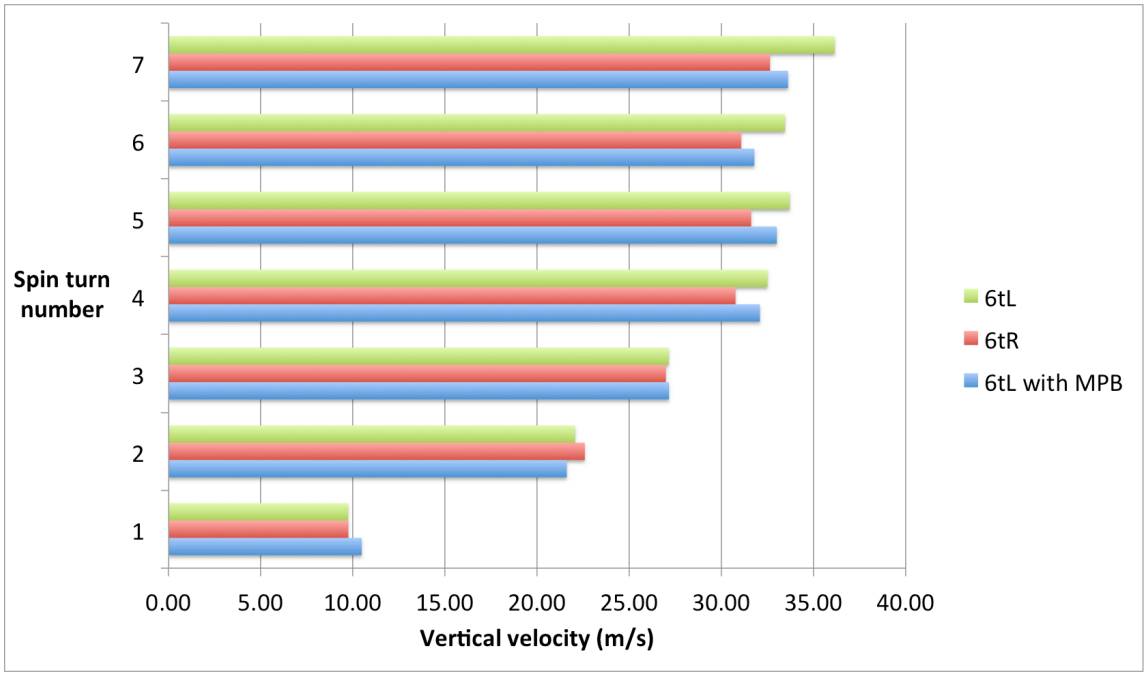

Figure 43. Average vertical velocity for the three groups of spins (6-turn left, right and left with MPB installed) shown in Table 10.

It is interesting to note that the average vertical velocity for the three groups of spins show a consistent trend, with vertical velocity increasing from the 1st to the 7th turn. In addition, from spin turn number 4 to 7, the average vertical velocity for the right turn spins were less than for the left turn spins. Although the Ω values are not completely steady, it can be observed in Figure 41 and Figure 42 that the right turn spins are oscillating about slightly higher Ω levels than the left spins in the developed phase of the spin. This indicates a relation between Ω and vertical velocity, i.e. a higher rotation rate result in less vertical velocity. So, based on the data presented above in Table 10 and Figure 43, it then follows that the difference in time per turn and altitude loss in the spin motion might depend on the Ω attained in any given spin.

4.6 Data obtained from the Vision Based State Estimation of the spinning Firefly

The angles used to determine the aeroplane position to the relative wind is of great interest for the spin motion analysis. However, the time histories of α and β have historically been difficult to obtain. In the early spin investigations, they were not able to establish a time history of β despite trying several techniques [30, 31]. More recently, for the spinning trials of the Tucano T Mk 1, it was reported that the boom-mounted sensors were only usable up to the point where the aeroplane departed [94]. Consequently, using

the boom-mounted sensors to obtain data for post-stall and spinning manoeuvres were not possible. These experiences correspond with the results from the present research programme. The ADP used on the Firefly research aeroplane, in addition to having limited ranges of measurement (+/- 20 degrees), also didn't record any reasonable relative wind angles during spins. Flow angle data obtained from an ADP must be corrected for upwash effects, i.e. corrected for the flow field disturbance due to the presence of the aeroplane (e.g. wing and fuselage depending on the point where measurements are made). For the complex spin motion, it is not difficult to envision the difficulty in obtaining correction factors for flow field disturbance for an ADP installation as shown in Figure 31. With the significant yaw rates typical of the spin motion the flow field will not only be disturbed by the presence of the wing, but also most likely due to the presence of the forward fuselage and the propeller. Therefore, due to these challenges, time histories of α and β during spins are rarely reported in spinning trials reports. However, the technical reports on spinning from NASA's comprehensive spin programme during the 1980's are the exceptions where complete α and β time histories were published. The research aeroplanes used by NASA, which were representative of typical single-engine light general aviation aeroplanes, had twin booms installed with ADP's at each wingtip [22,37,38].

High quality video imagery and camera tracking techniques resulted in a Vision Based State Estimation (VBSE) of the spinning Slingsby Firefly (as described in Section 3.5). Estimated β was obtained from the VBSE and is shown below in Figure 44. The VBSE shows maximum β values of +/- 38 degrees. Initially, these values appeared to be high (at least twice the value) compared to data from the NASA spin research programme [22,37,38]. However, the aeroplanes used in the NASA programme were representative of typical general aviation aeroplanes, not aerobatic military trainer types and therefore not directly comparable.

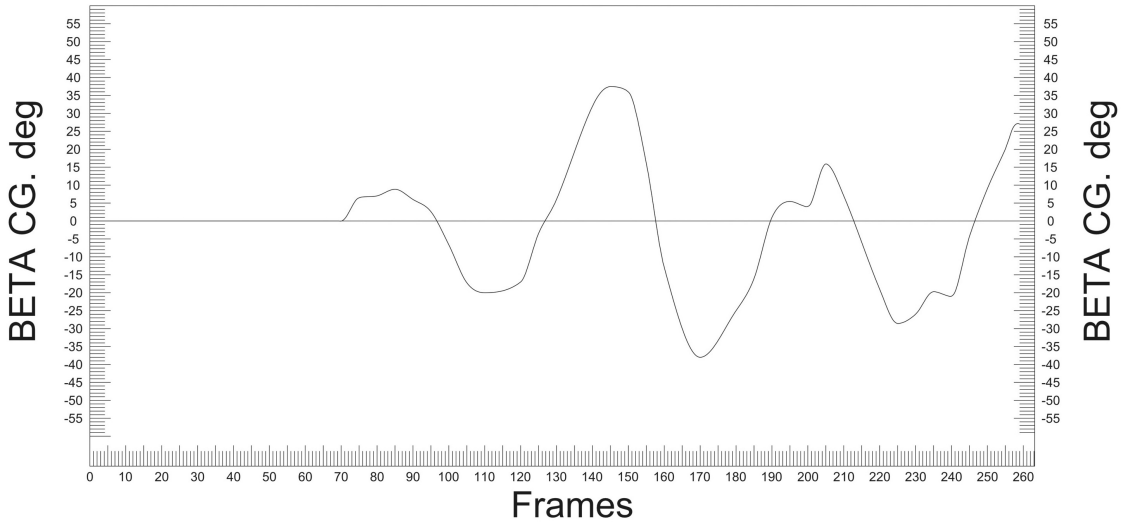

Figure 44. Estimated Beta (β) angle at the aeroplane CG for a left 2-turn spin in the Firefly.

To further investigate, and possibly establish if the VBSE was reasonably accurate, a point was placed 2.6 meters out from the centre of the aeroplane (in Y-axis direction) on the right wing of the Firefly model (hereafter referred to as the 'wing point' or WP), and its trackline during the spin motion was plotted in 3D. A comparison of this WP trackline and corresponding images obtained from the video imagery of the spinning Firefly with the 'smoke boom' is shown in Figure 45. The left column shows images of the smoke trail and the right column the corresponding screenshots from the VBSE. Assuming that the smoke trail will mainly follow the direction of the relative wind after leaving the trailing edge of the wing, and thus provide a visual estimation of β, this comparison showed good agreement between the results from the VBSE and the screenshots of the smoke trail from the video imagery.

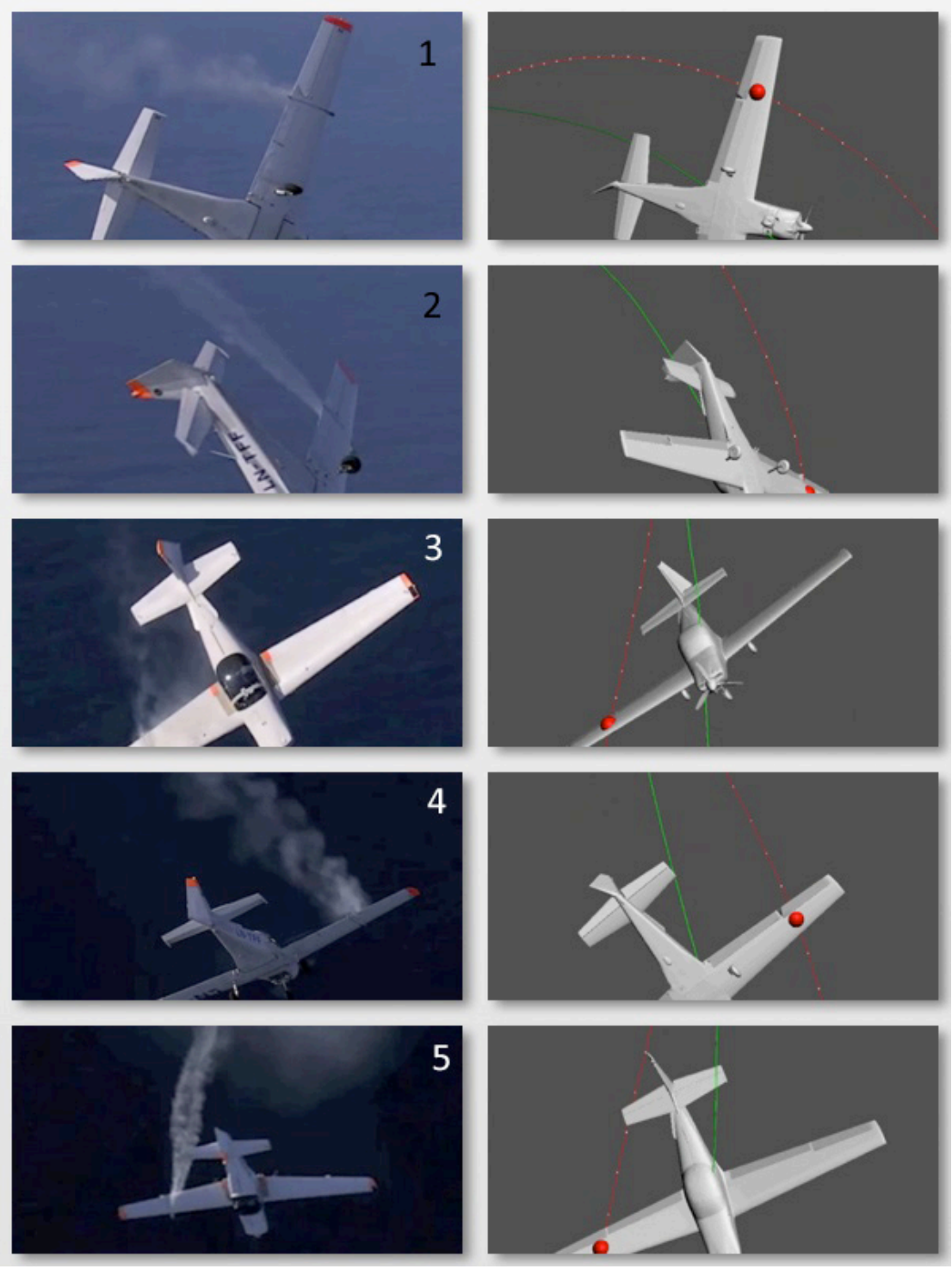

Figure 45. Comparisons of two left 2-turn spins in the Slingsby Firefly. 1) ¼-turn point 2) ½-turn point 3) Before 1-turn point 4) After 1-turn point 5) At recovery (rotation stopped)

Another comparison, enabling more quantitative results, was of the altitude loss and time per turn measured by using the VBSE and the experimental results presented in Section 4.5. However, it should be noted that the spin used for the VBSE was 2-turn spin entered at a density altitude of 3390 feet which was lower than the set of spins used in Section

4.5 above (which had a range from 5200 to 5960 feet). Figure 46 below shows data obtained from the VBSE. The altitude loss for 1st turn point for both spins (112 feet for left and 119 feet for right turn spin) compares well with the data in Table 10 since both values are within the minimum – maximum range and compares reasonably well with the average values which are 124 and 127 feet respectively. The average time per turn from Table 10 compared very well with the VBSE, with the left turn spins having the same values to 2 significant figures (3.9 sec for 1st turn and 2.2 sec for 2nd turn). For the right turn spin there was only a slight difference in values, with VBSE values of 4.1 sec and 2.2 sec for 1st and 2nd turn, compared to average values from Table 10 of 4 sec and 2.1 sec.

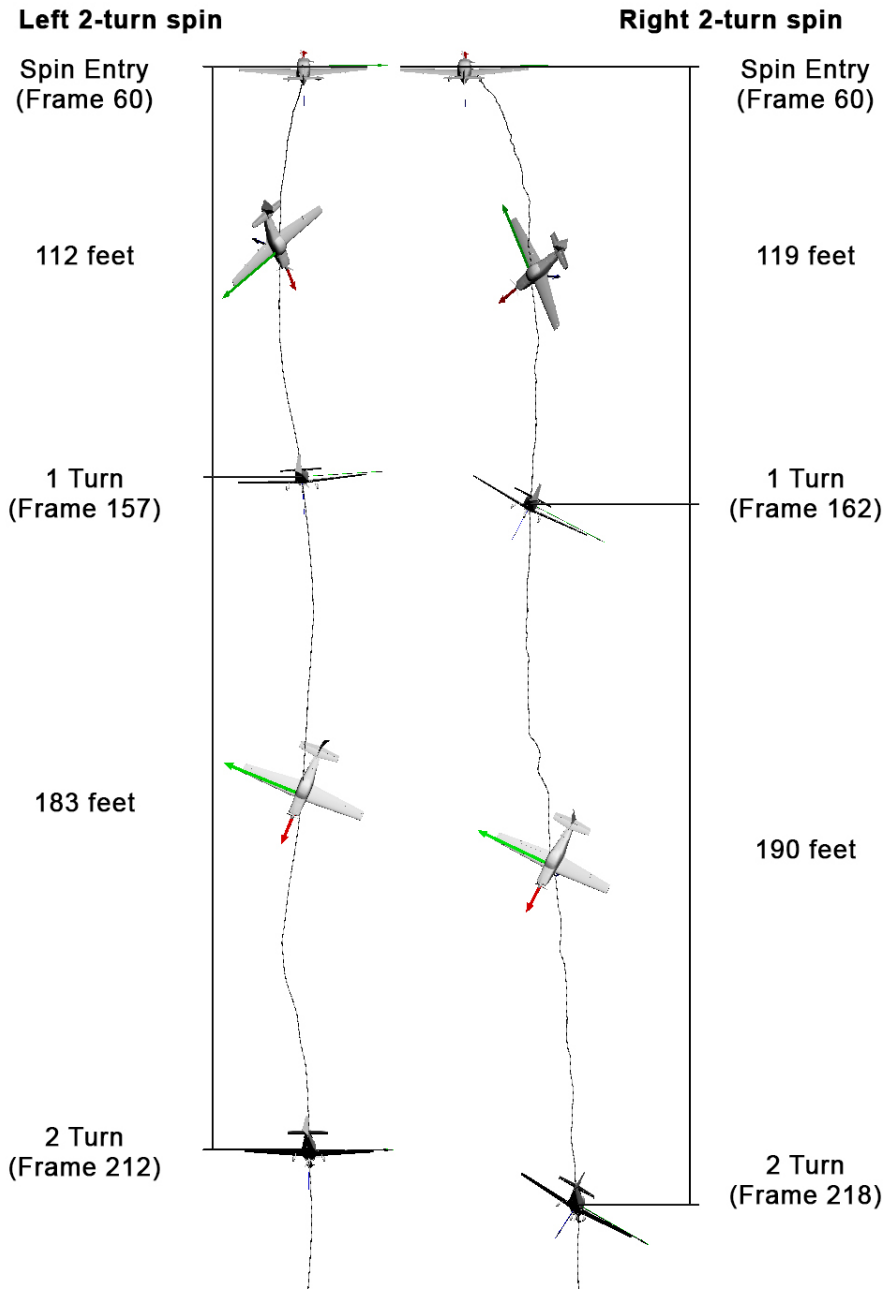

Figure 46. Left and right 2-turn spin data obtained from the VBSE.

Now, having established a reasonable accuracy of the VBSE method (by comparing data with other data sources), examples of the unique capability of this method to obtain data and to produce illustrations that will enhance the understanding of the complex spin motion will now be shown. Although the VBSE used in this research project is only limited to 2-turn spins, and thus unfortunately do not cover the developed phase of the spin, it can be used to obtain data that would otherwise be challenging to obtain using sensors and instrumentation on the aeroplane itself. In the first example, the path of the wing point (WP) in 3D described above and shown in Figure 45 was studied in the 3D

space. Figure 47 below shows 4 different view angles of the 1-turn point of the left 2-turn spin. Due to the spin motion the wing point will have a different track through the 3D space than the aeroplane CG. For example, it can be clearly seen in Figure 47 that the two tracklines are different at the 1-turn point in the spin. From the two bottom view angles, it is shown how the WP trackline was at a shallower angle than the CG trackline. Using the technique described in Section 3.5, the estimated α time histories for the WP on the right wing (outside wing in the spin) in addition to a WP placed in the same position but on the opposite wing (i.e. the left or inside wing in the spin) have been compared to the estimated α at the aeroplane CG and shown in Figure 48. It can be observed that

$$\alpha_{IWP} > \alpha_{CG} > \alpha_{OWP} \tag{4-2}$$

is valid from the start of the spin.

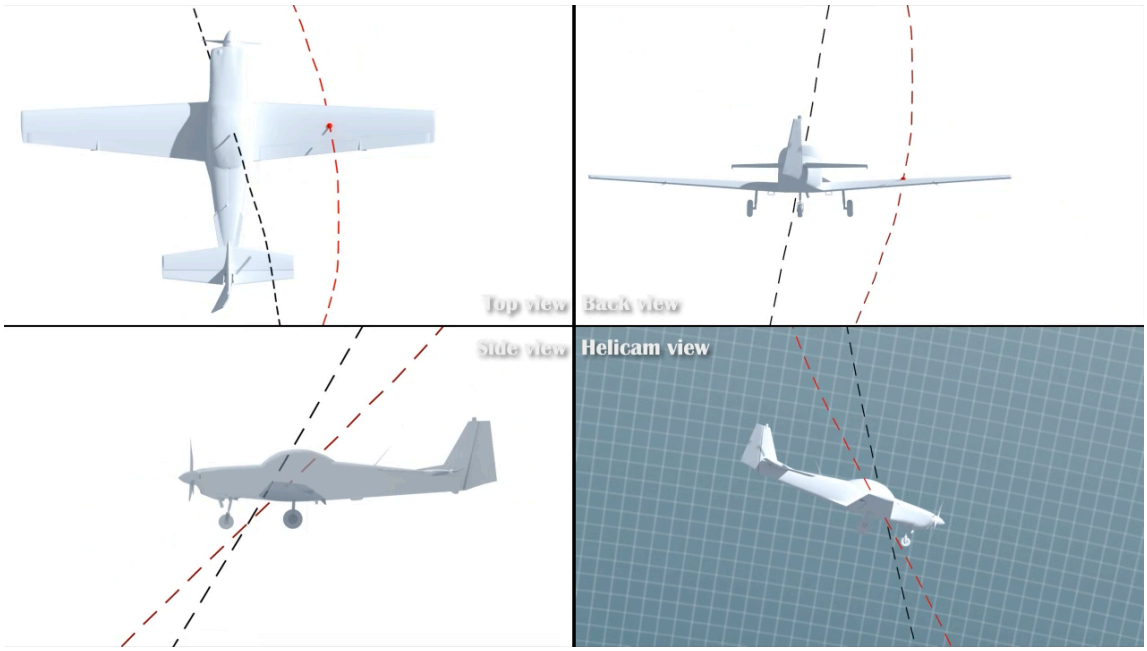

Figure 47. 4 different view angles of the aeroplane showing the CG (black) and the wing point (red) tracklines at the 1-turn point in the spin (frame 157).

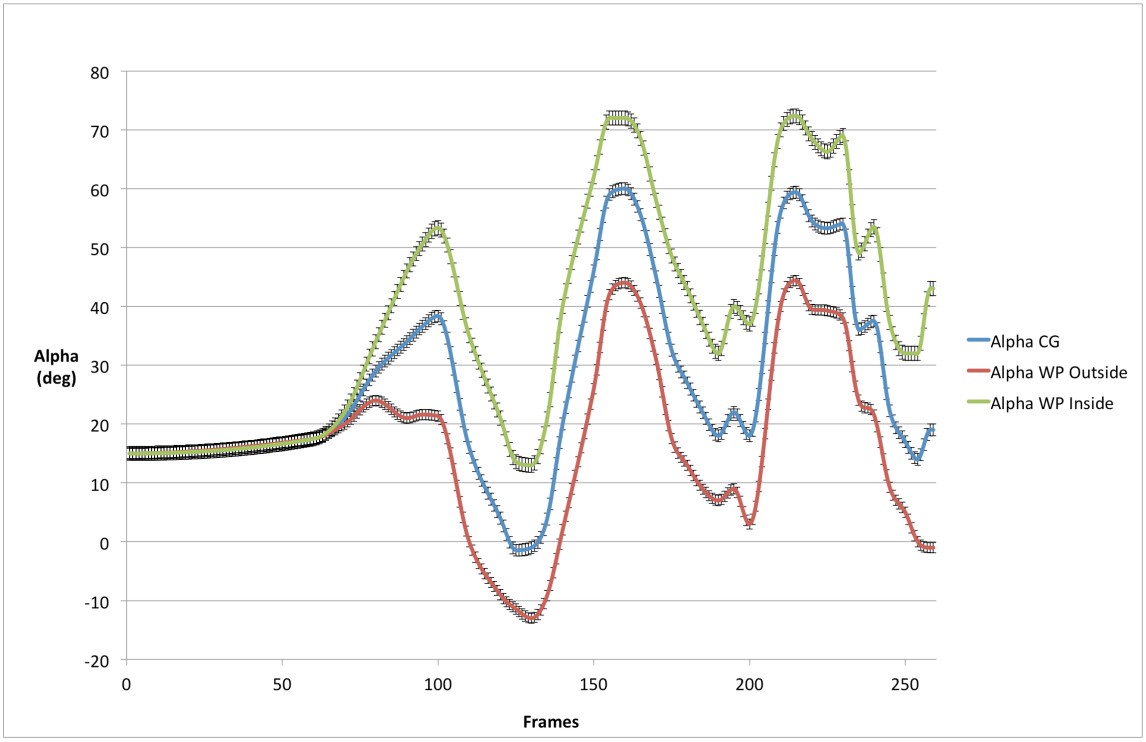

Figure 48. Comparisons of estimated α for the aeroplane CG and the two wing points (WP) placed 2.6 m from the aeroplane centre on the outside and inside wing respectively. Error bars were added for an estimated angle error of +/- 2.5 deg (see section 3.10.1).

Another example of the utility of the VBSE method is shown in Figure 49 below where a point has been placed on the vertical tail of the aeroplane. For illustration purposes, the spin axis was placed in the centre of the aeroplane CG trackline path. Thereafter a solid of revolution was obtained by using a lathe function in the visual 3D studio to rotate the tail point path about the spin axis in the 3D space. The radius of this solid of revolution was measured in the 3D space and shown at three different spin positions in the spin as shown in Figure 49. So, having established a VBSE enabling data acquisition with a reasonable accuracy, any points of interest on the aeroplane (e.g. wings, tail surfaces, propeller or fuselage) can be selected and their point tracklines plotted in the 3D space. Finally, angles or other properties of interest can be measured directly.

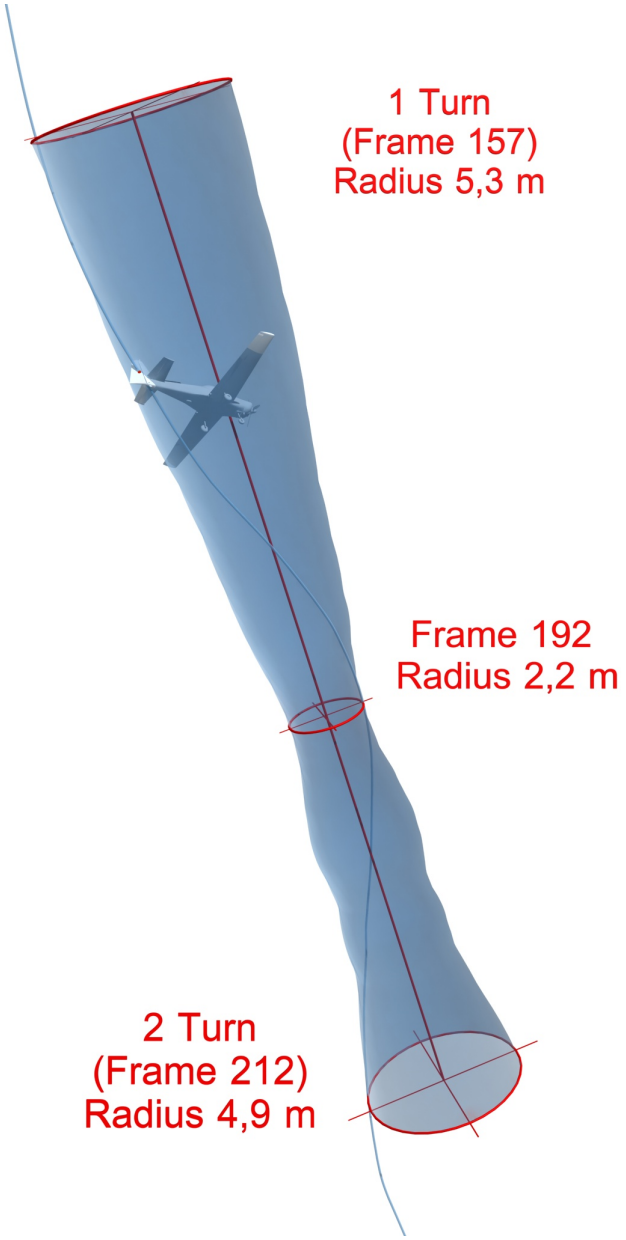

Figure 49. The trackline of a point placed at the aeroplane tail and its path in the 3D space.

5 Aerodynamic flow over wings and empennage

5.1 Introduction

A qualitative assessment of the aerodynamic flow over wings and empennage of the spinning Firefly was carried out using in-flight photographing of wool tufts. This technique for studying the flow on a spinning aeroplane has been used many times before. As early as 1932, Jones and Haslam [95] studied the airflow over the wings and tail by using wool tufts on a spinning Atlas biplane. The turbulent nature of the flow was clearly shown. About 4 seconds after the start of the spin the flow over the outside top wing was mainly irregular, but there was also areas with unsteady streamline and also reversed flow. The outside lower wing was mainly streamline with irregular flow on the inner section. However, the inside upper wing was irregular and the lower wing had very marked and steady reversed flow. In a more recent research program by Brown *et al* [96] at the National Research Council in Canada, the wings of a Harvard Mark 4 were tufted with wool tufts and the airflow studied while spinning by using video imagery. They describe the airflow in more detail, e.g. the authors' statement regarding the flow on the outside wing (in this case the left wing in an erect, right turn spin):

"*Although some large-scale eddy (LSE) coherence was evident at times (...), it is non-stationary. This is indicative of the temporal formation of LSE in the separated flow, followed by downstream eddy convection*".

Furthermore, Brown *et al* also describe the airflow on the inside wing:

"… *the tuft patterns appeared to be dominantly arranged about a ¼ chord vortex, of clockwise-rotational sense, located at the mid-span position. Video imagery tended to suggest the vortex was frozen, or quasi-stationary, with respect to the wing, rather than being formed and convected downstream*."

It is worthwhile to study in detail the aerodynamic flow on a more modern aeroplane design such as the Firefly. Furthermore, it is of interest to investigate the shielding of the tail effect, as this is the main assumption behind the tail design criterion [55]. The wake

from the tail plane is assumed to be in the region bounded by a 60° line from the leading edge and a 30° line from the trailing edge.

5.2 Flow over the wings of the spinning aeroplane

In order to describe the flow, as indicated by observing tufts on the wing, some definitions will now be made. The inside wing is the same side as the spin direction, e.g. in a spin to the left, the inside wing will be the left wing and the outside wing will be the right wing. Spanwise flow is either outwards (direction from wing root to tip) or inwards (direction from wing tip to root). Streamline flow is from leading edge of the wing towards the trailing edge. Conversely, reverse flow is in the opposite direction (from trailing edge to leading edge). Unsteady streamline is typically used for the case where flow is mainly in the streamline direction, but the flow has separated and is clearly turbulent. In the case of irregular flow, no principal direction of the flow is indicated and the tufts have no pattern of movement (erratic motion).

5.2.1 Spin entry and first turn

Considering now the outside wing in a left spin. As the elevator was deflected trailing edge up for the spin entry, unsteady streamline flow was observed at the trailing edge of the wing root. From the spin entry point, where full elevator up position was set, irregular flow had moved from the trailing edge and reached the leading edge of the wing in 8 frames. This only applied to the inner 2/3 section of the wing (from the wing root), and thus the flow was still attached (streamline) on the outer 1/3 section of the wing. At the point on the wing where the flap meets the aileron, a vortex flow structure was observed. This vortex structure was placed in the area where the flow transitions from irregular to streamline. When the Slingsby had rotated to a point where the wings were 90 degrees to the horizon, the flow returned to streamline over the entire wing. The flow was streamline for the next 90 degrees of rotation to the ½ turn point.

After the ½ turn point, a vortex formed and moved from the wing root (spanwise outwards). The rotational flow was clearly observed and it was a large vortex in the sense that its diameter seemed to be comparable to the wing chord (Figure 50). At just past the ¾ turn, the rotational flow was most apparent and the vortex core observed at the approx. 1/3 chord position (Figure 51). The flow behind the vortex was in the

spanwise outwards direction. At 1-turn the flow on the wing was predominantly spanwise outwards with a 90-degree turn towards the trailing edge, leaving the three outer row tufts in the streamline direction.

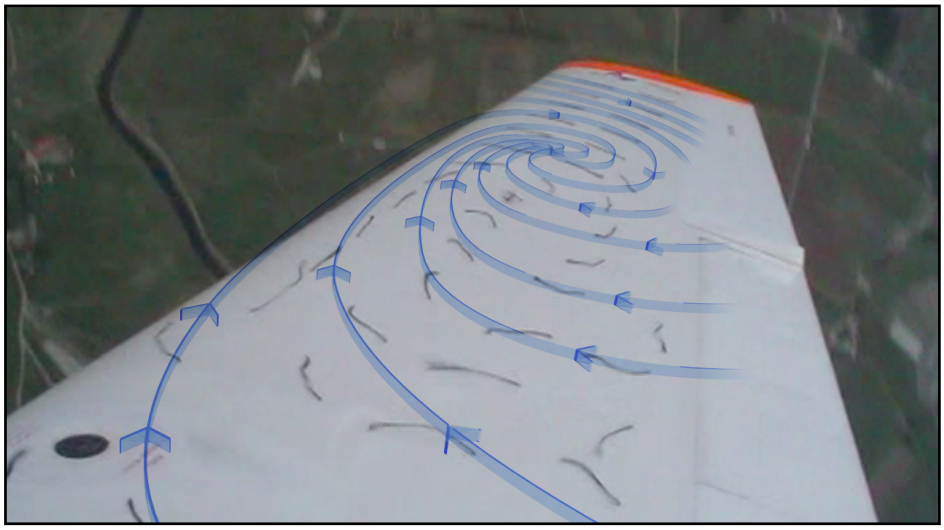

Figure 50. A large vortex forms on the outside wing as indicated by the wool tufts. The blue lines are drawn to illustrate how the shape of the vortex might be and arrows indicate flow direction.

Figure 51. Tufts on the wing at just past the ¾ turn in a left hand spin. The vortex on the outside (right) wing is clearly seen where the flap meets the aileron.

The tufts indicate a ‘twin peak’ in alpha during the first spin turn. The first peak is when the full spin controls are set. Then the angle of attack is apparently reduced, with streamline flow over the entire outside wing, before increasing again from the ½ turn to the 1-turn. This is consistent with alpha time histories of other spinning aeroplanes, e.g. published data from the NASA general aviation research programme [22,37,38], where this twin peak in alpha during the first turn is clearly apparent.

The same technique was used to study the inside wing, but with the camera mounted on the right hand side, a right hand 2-turn spin was naturally used. From spin entry, reverse flow develops, starting at the trailing edge and after 10 frames from spin entry the reverse flow has moved to the leading edge, thus covering the entire wing. The flow on the inside wing during the first turn is best described as a mix of reverse and irregular. On many frames the reverse flow is apparent. However, studying one tuft from frame to frame it can be observed that the direction might change from reverse to streamline in two frames.

5.2.2 Second turn and recovery

First, we will again consider the outside wing in a left spin. From the 1-turn and then 10 more frames, the vortex rolled back (inwards) so that the outer 7 rows of tufts were streamline. At 1.5 turns the vortex moved outwards again, and 4 rows of tufts were streamline. The spanwise outwards flow was clearly apparent at the 2-turn point, and only one row of tufts were streamline (Figure 52).

The spin recovery controls are set at the 2-turn point. Rudder is reversed in 7 frames and after 6 more frames the elevator starts to move. From this instant the vortex rolled inwards. One row at the time, from the wing tip towards to root, became streamline. The rate is such that after ½ turn in recovery the outer two rows are streamline and when the aeroplane had completed one full turn in recovery all of the outside wing tufts indicated streamline flow (Figure 53).

For the inside wing, the flow is best described as irregular. One tuft would typically rotate 90 degrees from one frame to the next. Mostly, no clear pattern was seen over the entire wing. This can be observed in Figure 51, with tufts indicating several directions

over the inside wing. However, at 1.5 turn and for a period of 11 frames the main direction of the flow can be described as reversed. From the point where spin recovery controls were set to just before recovery was complete (rotation ceased), the flow remained irregular (Figure 53). One frame before rotation stops, the flow over the entire inside wing was streamline. The transition from irregular to streamline commenced 6 frames before recovery, and developed from root to tip, indicating a gradual decrease in angle of attack towards the wing tip.

Figure 52. At the 2-turn point, spanwise outboard flow is clearly apparent on the outside wing. Only the outer row of tufts are streamline. Irregular flow can be seen on the inside wing.

Figure 53. The aeroplane just before completing one turn with recovery controls set (the third turn from spin entry, left hand spin). All of the outside wing tufts indicate streamline flow. Flow on inside wing is still irregular at this point.

The movement of the vortex on the outside wing (as described in this and the previous section), have been illustrated, related to the estimated α at the aeroplane CG and shown together with the Slingsby position in the spin. Estimated α_{CG} from the VBSE has been plotted and is shown in Figure 54. The corresponding slides are shown in Figure 55.

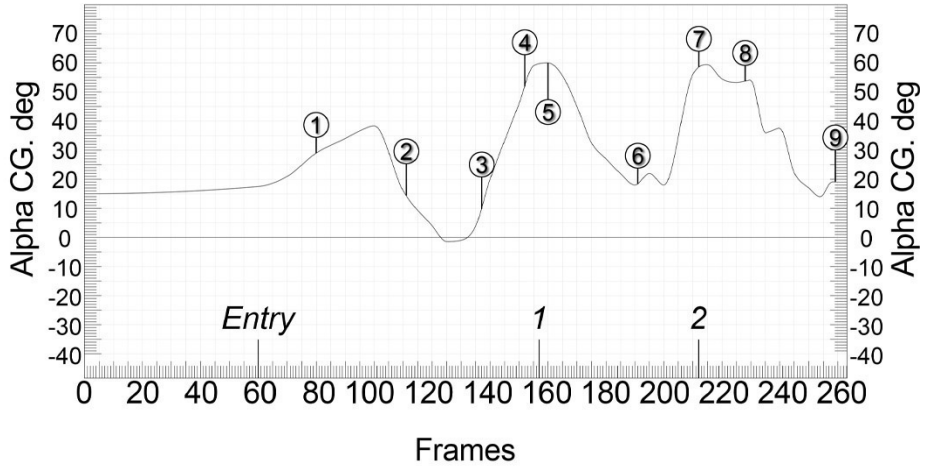

Figure 54. Estimated α at the aeroplane CG from the VBSE of a left 2-turn spin in the Firefly. The numbers marked on the alpha graph correspond to the slides in Figure 55.

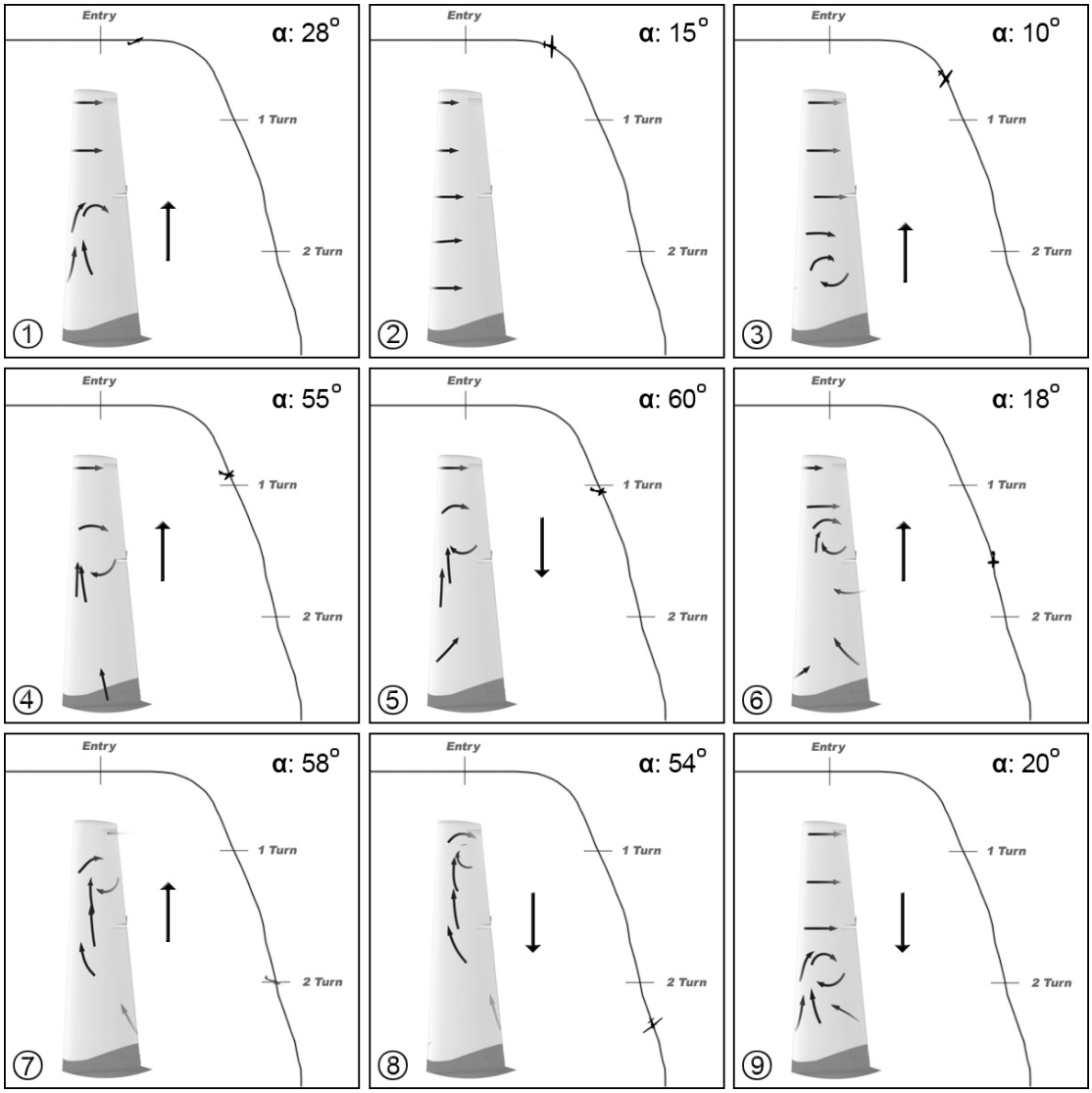

Figure 55. The vortex on the outside wing, shown together with the spin position and estimated α at the aeroplane CG. The arrows on the wing show the direction of airflow as indicated by the tufts. The large arrow behind the wing indicates the direction of vortex movement on the wing.

5.3 Flow across the vertical tail and aft fuselage

As the aeroplane was pitched up, but just before the controls were fully set for spin entry, the tufts at the inside fuselage indicated unsteady streamline flow. At entry, the flow on the inside vertical tail was unsteady streamline but deflected approx. 20 degrees upward above the horizontal tail and deflected downwards below. After 15 frames the flow became irregular at inside fuselage and vertical tail.

After an additional 7 frames, reversed flow was observed at the vertical tail, with the tufts pointing straight out from the leading edge of the vertical fin. This indicates the

presence of a vortex at the tail. When the aeroplane has rotated to a point where the wings are 90 degrees to the horizon, the flow at the tail is irregular, but direction is mainly in the streamline direction. Reverse flow, or rather highly irregular flow, was again apparent after the Slingsby had passed the ½ turn. This indicates that there might be a connection between the vortex forming on the outside wing and the irregular flow observed on the vertical tail.

The flow at the inside fuselage is irregular, however one flow direction seemed to be more dominant than the other, and that is 90 degrees to the fuselage streamline direction. This indicates a rotational flow around the fuselage with a right angle to the spin strake and horizontal tail. Just before the spin recovery is complete (8 frames before rotation ceased), the flow at both inside fuselage and vertical tail was again streamline.

Observing the tufts on the outside fuselage and vertical tail, the flow seemed to be similar to that described above for the inside. Again, the dominant flow direction at the fuselage was straight up. One exception is the flow under the horizontal tail, which appeared to be either unsteady streamline or deflected approx. 30 degrees downward. This difference in flow condition, from the inside to the outside, might correspond with the results from the wind tunnel investigation performed by Bowman, Hultberg and Martin [55] where they measured pressures on the tail and aft fuselage on a model spun in the wind tunnel. They found that the fuselage area on the outside under the horizontal tail contributes damping.

The tufts on top of the horizontal stabiliser indicate the presence of a leading edge vortex with rotation centre parallel to the leading edge. The second row (from the leading edge) of tufts on the inside stabilisator indicated reverse flow and on the outside stabilisator the flow was mainly spanwise outwards. This can be observed in Figure 52 and Figure 56. Again, it is interesting to compare this experimental observation with the pressure measurements from the wind tunnel [55]. In the wind tunnel, the negative pressures were larger on top of the outside stabilisator than the inside as shown in Figure 57. This might indicate that the vortex is generating a flow outwards, which result in more suction on the outside than the inside.

Figure 56. The tufts on top of the stabilisator indicate the presence of a leading edge vortex.

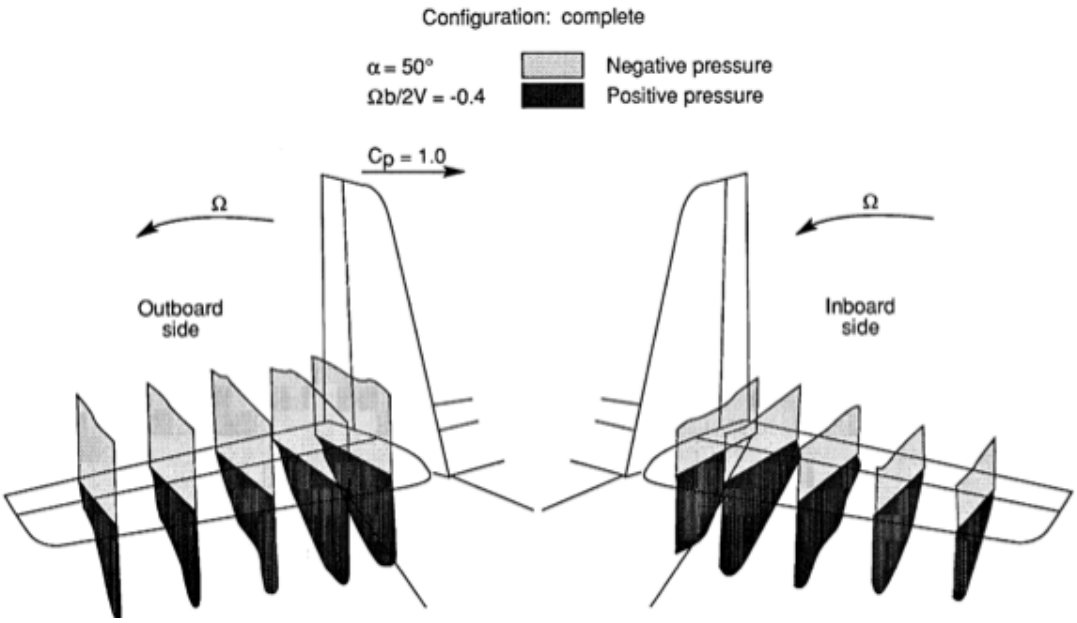

Figure 57. Measurement of pressures on horizontal tail surfaces from NASA wind tunnel spin research. Illustration is from NASA [55].

5.4 Upper Surface Vortex smoke visualization

Due to tuft observations on the vertical tail during the 2-turn Slingsby spin, it was hypothesized that the wake from the USV on the wing momentarily impinged the tail surfaces. To further investigate this possible turbulent wake generating effect and discover if it indeed impacted the tail, smoke was used to visualize the flow. It was also hoped that smoke would give a better 3D view of the turbulent upper wing boundary layer. The same methodology as described in section 3.4 (use of helicopter as chase aircraft) was used to capture video imagery of the spinning Firefly research aeroplane with the 'smoke boom' attached. However, the camera used in the helicopter was a newer model (Panasonic HPX3100), and the camera installed in the cockpit was the Casio Exilim F1 used in the 300 frames per second mode.

During the left spin entry, as the elevator was moved to the full up position, the wing on-surface vortex moves outwards and the smoke is pulled inwards and towards the fuselage. The angle of the smoke trail is initially towards the tail, but did not hit the tail itself (revealed by the tail-mounted camera). The smoke trail was clearly deflected upwards at the first peak in α, before it again followed the wing contour as the tufts indicated streamline flow over the whole wing.

From the ½-turn point, as soon as the vortex again formed on the outside wing, the smoke was pulled inwards toward the fuselage (Figure 58). From the ½-turn to 1-turn point, tail and aft fuselage was covered in smoke (Figure 59). From the 1-turn point, the smoke trail was aligned with (parallel to) the fuselage and did not interfere with the tail section of the aircraft. However, as the aircraft approached the 1½-turn point, smoke was visible towards the fuselage. The main smoke trail was going straight back from the wing, but a portion of the smoke was clearly deflected towards the fuselage.

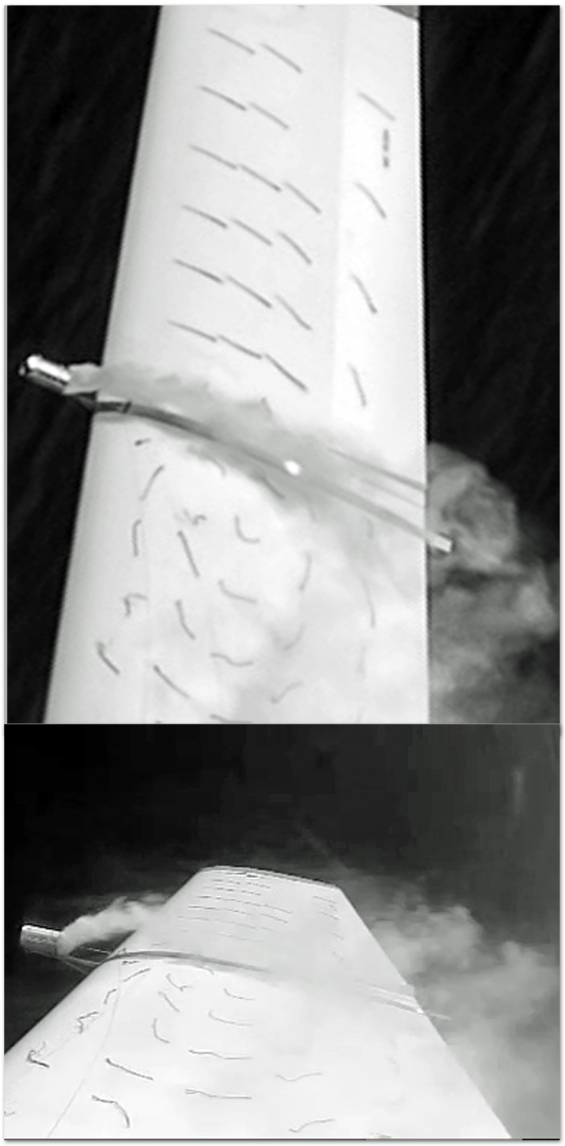

Figure 58. Smoke is pulled inwards by the USV as it moves towards the wing tip during the spin entry (from the ½-turn point). The top and bottom images, from the helicopter chase and the cockpit camera respectively, are synchronised.

Figure 59. Smoke visualization before the 1-turn point in the left spin.

From the 1½-turn point, smoke was clearly visible from the smoke source and over the entire wing towards the fuselage. Before the 2-turn point, smoke was also visible on the outer section of the wing towards the wing tip (Figure 60). This indicates that the observed on-surface vortex moving towards the wing tip sucks some smoke outwards. After the 2-turn point, and after recovery action commenced (with full right rudder), smoke was covering the whole length of the wing. As the elevator was moved forward for the recovery, the nose of the aircraft was pitching down and the smoke indicates transition to streamline flow. Figure 61 clearly shows the turbulent wake being left behind as the aircraft recovers and dives out of the spin.

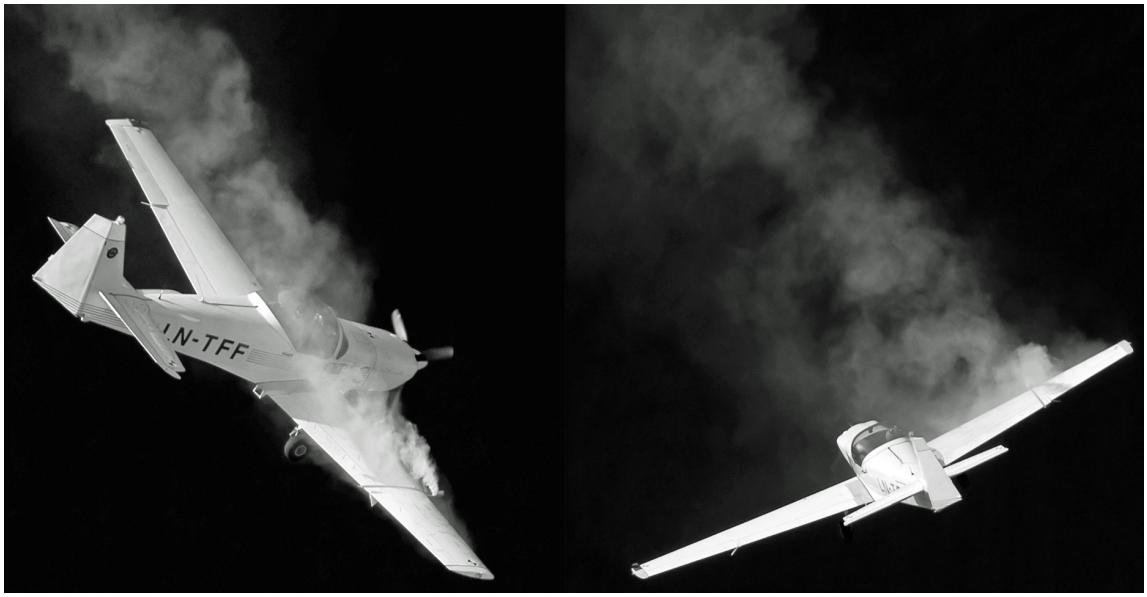

Figure 60. Before the 2-turn point (left image) in the spin, and after full right rudder was applied for the recovery at the 2-turn point (right image), smoke was visible towards the wing tip.

Figure 61. Aeroplane recovers from the spin.

5.5 Saab Safir: A special case of rudder control limiting

To check if the observed phenomenon, in particular the USV on wing and LEV on top of horizontal tail, was unique to the research aeroplane used, spin flights were also flown with the Saab Safir. The Safir has a special rudder design feature. The rudder is twisted so that it is more effective to the right than to the left. According to the Saab Safir Manual [69]:

"The rudder is slightly washed out to the right side to compensate torsion impulses from the propeller slip stream"

This rudder washout can be seen in Figure 62 below, and due to this design feature the Safir will only spin to the right (when using the standard spin entry technique). Spins to the right, using the same standard spin entry and recovery technique as used previously on the Firefly, were qualitatively similar to the Slingsby spin, with recovery normally after an additional ¾-turn for a 2-turn spin (after recovery controls were applied). For the 6-turn spins in the Safir, recovery was normally after additional 1¾ turn. As described earlier in Section 4.2.4, spin entries to the left resulted in a spiral mode. The difference in yaw rate values obtained from a total of six 2-turn spins (3 left and 3 right) can be seen in Figure 63. One left – right spin pair was flown with another Saab Safir. However, both Safir's have the same model designation as shown in Figure 11. The yaw rate in the spirals (2-turn left) was less than for the spins to the right. For example, after 2.2 seconds the left spins were in the range of 60 - 70 deg/sec and the right spins had 80 deg/sec. After 5.0 seconds the difference was 60 - 90 deg/sec for the left spins versus 110 – 120 deg/sec for right spins.

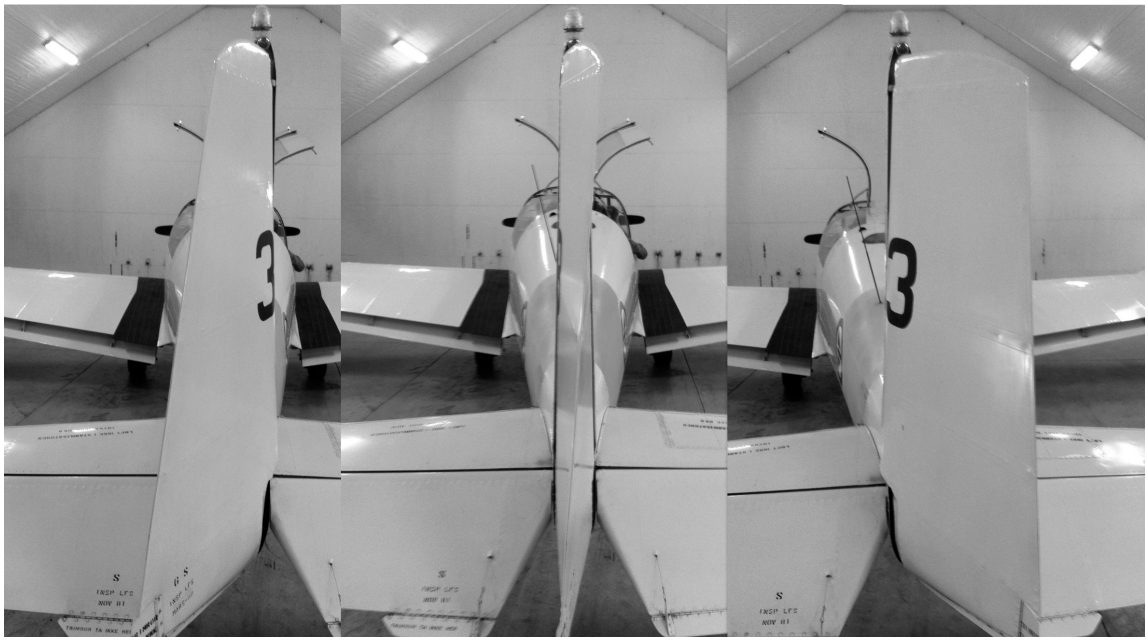

Figure 62. Pictures of the Safir rudder showing full left, neutral and full right positions. Note the twisted rudder and the difference in rudder angle when displaced full left and full right.

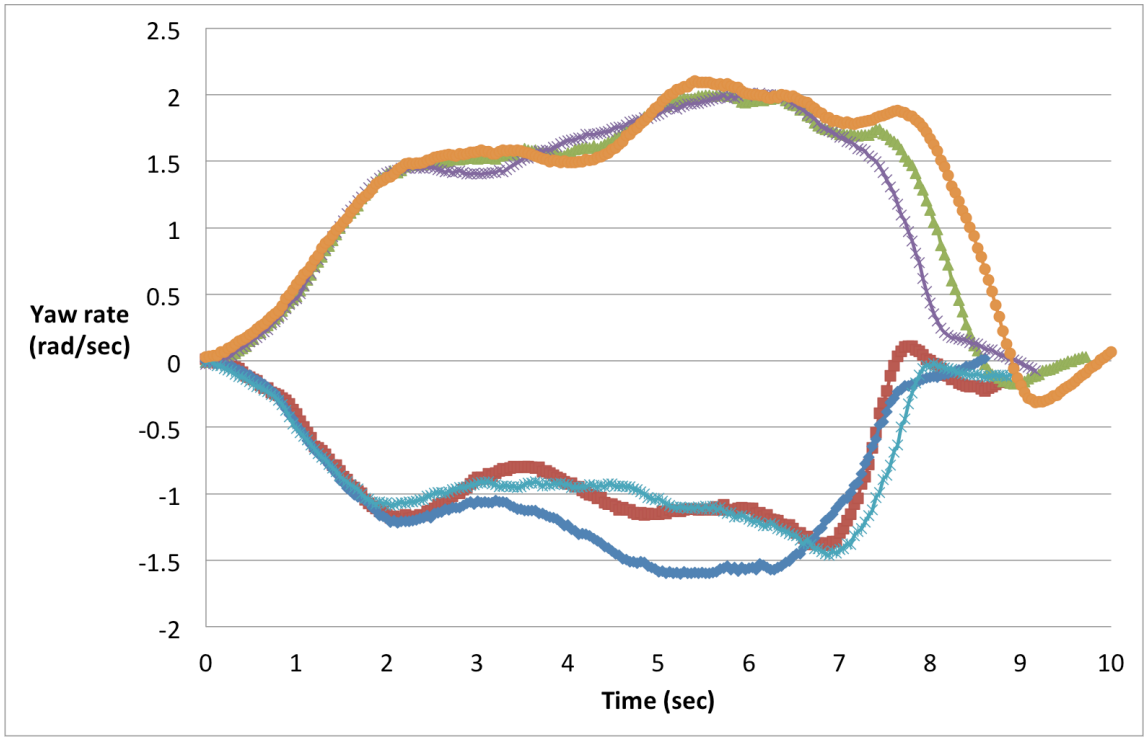

Figure 63. Measured yaw rates for three 2-turn left (spiral mode) and three 2-turn right spins in the Safir.

The recovery from the spiral mode was instant with no perceived back force on the stick (as compared to a right spin in the Safir where the stick must be pushed forward for recovery). Therefore, the Safir being rudder control limited to the left but not to the right

was believed to be an interesting case for studying the above mentioned flow conditions. The observed flow conditions, using tufts on the upper side of wing and horizontal tail, are described below.

5.5.1 Saab Safir: Outside wing in a right 2-turn spin

Before spin entry, airflow separation was evident from inboard trailing edge. Flow outboard of the landing light at approx. half semi-span was still streamline. At spin entry, tufts indicated unsteady flow but direction was predominantly spanwise (towards the wing tip). At ¼-turn point, a vortex centre was observed at mid-wing (just inboard of landing light position). In one of the video imagery sequences, rotational flow was clearly apparent with one tuft, second row inboard of landing light, rotating twice (720 degrees) about its centre anti-clockwise in 0.2 seconds (54 frames, 300 frames per second video imagery). In another video sequence, the same tuft was also observed to rotate, but only once (360 degrees) in 27 frames (0.1 sec), half the time of the previously mentioned double rotation. This tuft rotation rate is about 30 times the rotation rate of the aeroplane, which is at least an order of magnitude difference.

Towards the ½-turn point, the outer part of wing from 2 rows of tufts inboard of landing light were streamline. After the ½-turn point the vortex moved outwards again and at ¾-turn flow were streamline from 2 rows of tufts outboard of landing light, with the flow predominantly spanwise behind. Spanwise flow was still predominant at 1-turn point with tufts deflecting aft (streamline) at the wing-tip area. However, from the 1-turn point, a dipolar vortex structure was observed, with anti-clockwise rotational flow outboard of landing light and 3-4 rows of tufts inboard of landing light were indicating reverse flow. The tufts furthest inboard (nearest the fuselage) were temporarily deflected in the clockwise direction. An illustration of this flow structure can be seen in Figure 64. However, although this flow structure was observed in the video imagery over several frames (about 50 - 60 frames which is 0.16 – 0.2 seconds) the flow was very unsteady with every single tuft deflecting slightly from frame to frame, sometimes against the ‘perfect’ circular flow direction.

Figure 64. Illustration based on the flow direction indicated by tufts, showing the dipolar vortex structure temporarily observed on the outside wing of the spinning Safir after the 1-turn point in the right spin.

Vortex rolls back from 1¼ turns and the tufts outboard of landing light were streamline again. However, from 1½-turn point vortex rolls out again and the aforementioned dipolar structure are again evident at 2-turn point. Spin recovery actions were started from 2-turn, and the vortex started to move back from 2½-turn and recovery was complete at 2¾-turn where rotation ceased and flow became streamline over wing. A summary of observations as described in this section is shown in Table 11.

Time (sec)	Spin position	Tuft observations
0	0	Airflow separation from inboard trailing edge. Predominantly spanwise flow (outwards) from spin entry.
1	¼	Vortex centre at mid-wing (just outboard of landing light).
2	½	Outer part of wing had streamline flow.
3	¾	Vortex moved outwards, with flow predominantly spanwise behind. Outer part of wing was still streamline.
4	1	Spanwise flow predominant over wing, except the wing-tip area, which had streamline flow.
4+	1¼	Dipolar vortex structure, anti-clockwise rotational flow outboard, reverse flow in-between and clockwise rotational flow inboard.
5	1½	Outer part of wing had streamline flow again.
6	2	Dipolar vortex structure as described above was again evident.
7	2½	Vortex moved towards fuselage, flow over wing becoming streamline.
8	2¾	Spin recovery (rotation ceased) and flow streamline over full wing.

Table 11. Summary of tuft observations on outside wing from the Safir 2-turn right spin.

5.5.2 Saab Safir: Inside wing in a left 2-turn spin (spiral mode)

Spin entry to the left was initially similar to the right spin entry, with separation starting at inboard trailing edge and flow deflecting outboard as the stall progresses. However, with the relative back- and downward motion of the left wing in a left spin, the flow quickly separates on the whole wing surface. The flow was unsteady and irregular, with some of the tufts along the leading edge temporarily going straight up, normal to the wing surface. At ¼-turn the flow is still irregular, but reverse flow on most of the wing surface is predominant. Compared to the outside wing flow, the row of tufts on the wing tip on inside wing, was indicating either reverse or spanwise flow. Also, it was difficult to observe any clear pattern, e.g. with one tuft in streamline direction and the next in reverse direction (erratic motion). From ¼-turn, this flow condition continued until spin

recovery, but with some time frames where reverse flow was more apparent. At recovery, flow reattachment started from the wing tip and after 48 frames ($^1/_6$ sec) the whole wing was streamline again.

5.5.3 Saab Safir: Outside wing in a left 2-turn spin (spiral mode)

At entry flow separated from inboard trailing edge and flow was deflected outboard, indicating spanwise flow. However, flow outboard of landing light remained streamline, and after ¼-turn towards the ½-turn point, more flow became streamline and only an area inboard towards the trailing edge was separated. After ½-turn point the tufts again indicated spanwise (outward) flow, but flow outboard of landing light was still streamlined and remained so for the rest of the spin. From the 1-turn point, again only an area inboard, aft at the trailing edge was separated and the row of tufts along the leading edge was all streamline. All the tufts indicated streamline flow from the 1½-turn point to the (instant) recovery at 2-turns.

5.5.3 Saab Safir: Description of observed flow on the horizontal tail surfaces

Due to limitations on the small tail camera used (only 20 frames per second), it was not possible to study the flow in the same fidelity as on the wing where a camera capable of 300 frames per second was used. However, it was still possible to see some notable differences, depending on spin direction, in flow conditions on the horizontal tail.

- **Left 2 turn spin (spiral mode)**

  Right horizontal tail: As the elevator was moved to the full up position (stick full back position) and the aeroplane started to rotate left, the tufts on top of the horizontal tail surface indicated flow separation (erratic motion). At the ¼-turn point, the tufts indicated unsteady, but streamline flow. Temporarily, the tufts indicate unsteady flow, but clearly the flow was predominantly in the streamline direction during the rest of the spin.

  Left horizontal tail: At spin entry flow separated, tufts indicated mostly erratic flow, however some frames showed spanwise (outwards) and some frames indicated unsteady streamline flow. Two frames before elevator moved down, the

tufts indicated unsteady streamline flow. As the elevator reached the neutral position, the tufts indicated streamline flow (Figure 65).

- **Right 2-turn spin**

Right horizontal tail: Flow separated at entry, indicating erratic flow motion. However, from just before 1-turn point, the tufts on the leading edge indicated spanwise flow (toward the fuselage). This continued for another 9 frames (20 frames per second). The flow was clearly unsteady, but a predominant direction was towards the fuselage. At 2-turn point the tufts indicate erratic flow. As the elevator started moving down (for the spin recovery), separated flow was still indicated for the next 6 frames, before it became streamline.

Left horizontal tail: Flow separated at entry and was erratic up to the ¾-turn point, where tufts indicated flow in a predominantly spanwise outward direction (Figure 66). Like for the inside tail surface in a 2-turn right spin, the tufts indicated flow mostly in the spanwise direction, although some frames showed erratic flow motion. Again, as the elevator started to move down for the spin recovery, the flow remained separated for 6 more frames. The elevator had moved to its neutral position after 4 frames.

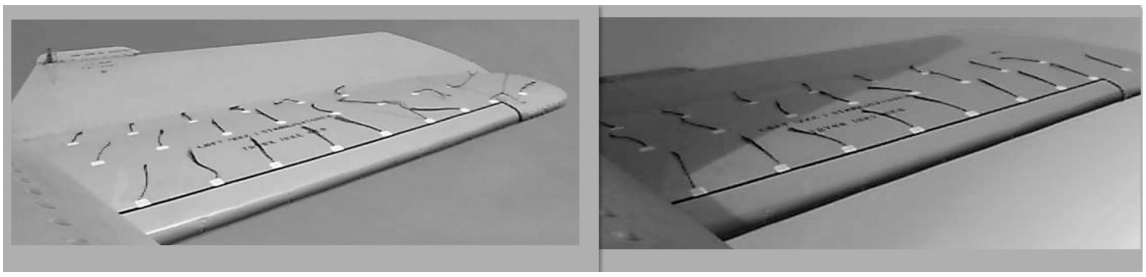

Figure 65. Tufts indicating unsteady streamline flow on left horizontal tail surface in a left, 2-turn spin, just before the elevator moves down for the recovery to the left, and elevator in neutral position on the right.

Figure 66. Tufts indicating spanwise flow on the left horizontal tail surface in a right hand 2-turn spin (at approx. the ¾-turn position in the spin).

6 Point measurements of differential pressure between upper and lower horizontal tail and wing surfaces

6.1 Introduction

For the horizontal tail and wing point differential pressure (dP) measurements, data has not been found in literature that would enable a comparison of the results. Before the Safir horizontal tail dP measurements, data was obtained for the pre-stall regime to check if dP varied with airspeed. For the Firefly wing point dP measurements, a gradual build-up approach was used starting with two stalls, then a post-stall Large Amplitude Wing Rock (LAWR) mode and then finally the spins. At each step, the differential pressure measurements were compared with the corresponding video imagery of the tufts positioned near and around the static sink ports on the wing. When possible, data from other sources was used to gain further insight, e.g. for the stalls AoA time history from the ADP was used.

The reason for these point measurements of differential pressure was not to map the complete wing pressure field, or quantitatively establish the total lift distribution over the wing. With only two pressure sensors available, such a goal would be inappropriate. The aim was merely to obtain measurements to supplement the analysing of the observed flow as indicated by the tufts. For example, the observation of the peculiar USV on the wing (e.g. as shown in Figure 51), with its perfect circular shape, conjectures a change in pressure. Therefore, a point measurement of differential pressure where one port is placed on top of the wing surface where the USV transits could possibly indicate if there was a change in pressure compared to flow conditions where the USV was not observed. Therefore, it also follows that the exact value of the dP measurement was not important, but rather the relative values of the different measurements were important to consider.

There was a time period in the research program where the Slingsby research aeroplane was not available due to operational reasons. Therefore, when the PSS-8 pressure sensor system became available it was first used on the Saab Safir to measure the difference in pressure between the upper and lower horizontal tail surface during spins. These results will be discussed first.

6.2 Differential pressure between upper and lower horizontal tail surfaces during spins in the Safir

The difference in pressure was measured at two points on the horizontal tail surface of the Safir as shown in Figure 27. In pre-stall flight, the horizontal tail surface exerts a down force. This was confirmed in the measurements, as the pressure was relatively lower on underside, which means relatively higher pressure on the upper surface. The speed was varied during two cycles of forward and aft stick (elevator moved forward then down) and the pressure difference changed with varying speed. Then the speed was decayed towards stall, and the pressure difference went correspondingly towards zero. Thereafter, a series of spins were flown and the pressure difference measured. Below in Figure 67 and Figure 68 are the results from a 6-turn right spin. The points are designated dP1 and dP2, where dP2 is the point nearest the aft fuselage and dP1 is the point furthest out on the horizontal stabiliser (see Figure 27). The '-' port of the differential pressure sensor was placed at the upper surface.

The results shown in Figure 67 and Figure 68 below show a positive pressure delta, which means a relatively higher pressure on the lower side of the horizontal stabiliser. Therefore the relatively lower pressure on the upper side exerts an up force at the tail. Note the increase in pressure difference at the ¾-turn point in the spin and a further increase at the 1½-turn point in the spin. Thereafter, the pressure delta stabilises at approximately the 8 hPa level from the 2-turn point. At recovery, the pressure difference changes sign back to negative as it was for the pre-stall flight regime which was lower pressure on the underside, exerting a down force at the tail.

It is interesting to note the fluctuations in dP values that can be observed in Figure 67 and Figure 68. It is possible that these fluctuations are due to the presence of the observed vortices (see section 5.3). A spectrum analysis of the dP time histories has not been conducted, but this could be an interesting topic for future research.

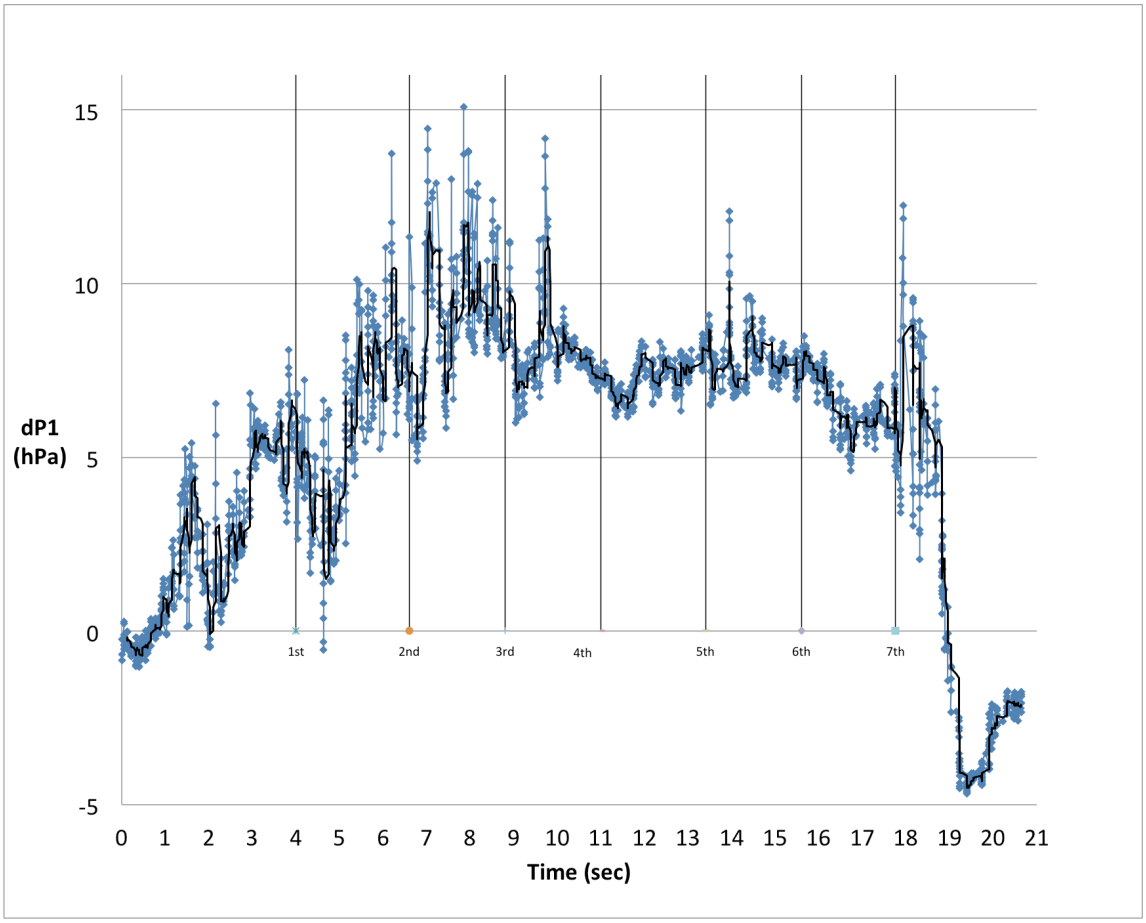

Figure 67. Difference in pressure measured at point dP1 during a 6-turn right spin in the Safir (CG at 11% MAC, weight was 980 kg and spin entry was at approx. 4800 feet density altitude). A 10-point moving average trend is shown as a black solid line.

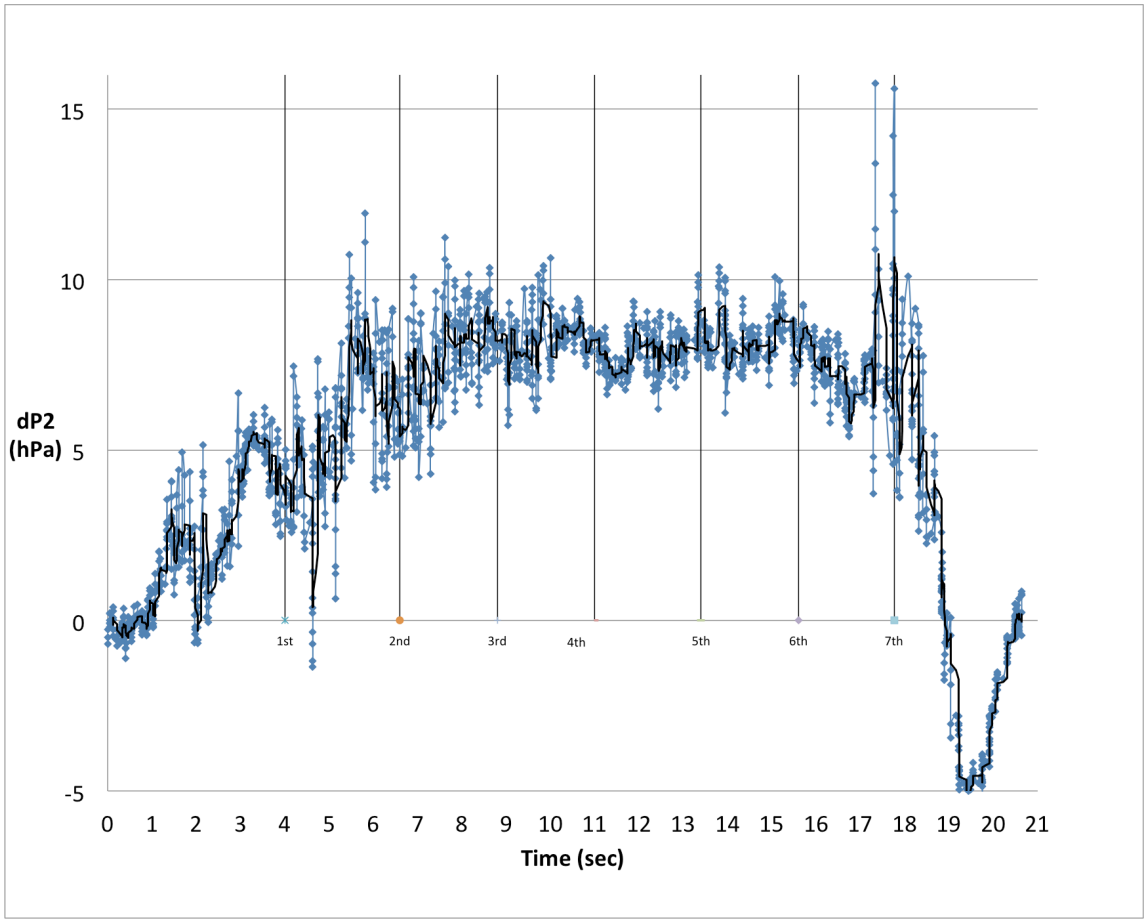

Figure 68. Difference in pressure measured at point dP2 during a 6-turn right spin in the Safir (exactly same spin as above for the dP1 measurement). A 10-point moving average trend is shown as a black solid line.

6.3 Slingsby Firefly stalls

As a preparation for the spinning point differential pressure measurement on the wing, and to compare pressure measurements with observations of tufts on the wing, stalls were flown in the Firefly research aeroplane.

First a 1 kn/sec deceleration rate was used for the stall entry (with idle power) and the stall recovery actions were applied at the first indication of stall as perceived in the cockpit. For the Firefly T67MX, a slight nose drop marked the stall before the stick reached the backstop. At the indication of stall, the stick was moved forward before power was increased (FAA stall recovery method [97]). Figure 69 shows the increasing α (AoA) as the stick is moved backwards to decelerate the aeroplane towards stall. The differential pressure at point dP2 (see Figure 10 for the position of point dP2 on the right

T67MX wing) was gradually decreasing as α reached its maximum value and then there was a dip in differential pressure as the wing was unloaded in the stall recovery (stick moved forward to decrease α). The video imagery of the tufts shows that the single tuft just before and the tuft aft of the dP2 point remain in the streamline direction. However, the tufts from the approx. mid-chord position towards the trailing edge of the wing indicate separated flow at the stall.

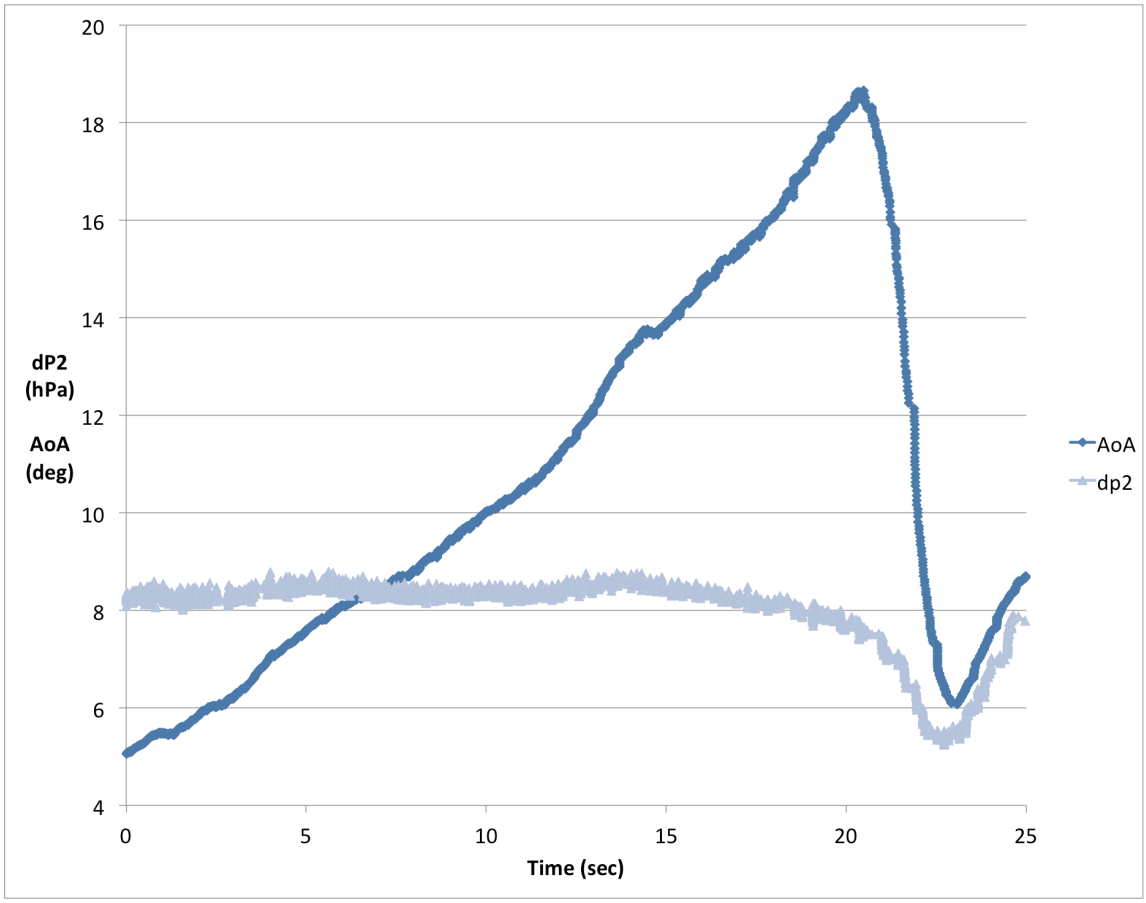

Figure 69. Stall flown in the Firefly T67MX with the FAA method used for stall recovery.

Thereafter, another stall was flown using the same entry technique described above. However, this time a pitch delayed stall recovery method was used. At the indication of stall, full power was applied but the stick was held in position for about 2 seconds before the stick was moved forward to affect the recovery (i.e. pitch delayed [97]). The first peak in α in Figure 70 was at the approximate same value as in Figure 69 (both were in the range of 18-19 degrees). Thereafter, there was a drop in α indicating a slight pitch-down at the stall. When engine power was increased from idle to full power, there was a sharp increase in α (last value recorded before α went outside the measureable ADP

range was 22.7 degrees). This indicates that an even higher α, past the stall α using idle power, was reached when power was increased from idle to full while the stick was held in the same position.

Finally, when the stick was moved forward to affect recovery from the stall, α decreased rapidly. The differential pressure time history followed the same development as the previous stall up to the time where the first peak in α was observed. Thereafter, as α remained high, unsteadiness in the differential pressure reading was observed. During the recovery with α reducing, the same drop in differential pressure value was observed when the wing was unloaded. Observations from the video imagery correlate well with the data presented in Figure 70. All the tufts near the dP2 point indicated temporary flow separation as α increased after the first peak in α. There was also a slight right wing drop before α was reduced during the recovery after which all the tufts indicated streamline flow again.

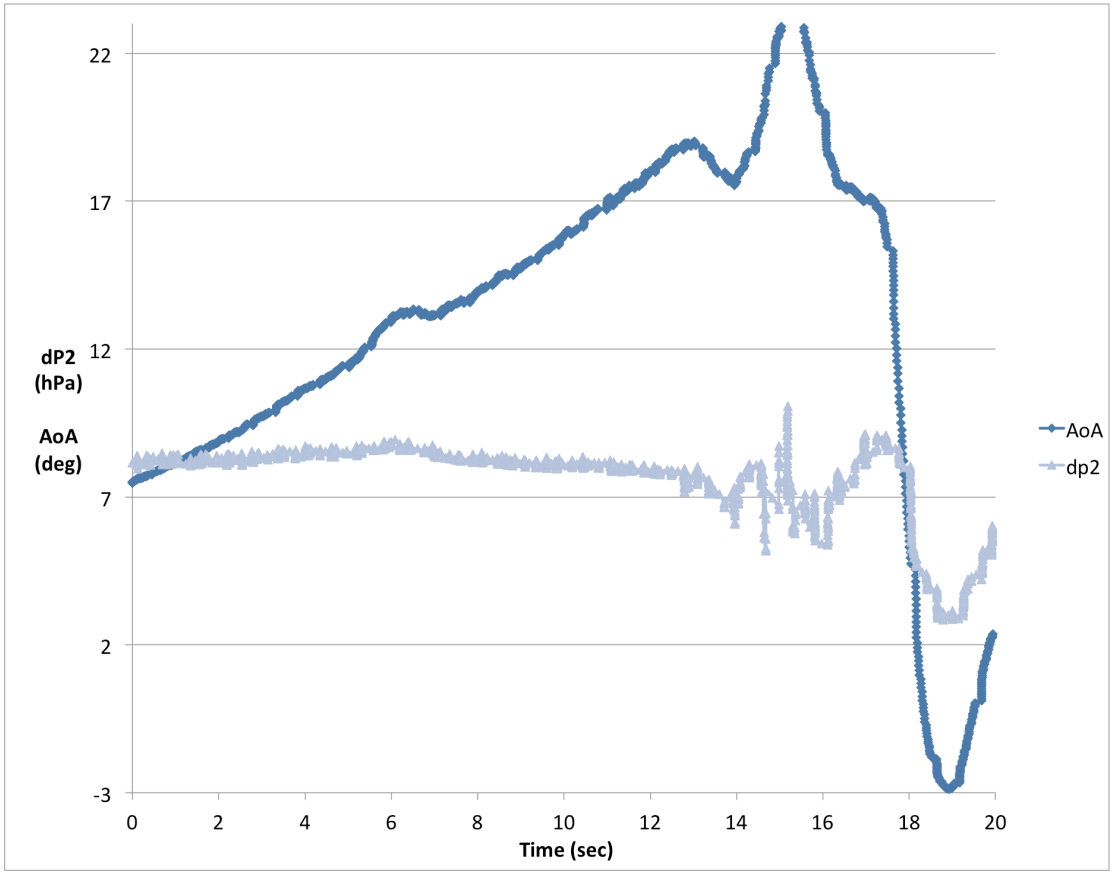

Figure 70. Time history for a pitch delayed stall recovery, which resulted in an even higher α (AoA).

6.4 Post-stall Large Amplitude Wing Rock (LAWR) mode

The post-stall flight regime was further explored by entering a LAWR mode. This post-stall manoeuvre is particularly interesting to study, since the aeroplane state is crossing in and out of the stability boundary, between the stable pre-stall and unstable post-stall regime.

In the Firefly research aeroplane (T67MX), the LAWR mode was deliberately entered from the stall with the power at idle. At the stall point, the stick was brought back to the stop (elevator at full up position). At the first wing drop to the right hand side, opposite rudder was temporarily used to raise the falling wing towards a wings level attitude. This use of the rudder to raise the falling wing was continued for a few cycles before the rudders were kept centred. With stick full back and centred, and the rudders also at centre position, the aeroplane continued with periodic LAWR cycles until recovery from this post-stall mode was affected by pushing the stick forward. As with the spins, the recovery to normal flight was affected by entering a dive with subsequent increased airspeed and substantial height loss.

After the initial stall and wing drop, the following cycles can be described as follows: Starting with the right hand side, high-wing position, there was rotation about the Z-axis (left yaw) and rotation about the Y-axis (pitch-up). The wing plunged as the flow separated on the wing surface. At the low-wing position there was flow re-attachment, right yaw and pitch-up. Thereafter, the wing rises and flow separates again, however the tufts indicated less flow separation (first row of tufts closest to the leading edge streamline and the rest unsteady streamline and slightly deflected) for the up-going wing as compared to the plunging wing (reverse and very unsteady flow over the full wing surface). At the high-wing position, there was flow re-attachment before the cycle started again. The high-wing position, with flow separated and just before the wing plunges, is shown in Figure 71 below. The subsequent wing-low position, where the flow has reattached, is also shown in the same figure. Note the large amplitude of the wing rock. At the high-wing position the horizon is barely visible in the lower left corner, and in the low-wing position the ‘blue sky’ is replaced by a view of the ground landscape.

Figure 71. The high- and low-wing positions during the post-stall LAWR motion.

In the previous paragraph the aeroplane position was described together with the tuft observations from the video imagery. It is interesting to study the aeroplane stability characteristics and how they keep changing from stable to un-stable during this manoeuvre. Apparently, the rolling motion reduces α and roll damping engages with flow re-attachment and thereby stops the rolling motion. Also, with the reduction in α and the accompanying re-attachment of flow, it is possible that directional stability engages which would result in a rotation about the Z-axis (yaw). However, with the continuation of full back stick, the elevator commands an increased α and subsequent flow separation at the critical α. With flow separation and loss of stability the roll damping becomes negative and the wing plunges starting the cycle again. A more detailed investigation into the stability characteristics of the aeroplane during this post-stall mode could be an interesting topic for future research.

The above description of the LAWR motion of the Slingsby can be viewed as a limit cycle due to the apparent self-sustained periodic motion as the aileron and rudders were kept neutral. After reviewing the point measurements of differential pressure, it was found that there was a repeatable structure in the measurements. Apparently, the differential pressure drop at flow separation as the wing plunges was to a lower level than the corresponding pressure drop at flow separation as the wing was rising. This is shown in Figure 72 below, where the different levels in differential pressure drop as the flow separates are shown as two black horizontal lines. One of the black lines is for the plunging wing minimum values (approx. 2.5 hPa) and the other for the rising wing values (approx. 6.5 hPa). A total of 7 cycles was completed before recovery was affected by using forward stick. The flow separated twice every cycle, both during the plunging motion and when the wing was rising, resulting in a total of 14 minimum differential pressure values.

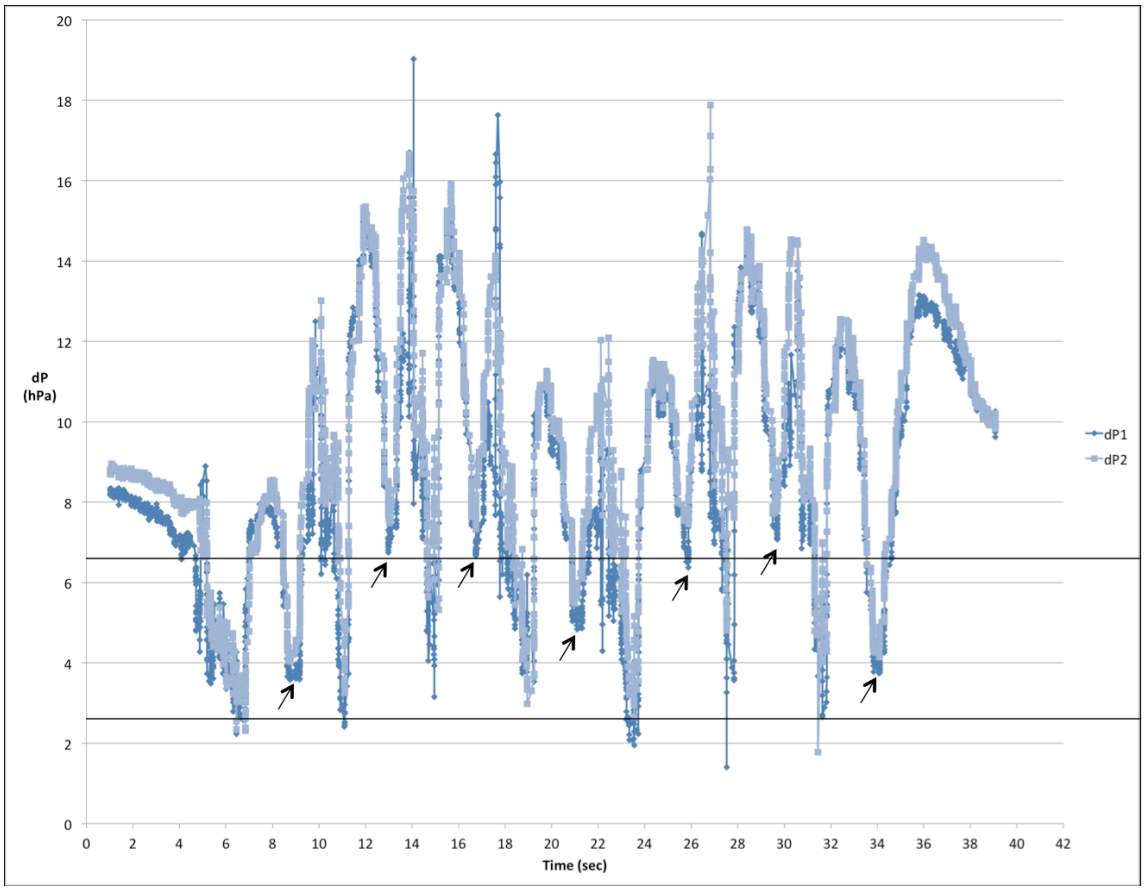

Figure 72. Point differential pressure measurements for the LAWR mode in the Firefly research aeroplane. The dP1 and dP2 points where placed on the right hand side wing as shown in Figure 29. The small arrows point to the minimum dP values as the flow separates on the up-going wing.

These different levels in minimum dP values indicate that the rising wing had a higher lift component than the plunging wing, and thus there was an unbalanced moment sustaining the wing rock motion. Apparently, the plunging wing 'stalls deeper' than the rising wing, and this was confirmed by the tuft observations as described above. As we have seen in Figure 72, the enhanced and dramatic flow separation of the plunging wing resulted in a differential pressure drop to a lower level, below the lowest level shown in Figure 70 for a pressure drop due to a prolonged stall caused by a mishandled stall recovery.

6.5 Differential pressure measurements between upper and lower wing surfaces during spins in the Firefly

Having established a correlation between the tuft observations and the point differential pressure measurements during stalls and LAWR motion described in the section above, dP measurements were then conducted during spins in the Firefly research aeroplane (T67MX).

Figure 73 below shows the dP time histories for a 6-turn left spin and for comparison the same measurements for a 6-turn right spin are shown in Figure 74. It was desirable to have dP measurements for both the inside and outside wing in the spin. However, it was only possible to mount the PSS-8 system on one side. Therefore, a left spin was flown to obtain measurements for the outside wing and correspondingly a right spin flown to obtain inside wing measurements. The positions of the static ports are shown in Figure 10.

The dP plots for the initial stall and flow separation (before 1 second) are both similar in shape and values. However, in the period from 2 to 5 seconds there was a distinct difference in dP values. For the right spin (inside wing), there was a drop in dP level down to about 4 hPa at the 1-turn point in the spin (just before 4 seconds). For the left spin (outside wing), the dP level increased from 2 seconds and dP1 was at 8 hPa just before, and dP2 was at the 8 hPa level just after the 1-turn point in the spin. Interestingly, the increase in dP values for the outside wing corresponds with the time (from 3 seconds or ¾-turn point in the spin) when the USV was moving spanwise towards the wing-tip.

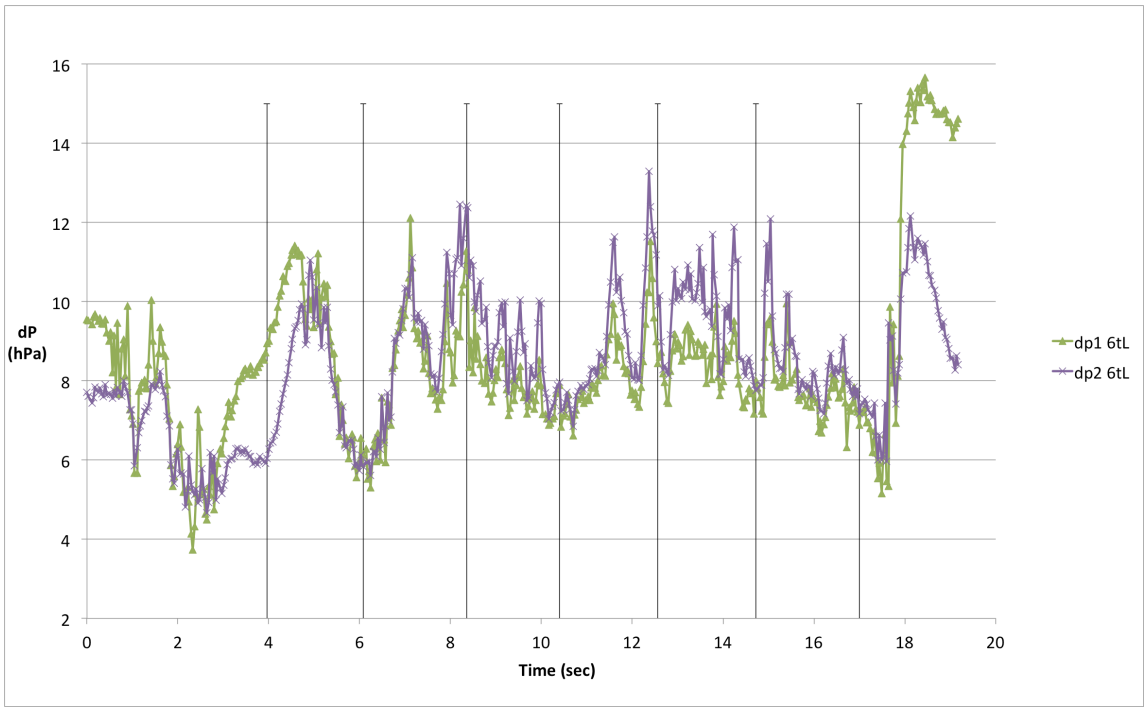

Figure 73. Point differential pressure measurements for the 6-turn left spin in the Firefly research aeroplane. The vertical lines represent the turn completions in the spin.

After 5 seconds, the dP values for the inside wing is first oscillating between the 6 and 10 hPa levels and mainly between 8 and 10 hPa levels after the 3-turn point in the spin (Figure 74). The dP measurements for the outside wing were considerable more unsteady with fluctuations in dP values. This was particularly apparent after the 3-turn point in the spin. There was also some difference between the dP1 and dP2 values, e.g. dP2 having a higher average value from the 5-turn to the 6-turn point in the spin than dP1 (Figure 73).

At the spin recovery there was an increase in dP value for both cases as the flow re-attached. The following decrease in dP value at the very end of the plots was due to the unloading of the wing (depending on the elevator position at flow re-attachment) as the aeroplane dives to regain airspeed before the pull-out from the ensuing dive.

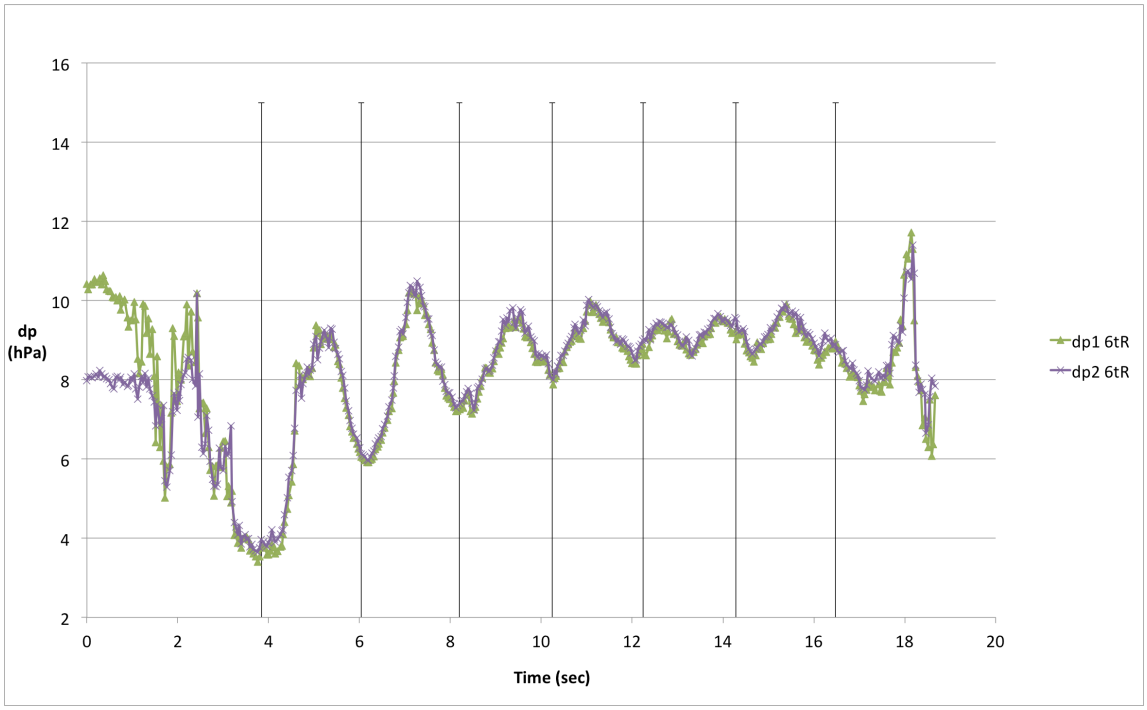

Figure 74. Point differential pressure measurements for the 6-turn right spin in the Firefly research aeroplane.

7 Discussions and Conclusions

7.1 Vision Based State Estimation (VBSE)

Challenges were encountered during state estimation of the spinning aeroplane in 3D using a vision based approach. It was a challenge to track both the aeroplane and camera simultaneously and post-flight corrections had to be applied. The background points used for tracking the camera motion were required for estimating the translational motion of the aeroplane. Furthermore, the flight path of the helicopter camera platform had to be estimated in the visual 3D studio. Motion data from a FDR in the helicopter would have been very helpful for post-flight processing of data, but unfortunately no such data was available. However, both qualitative (video imagery of the spinning Firefly with a smoke source) and quantitative (angular velocity and GPS altitude data from the FDR) comparisons of data indicated reasonable accuracy.

7.2 Qualitative assessment of the aerodynamic flow

The qualitative assessment of the airflow on the spinning Firefly indicated that a vortex forms on the outside wing. This USV, how it forms its movement on the wing, has been related to the spin motion and data from the VBSE. Furthermore, it is likely that the turbulence observed on the empennage is partly from the vortex formed on the wing. It was therefore hypothesised that the USV was partly the source of turbulent flow over the empennage. Smoke, used for flow visualization, revealed wing flow interference over the empennage during the spin entry. Apparently, even at high alpha, the smoke was pulled inwards on the wing and over the empennage before the 1-turn point. From the single smoke source, smoke was distributed over the whole wing surface, reinforcing the results from tuft observations, e.g. the existence of USV and spanwise flow.

Qualitative assessment of the flow across the tail and aft fuselage has shown 3 dimensional effects and vorticity, including indications of a leading edge vortex on top of the horizontal stabiliser. This is not in agreement with spin theories of the past, where the horizontal tail was believed to be the cause for the ‘blanking’ of the vertical tail. Furthermore, using a 2 dimensional view, the assumed effect of the vertical tail in the spin were believed to be dependent on its geometry alone without considering other effects from the complete aeroplane configuration.

It has been said earlier that to be able to understand aerodynamics one must try to 'see' the airflow. An extension is that to understand high-angle of attack flight one must try to see the vortices. Based on the results so far, it is likely that any spin prediction criteria based on simplistic 2 dimensional effects and localised flow phenomena will continue to fail.

7.3 Initialisation of the Upper Surface Vortex (USV)

A closer look at the initialisation of the USV is of interest. Vortical flow was first observed as the aeroplane started the spin entry (see for example slide no. 1 in Figure 55) and then in the period from the ½-turn to the 1-turn point in the spin (Figure 58). A common condition for both these cases was a positive ß value (Figure 44). The gradual development of the USV is shown below in Figure 75. In particular for the first slides numbered 1-3, the deflection of the streamlines due to positive ß is apparent. From slide no. 1 the tufts indicate separation of the flow starting inboard and progressing spanwise outwards. Assuming now that the separation starting from the wing root result in a spanwise pressure gradient, which in-turn result in a pressure-driven flow velocity parallel to the leading edge. It is suggested that these two components, the deflection of the streamlines due to positive ß combined with a spanwise pressure gradient, initialise the USV.

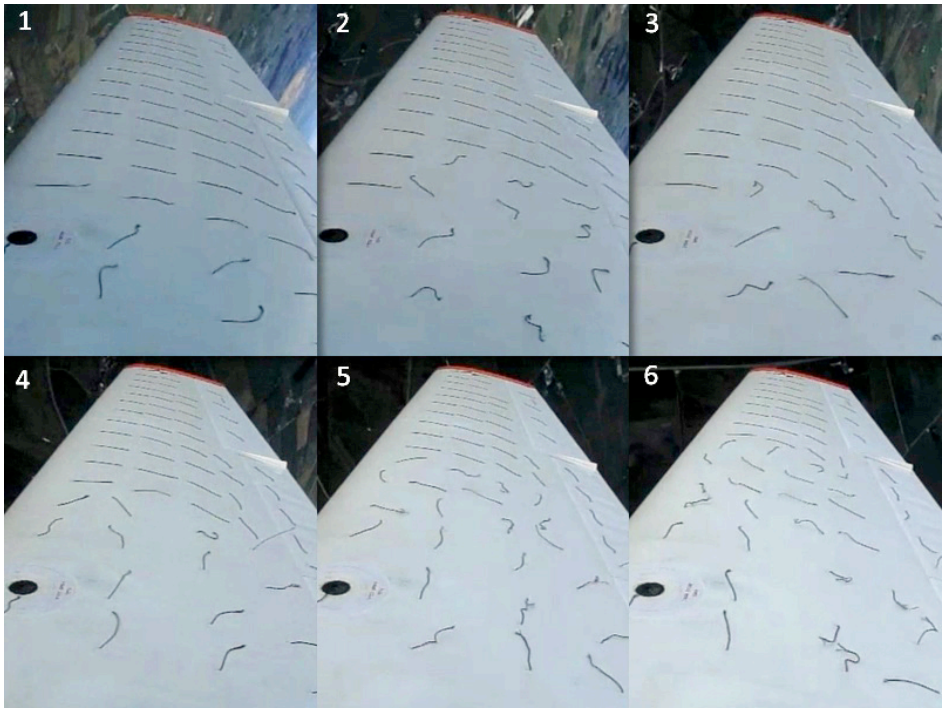

Figure 75. Slides showing the initialisation of the USV. Time in-between the slides was 20/300 seconds (frame rate was 300 Hz).

7.4 Rotational aerodynamic flow effects

Whilst studying the flow structure on the Safir, it was found that the flow structure on the outside wing was periodic as opposed to irregular and random vortices. Although the flow in the turbulent boundary layer was very unsteady, a repeatable structure was found when examining several spins. Although the USV observed on the Safir outside wing did not have the same perfect circular shape as seen on the Firefly (e.g. the vortex visualized by smoke and tufts in Figure 58), and although the flow condition was very unsteady, vortical flow was observed. Furthermore, the same anti-clockwise rotation of a single tuft was observed in three different video sequences of the same type of spin (2-turn right), at the same position in the spin. This indicates periodic and structured flow motion as opposed to random flow circulation. In addition, vortical flow was also observed on the upper surface of the Firefly wing after the 1-turn point (see Figure 55) where ß changes from positive to negative, indicating ß sign independency after the USV has been initialised as described in section 7.3 above.

The fact that the rotation was against the spin direction, and given that the shape shown in Figure 64, resembles a source – sink pair with a saddle point in-between, lead to the

suggestion that the turbulent layer flow structure was due to the rotation of the aeroplane. This structure is similar to what can be observed in the earth atmosphere, in the form of a high-pressure, low-pressure system pair (or anticyclone – cyclone pair called a Rex block in meteorology [98]) having its characteristic shape due to the rotation of the earth.

The aeroplane in a spin must be considered as a rotating frame of reference. A fluid in motion in this frame of reference (e.g. moving on top of the outside wing) will have additional accelerations due to the aeroplane rotation. These additional acceleration terms are the centrifugal, Coriolis and Euler accelerations.

Initially, at spin entry as the flow starts to separate from the inboard trailing edge and flow outboard was still streamline, the pressure is lower on the outside part of the wing than the inside. Therefore, the tufts indicate spanwise outward flow as the air particles moves from relatively higher pressure to lower pressure at the outer section (towards the wing tip). As the aeroplane starts to rotate in the spin, this layer of separated flow close to the wing surface is then subject to additional acceleration terms. The total flow acceleration vector is given by (e.g. see discussion on motion relative to rotating axes in Ref. [99], or alternatively the research on the flight of the fly by Lentink and Dickinson [100]):

$$a = a_u - 2\Omega \times v - \Omega \times (\Omega \times R) - \frac{d\Omega}{dt} \times R \qquad (7\text{-}1)$$

where $\boldsymbol{a_u}$ is the local flow acceleration vector (e.g. due to difference in pressure on the wing upper surface), Ω is the angular velocity vector, $\boldsymbol{v}$ is flow velocity vector and $\boldsymbol{R}$ the radius vector. The minus sign in front of these vector cross products are due to the direction definition in the coordinate system. Coriolis acceleration varies with rotation rate and flow velocity, centrifugal acceleration varies with rotation rate squared and radius and Euler acceleration varies with the time derivative of rotation rate and radius. As earlier described, this flow structure was observed on the outside wing. The inside wing has different initial conditions during spin entry. As the inside wing rotates aft and downwards, the flow on the whole wing separates at the same time, and this difference in pressure due to streamline flow on the outer part of the outside wing might not exist on the inside wing.

Applying the right-hand rule, and using equation (7-1), the Coriolis force is deflecting flow against the spin direction, the centrifugal force has direction spanwise outboard and Euler force is deflecting flow in either the streamline or reverse direction, depending on the angular acceleration vector direction. Therefore, there is correlation between the theoretical flow influences due to equation (7-1) and the observations, and the following hypothesis is put forward: The turbulent layer on the upper surface, on the wing of a spinning aeroplane, is accelerated due to additional, spin induced accelerations.

To further investigate the likelihood of the Coriolis force deflecting the flow field on the upper wing surface, the Rossby number [101] was considered. The Rossby number, which is the ratio of inertial to Coriolis force, signifies a system affected by Coriolis acceleration if this number is small (e.g. a value of 1 or less signifies a system where Coriolis force should be considered):

$$Ro = \frac{U}{fl} \tag{7-2}$$

where U is flow velocity, l the length scale, and f the Coriolis parameter:

$$f = 2\Omega\cos\varphi \tag{7-3}$$

where Ω is the rotation rate and φ the roll angle. Coriolis acceleration affects fluid motion perpendicular to the spin axis and vanishes for motion parallel to the axis. It is the spanwise flow on the upper surface of the wing that is of interest, so for example at the 1-turn point in the spin where the wings are approximately level and φ close to 0, the Coriolis acceleration will be at maximum. Furthermore, Coriolis acceleration will be reduced at roll angles when the accelerated flow is constrained by the surface of the wing when angle of attack is high (i.e. wing chord not parallel to the spin axis). Using the 1-turn point in a left Firefly spin as an example, flow velocity U was estimated to 5 m/s by observing the movement of the USV spanwise over a measured distance, Ω = 2.9 rad/sec (from Figure 42), applying the Firefly MAC (1.2 m) as length scale and finally assuming φ close to 0 we get:

$$Ro = 0.7 \tag{7-4}$$

which signifies a system affected by the Coriolis acceleration. However, with higher flow velocities the Rossby number will increase and the system will be less affected by Coriolis acceleration.

7.5 The change in flow condition over the horizontal tail

A sudden change in flow condition over the horizontal tail surfaces on both the Firefly and the Safir was observed at the ¾-turn. The flow was mainly in the spanwise direction over the outside horizontal tail, as shown in Figure 66 for the Safir and similarly as observed on the Firefly in Figure 56. It has been suggested that this might be a leading edge vortex, similar to what have been found on delta wings. However, not having been able to use smoke to visualize the flow structure over the tail, the exact structure of this flow is unknown.

It is interesting to note a change in the spin motion of the aeroplane, which might be related to this sudden change in flow condition over the horizontal tail. On both the Firefly and the Safir, it has been observed that the aeroplane has its flattest attitude at the 1-turn point. After 1-turn, the nose pitched down and the aeroplanes spun at a steeper nose down attitude and the rotation rate increased. At this stage in the spin entry, rolling, yawing and pitching rotary moments are in effect (see Figure 38). So, a pitch down rate (q) imposed on the yawing momentum precesses and result in an increased roll rate (p), which again result in an increased yaw rate (r).

The data from the measurement of pressure difference between the lower and upper surface of the horizontal tail (Figure 67 and Figure 68) indicates a reversal of horizontal stabiliser effect in the spin. The relative negative pressure measured on the upper surface is a reversal of horizontal stabiliser effect during the spin, from exerting a net nose up (down-force at the tail) to a nose down moment (up-force at the tail). From the pilots' viewpoint the aeroplane is pitching nose down despite full back-stick input, which normally commands a nose-up movement, but as described above the nose of the aeroplane pitches down after the first turn in the spin. Furthermore, the differential pressure measurement corresponds with the visual observation of the sudden change in flow condition, with the differential pressure value increasing from the ¾-turn point in the spin.

7.6 Autorotation of the wings

The outside wing motion is characterised by persistent up-stroke (X-axis rotation due to roll), rotation about the Z-axis (due to positive and negative sideslip), rotation about the spin axis and periodic rotation about the Y-axis (due to oscillation in pitch). Conversely, the inside wing motion is characterised by persistent down-stroke and relative backward motion about the spin axis. However, it will naturally have the same rotation about the Z-axis and the same periodic rotation about the Y-axis as the outside wing. Due to this complex wing motion, combined with high Reynolds number, the autorotation of the wings is challenging to model accurately with CFD using current technology. Therefore, the exact aerodynamic force contribution, or more specifically the detailed lift distribution due to autorotation of the wings remains difficult to quantify.

The USV spanwise movement in- and outwards on the outside wing appears to be governed by the periodic rotation of the wing about the Y-axis. The USV moves outwards when α increases and moves inwards when α decreases. It is possible that lift enhancing streamline flow on the outer part of the outside wing, and the relative higher drag of the inside wing due to reversed and irregular flow, defines autorotation of the wings for the light aeroplane. It is also possible that a certain additional lift is due to the spanwise flow observed on the outside wing. This spanwise flow might be accelerated due to the rotational aerodynamic flow effects described above.

7.7 The importance of the dynamic effects for the development of the spin

In addition to the lift overshoot caused by a pitching wing, the LAWR mode data obtained (as shown in Figure 72) indicate also the lift undershoot caused by the plunging wing. Apparently, the concurrent lift overshoot of the pitching wing with the lift undershoot of the plunging wing, provides a couple with a resultant rolling moment. From an aeroplane stability and control viewpoint, this arrangement of lift under- and overshoot can be viewed as the ‘dark side’ of dynamic stall as it might lead to an unstable flight path.

Ericsson discusses accelerated flow and moving wall effects and notes that these dynamic flow effects occurs in rolling motions [65], and he describes wing rock motions in this context. The data obtained from the Firefly post-stall LAWR mode presented in

section 6.4 might be another full-scale (at $Re_c = 2.2x10^6$) example of these flow effects induced by the motion of the aeroplane.

In particular, two cases introduced in Section 2.2 can be discussed in the context of dynamic stall leading to departures from controlled flight. First, for the Cessna T-37 (Figure 2), a rolling departure from controlled flight was discovered after 40+ years in military training service [23]. Secondly, the Aermacchi Impala was probably prone to depart in the same manner as indicated by an operational supplement to the flight manual [24].

From tuft observations (section 5.2.1), and from reasoning based on the dynamic stall effects discussed above, one could assume that a significant asymmetry in lift condition would be in the time frame where the up going wing has streamline flow and the down going wing has reverse separated flow. However, the dP measurements (Figure 73 and Figure 74) indicate that from the ¼-turn to the ½-turn point in the spin, where the tufts indicated streamline flow over the outside wing, there was not the largest dP difference between inside and outside wing. The most likely explanation for this is that the outside wing was pitching down and not at an effective angle of attack for most of this period. Using the estimated alpha from the VBSE (Figure 48), the outside wing point had a reduction in α_{OWP} from 15 degrees to -13 degrees during this period. However, from the ½-turn to the 1-turn point in the spin, α_{OWP} was increasing from -13 deg to 44 deg, passing through an alpha range where the outer wing section was most likely to be effective in producing lift. In addition, the α_{OWP} rate of change for this period was 53 deg/sec and therefore dynamic stall effects, e.g. a delayed stall-onset [65, 66], were likely to occur during this same time period.

During the same period (from the ½-turn to the 1-turn point) the inside wing was at a very large alpha (α_{IWP} from 13 to 72 deg), where lift generation is less likely. This difference in estimated α was due to the spin motion of the aeroplane (as shown in Figure 47). The outside wing point had a different path through the 3D space as compared to the aeroplane CG. This difference in α, for the inside and outside wing, due to the spin entry motion can be considered a geometric modification of α.

Apparently, it is the time period where the USV was observed that might be most

important for the development of the spin. This is the time frame where the difference in dP between the up and down-going wing was largest, indicating the largest asymmetric lift condition in the spin entry phase.

7.8 Conclusions

This research project, which started with the challenges encountered during spin flight testing of a light aeroplane with a modified tail, has considered the aerodynamic flow conditions in relation to the spin motion of the aeroplane. Due to the challenges of obtaining data for analysis, an alternative Vision Based State Estimation method was used in the investigation. In particular for the spin entry phase, the VBSE was a valuable tool for understanding the complex spin motion, and unique illustrations have been made that can be useful for future flight training programmes. It is proposed that the VBSE method can be an alternative and viable state estimation method for the aeroplane spin.

It is clear that just as the aeroplane stability characteristics just before and at the stall determine if a spin develops or not, the spin entry affects how the spin will develop and if it will become recoverable or not. A spin prediction method based on the aeroplane geometry alone will be unreliable due to the fact that it doesn't account for the dynamic effects of the spin entry. In addition to the dynamic stall effects that have been previously known, this research has led to the suggestion that an additional dynamic effect might exist; the acceleration of the turbulent boundary layer due to the rotational motion of the aeroplane in the spin. Furthermore, a reliable spin prediction method to be used during the design phase has to consider the effectiveness of the aerodynamic controls at high angles of attack and the gyroscopic effects when rotation has started.

However, the positions of the tail surfaces are clearly important to consider for the complete aeroplane configuration. In the present investigation, we have discussed the effect on the spin due to the horizontal tail surface and the importance of the pitch-down moment exerted by the tail section for the development of the spin.

8 Suggestions for future research

The following topics are suggested for future research to further advance the understanding of the aeroplane spin and progress towards a model capable of a more reliable spin recovery prediction:

In this research project, the aerodynamic flow field structure has been studied and documented using tufts on wings, aft fuselage and empennage and a smoke source in front of the wing. Further study of the full-scale, 3-dimensional aerodynamic flow structure over the wings, around the tail surfaces and the fuselage could possibly result in an even better understanding of the aerodynamic flow about a spinning aeroplane. More pressure measurements, ideally resulting in a pressure distribution mapping of the wings and tail surfaces, would give an even better overview of the aerodynamic forces during the spin phases, and might provide further insights into how the dynamic effects influence the development of the aeroplane spin.

Experimental data has been obtained by using an alternative Vision Based State Estimation in conditions where data acquisition has historically been very challenging. It is suggested that these unique data should be used to enhance mathematical modeling and CFD analysis in an effort to recreate the distinct aerodynamic flow conditions observed.

It has been hypothesized that an additional lift component exists due to the additional acceleration of the turbulent boundary layer, induced by the rotation of the wings. The data obtained in this research project, indicate that aerodynamic lift in the developed spin might be a function of Ω. First, as shown in Figure 43, the right turn spins (which had a higher rotation rate) had a lower vertical speed than the left turn spins. Secondly, when plotting point dP measurements from left and right turn spins in the same figure, the right turn spins typically had higher average dP values in the developed spin phase. It should be further investigated if indeed an accelerated spanwise flow component does provide additional lift for a spinning wing.

References

1 Sobie, B. PICTURE: Flight gets first look at redesigned SkyCatcher, Flightglobal.com, Business & GA Article, 3 February 2009

2 Trimble, S. SkyCatcher future in doubt after second flight test crash, Flightglobal.com, News Article, 20 March 2009

3 Fox, L.A. Lancair 400 Spin Testing and Spin Chute Release Failure, Proceedings of the 48th Annual SETP Symposium, 2004

4 Roberts, S.C. Flight Test Lessons Learned from the Spinning Trials of the Gippsland GA-8 Single Engine General Aviation Aircraft, Proceedings of the 44th Annual SETP Symposium, 2000

5 Sling LSA Prototype Lost During Spin Testing, EAA News, February 25, 2010

6 South African Civil Aviation Authority, Aircraft Accident Report and Executive Summary, Sling, ZU-TAF, Ref. CA/18/2/3/8756

7 Philipp, H. Bailout during spin tests, SETP European Symposium, Dresden, Germany, 2006

8 Paranjape, A.A., Ananthkrishnan, N. Analytical Criterion for Aircraft Spin Susceptibility, *Journal of Aircraft*, Vol. 47, No. 5, September – October 2010

9 US Federal Aviation Administration, Advisory Circular 23-8C, *Flight Test Guide for Certification of Part 23 Airplanes,* dated 16 November 2011

10 UK Civil Aviation Authority, British Civil Airworthiness Requirements, Section S, *Small Light Aeroplanes*, CAP 482 issue 3 dated 15 August 2003

11 European Aviation Safety Agency, Certification Specifications CS-VLA, *Very Light Aeroplanes*, Decision No. 2003/18/RM dated 14 November 2003

12 European Aviation Safety Agency, Certification Specifications CS-22, *Sailplanes and Powered Sailplanes*, Decision No. 2003/13/RM dated 14 November 2003

13 European Aviation Safety Agency, Certification Specifications CS-23 for *Normal, Utility, Aerobatic, and Commuter Category Aeroplanes*, Decision No. 2003/14/RM

14 US Federal Aviation Administration, Federal Aviation Regulation Part 23 *Airworthiness Standards: Normal, Utility, Acrobatic, And Commuter Category Airplanes,* Amdt. 23-34, Eff. 02/17/87

15 Defence Standard 00-970 Part 1 Issue 5 – Section 2: Flight, 23 February 2007

16 MIL-F-8785C: Military Specification, *Flying Qualities of Piloted Airplanes,* November 1980

17 Neumann, H. “Drooped Leading Edge”, Flight Test Evaluation with a small General Aviation Airplane, 2006-03-07, SETP European Symposium, Dresden, Germany, 2006

18 Anderson, S.B. Historical Overview of Stall/Spin Characteristics of General Aviation Aircraft, *Journal of Aircraft*, Vol. 16, No.7, Article No. 78-1551, July 1979

19 Anderson, S.B. A Look at Handling Qualities of Canard Configurations, *Journal of Guidance,* Vol. 10, No.2, March-April 1987

20 Morris, D.E., Port, W.G.A., Flight Test of a Tailless Glider of V Planform with 28.4 deg. Sweepback*,* Report No. Aero 2394, Royal Aircraft Establishment, Farnborough, UK, January 1951

21 Veillette, P.R. Rudder and Elevator Effects on the Incipient Spin Characteristics of a Typical General Aviation Training Aircraft, AIAA-93-0016, University of Utah, Salt Lake City UT, 199

22 Stewart, E.C., Suit, W.T., Moul, T.M., Brown, P.W. Spin Tests of a Single-Engine, High-Wing Light Airplane, NASA Technical Paper 1927, Langley Research Center, Hampton VA, January 1982

23 Davis, G. Just Another Spin? (handling the T-37 plane), 89 FTS, Sheppard AFB, TX, USA, From: Flying Safety 11/1/2001, Brief Article, Encyclopedia.com

24 Aermacchi MB-326M, Flight Manual, Aermacchi Technical Publications Department, P.I. 1T-MB326M-1, 10 Feb 1977, Change 2, 15 Feb 1982

25 Courtney, F.T. Spins and things, *Aeronautics*, Vol.45 no.1, November 1961

26 Berriman, A.E. Parke’s Dive, *Flight*, No. 192, August 31, 1912

27 Lindemann, F.A. Glauert, H., Harris, R.G. The Experimental and Mathematical Investigation of Spinning, Reports and Memoranda No. 411, London, UK, March 1918

28 Pilot’s Flying Log Book, F.A. Lindemann, Royal Aircraft Factory, Log entries from 9.9.1916 to 3.1.1919

29 Glauert, H. The Investigation of the Spin of an Aeroplane, Reports and Memoranda No. 618, London, UK, June 1919

30 Bryant, L.W., Gates, S.B. The Spinning of Aeroplanes, *The Journal of The Royal Aeronautical Society*, Fifth Meeting, 62nd Session, March 1927

31 Irving, H.B., Stephens, A.V. Safety in Spinning, *The Journal of The Royal Aeronautical Society,* No. 255, Vol. XXXVI, March 1932

32 Durand, W.F., Jones, B.M. *Aerodynamic Theory Vol V, Div N Dynamics of the Airplane*, Julius Springer, Berlin 1935

33 Accidents Investigation Branch, Aircraft Accident Report No. 3/77, EW/C555, UK, 1977

34 Air Accidents Investigation Branch, AAIB Bulletin: 3/2008, EW/C2007/08/12, UK, 2008

35 Stowell, R. *Stall/Spin Awareness*, Rich Stowell Consulting, Ventura, CA, 2007, ISBN 978-1-879425-43-9

36 Wittwer, P., Masefield, O. Spin Behaviour of the Pilatus PC-7 Turbo Trainer, ICAS-82-3.6.1, Pilatus Aircraft Ltd., Stans, Switzerland

37 Stough III, H. P., Patton, Jr., J.M., Sliwa, S.M. Flight Investigation of the Effect of Tail Configuration on Stall, Spin, and Recovery Characteristics of a Low-Wing General Aviation Research Airplane, NASA Technical Paper 2644, Langley VA, October 1986

38 Stough III, H. P., DiCarlo, D.J., Patton, Jr., J.M. Flight Investigation of Stall, Spin, and Recovery Characteristics of a Low-Wing, Single-Engine T-Tail Light Airplane, NASA Technical Paper 2427, Langley VA, October 1985

39 Department of Transportation, Federal Aviation Administration, Type Certificate Data Sheet No. A00003SE, Revision 9, May 30, 2003

40 Department of Transportation, Federal Aviation Administration, Type Certificate Data Sheet No. A00009CH, Revision 4, March 14, 2002

41 Stough III, H. P., DiCarlo, D.J. Spin Resistance Development for Small Airplanes – A Retrospective, NASA Langley Research Center, SAE Technical Paper Series 2000-01-1691, May 2000

42 Aeroplane and Armament Experimental Establishment, Tucano T Mk 1 Spinning Assessment, Letter Report TM 1966, Boscombe Down, June 1992

43 Norris, E.J., Sandford, R., Tonkinson, B.J. Jet Provost T.Mk.5 Handling and Performance Assessment for Service Release, Aeroplane and Armament Experimental Establishment, Report No. A&AEE 875/6, Boscombe Down, March 1970

44 McAvoy, W.H. Piloting technique for recovery from spins, NACA Technical Note No. 555, Washington, February 1936

45 Shiel, W. *Cessna Warbirds*, Jones Publishing, Inc., WI, USA, 1995, ISBN 1-879825-25-2

46 Air Publication, AP.101B-2305-15, AL15, Jet Provost T Mk 5 A, Handling in Flight, UK

47 Borton, A. J. Spin testing the T-3A Firefly, Major, USAF, USAF Test Pilot School, Edwards AFB, CA

48 Neihouse, A. I. A mass-distribution criterion for predicting the effect of control manipulation on the recovery from a spin, NACA Wartime Report L-168, WA, August 1942

49 Harper, D.J. Comparison of Model and Full Scale Spinning Tests on a Basic Trainer (Percival Prentice), Royal Aircraft Establishment, Report No. Aero 2298, Farnborough, November 1948

50 Mortensen, J.A., Hamilton, L.J. U.S. Navy T-45A Departure and Spin Evaluation, T-45 Project Coordination Office, Naval Air Warfare Center, Aircraft Division, Patuxent River MD

51 Holcomb, M.L. The Beech Model 77 "Skipper" Spin Program, AIAA Aircraft Systems and Technology Meeting, NY, August 1979

52 Burk, Jr., S. M., Bowman, Jr., J.S., White, W. L. Spin-tunnel investigation of the spinning characteristics of typical Single-Engine General Aviation Airplane Designs. I – Low-wing model A: Effects of tail configurations, NASA Technical Paper 1009, Langley VA, September 1977

53 Finn, E. Analysis of routine tests of monoplanes in the Royal Aircraft Establishment Free Spinning Tunnel, Report No. B.A. 1409, June 1937

54 Bowman, Jr., J.S. Summary of spin technology as related to light General-Aviation Airplanes, NASA TN D-6575, Washington DC, December 1971

55 Bowman, Jr., J.S., Hultberg, R.S., Martin, C.A. Measurements of Pressures on the Tail and Aft Fuselage of an Airplane Model During Rotary Motions at Spin Attitudes, NASA Technical Paper 2939, Langley VA, 1989

56 Thompson, W.D. *Cessna Wings for the world, The Single-Engine Development Story*, ISBN 0-89288-221-2, USA, 1991

57 Meyer, C.H. *Corky Meyer's Flight Journal, A Test Pilot's Tales of Dodging Disasters – Just in Time*, ISBN 1-58007-093-0, USA, 2006

58 Stinton, D. *Flying Qualities and Flight Testing of the Aeroplane*, AIAA Education series, Reston VA, Third Edition, ISBN 1-56347-281-0, 1999

59 Englert, S. Lancair Columbia 400 Spin Recovery Testing, SETP Symposium, LA, 2005

60 Kimberlin, R.D. *Flight Testing of Fixed-Wing Aircraft*, AIAA Education Series, ISBN 1-56347-564-2, 2003

61 Janssens, L.G., Kimberlin, R.D. Micco MAC-145B Spin Tests, Part I, 2000 World Aviation Conference, San Diego, CA, October 2000

62 Janssens, L.G. Micco MAC-145B Spin Tests, Part II and III, SETP European Symposium, Lucerne, Switzerland, May 2002

63 Neihouse, A. I. The Effect of variations in Moments of Inertia on Spin and Recovery Characteristics of a Single-Engine Low-Wing Monoplane with Various Tail Arrangements, including a Twin Tail, NACA Technical Note No. 1575, Washington DC, May 1948

64 Ericsson, L.E., Beyers, M.E. Flat Spin of Axisymmetric Bodies, *Journal of Aircraft*, Vol. 32, No. 6, Nov – Dec 1995

65 Ericsson, L.E. Dynamic Airfoil Flow Separation and Reattachment, *Journal of Aircraft*, Vol. 32, No. 6, Nov – Dec 1995

66 Beyers, M.E. and Brown, A.P. Pitch-Rate Induced Abrupt Wing Stalling of Straight Wing Aircraft, AIAA Atmospheric Flight Mechanics Conference and Exhibit, 21-24 August 2006, Keystone, Colorado

67 The Slingsby T67M200 Pilots Notes, incorporating the CAA approved flight manual, Slingsby Aviation PLC, UK, August 1985

68 European Avaition Safety Agency, Type-Certificate Data Sheet A 390, Slingsby T67, Issue 02, 3 September 2007

69 Airplane Manual SAAB SAFIR 91B-2, Description.

70 Rutter, M. Airworthiness Co-ordinator, Composite Engineering Group, Marshall of Cambridge Aerospace Ltd. Private Correspondence, 14 January 2014

71 Holmström, S. Private Correspondence, 14 March 2013

72 Leica HDS 6000 Scanner, http://hds.leica-geosystems.com/en/HDS-Laser-Scanners-SW_5570.htm (Retrieved 11/01/11)

73 Leica Cyclone 6.0, http://hds.leica-geosystems.com/en/Leica-Cyclone_6515.htm (Retrieved 11/01/11)

74 3Dreshaper 5.2, http://www.3dreshaper.com/en1/En_PointCloudProcess.htm (Retrieved 11/01/11)

75 Ferreira, R. Project report on creation of high precision model of the airplane Slingsby (not published), Asis Grenland Group, Norway, May 2010

76 Panasonic, Operating Instructions, Memory card Camera-Recorder, Model No. AG-HPX500, DVCProHD, 2007 Matsushita Electric Industrial Co., Ltd.

77 Kenyon Laboratories, http://www.ken-lab.com/stabilizers.html (Retrieved 21/11/11)

78 Pentax, SLR Digital Camera, K20D, Operating Manual, Pentax Corporation 2008

79 SynthEyes 64-Bit Version 2008.1.1028, 2009 Andersson Technologies LLC

80 Autodesk 3ds Max 2011, 2010 Autodesk, Inc.

81 Sony, Handycam HDR-CX105, 2009 Sony Corporation

82 JVC Everio G, Hard Disk Camcorder, GZ-MG840BE, HDD, 2008 Victor Company of Japan, Limited

83 Muvi Micro DV Camcorder, http://www.veho-uk.com/main/index.aspx (Retrieved 7/02/11)

84 MTi-G User Manual and Technical Documentation, Xsens Technologies B.V., Document MT0137P, Revsion H, 15 Oct 2010

85 Muller, D. and Pommera, G. Spinning the modified ROBIN R2160, Cockpit, The Society of Experimental Test Pilots, April, May, June 1999

86 Pitot-Static System PSS-8, Interface Definition Document, Simtec Buergel AG, Issue 1, August 28, 2012

87 Comet, Smoke Signals for Parachutists, Data Sheet, Issue 24.04.2003

88 RTMC and ADP5 User Manual, Rev. 6, Simtec Buergel AG, November 25, 2010

89 Buergel, V. Private correspondence, Simtec Buergel AG, November 21, 2012

90 Engelsvoll, J. Private correspondence, November 3, 2014

91 NDN Firecracker, Aircraft Flight Manual, N182FR, NDN 1.2. Iss.1, 24 May 1979

92 Hoff, R.I., Gratton, G.B., Gee, A.E. Estimating Sailplane Mass Properties, *Technical Soaring*, Vol. 34, No. 4, October – December 2010

93 Grier, P. ”Gary, You Better Get Back In It!”, AIR FORCE Magazine, April 2009

94 Defence Test and Evaluation Organisation, Tucano T Mk 1 Assessment of possible unified spin recoveries, Report No DTEO/A&E/BD/95/128, Boscombe Down, December 1995

95 Jones, B.M. and Haslam, J.A.G. Airflow about Stalled and Spinning Aeroplanes shown by Cinematographic Records of the Movements of Wool-Tufts, Aeronautical Research Committee, T.3291, August 1932

96 Brown, A.P., Dillon, J., Craig, G. and Erdos, R. Flight Manoeuvre and Spin Characteristics of the Harvard Mk 4: Application to Human Factors Flight Research, AIAA Atmospheric Flight Mechanics Conference and Exhibit, Providence, Rhode Island, Aug. 16-19, 2004, 2004-4815

97 Gratton, G.B., Hoff, R.I., Rahman, C., Harbour, C. and Williams, S. Evaluating a set of stall recovery actions for single engine light aeroplanes, *The Aeronautical Journal*, Volume 118, No. 1203, May 2014

98 Pettersen, S. Weather Analysis and Forecasting, Second Edition, Vol 1, Motion and Motion Systems, McGraw-Hill Book Company, Inc., 1956

99 Meriam, J.L. and Kraige, L.G. Engineering Mechanics, Dynamics, Vol. 2, Third Edition, ISBN 0-471-59273-0, 1993

100 Lentink, D. and Dickinson, M.H. Biofluiddynamic scaling of flapping, spinning, and translating fins and wings, *The Journal of Experimental Biology* 212, 2691-2704, 5 February, 2009

101 Rossby, C.G. On the momentum transfer at the sea surface, *Papers in Physical Oceanography and Meteorology,* Vol. IV, No. 3, June, 1936

Appendix 1

Installation and flight calibration of the Air Data Probe

1. Introduction

A Multi Purpose Boom (MPB) was designed and built for the spin research programme at the Brunel Flight Safety Laboratory. The MPB was mounted onto the right hand wing of the Slingsby T67MX Firefly research aeroplane and approval was obtained to carry either a smoke source (used for flow visualization) or an Air Data Probe (ADP). This appendix describes first the installation of the ADP on the right hand wing of the Firefly and then the subsequent flight calibration of the system.

2. ADP installation

The ADP was mounted with a negative incidence of 3.5 degrees measured against level (Figure 1). This was done to enable a higher positive angle of attack (AoA) measurement when considering the maximum +20 degree AoA limit of the ADP. The wing chord, at the spanwise wing point where the MPB was mounted, was measured to 3 degrees (parallelogram shown in Figure 1) against level. This angle was confirmed by measurement on the CAD Firefly model as shown in Figure 2 below.

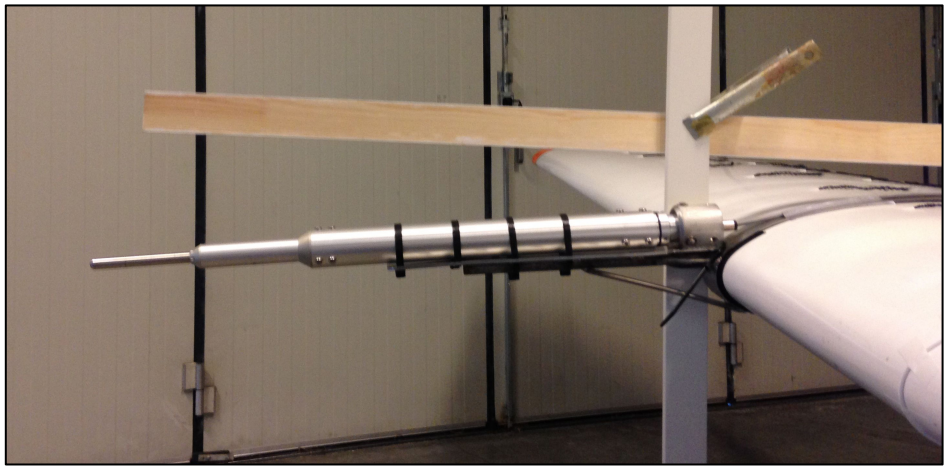

Figure 1. The probe angle is -3.5 degree measured against level.

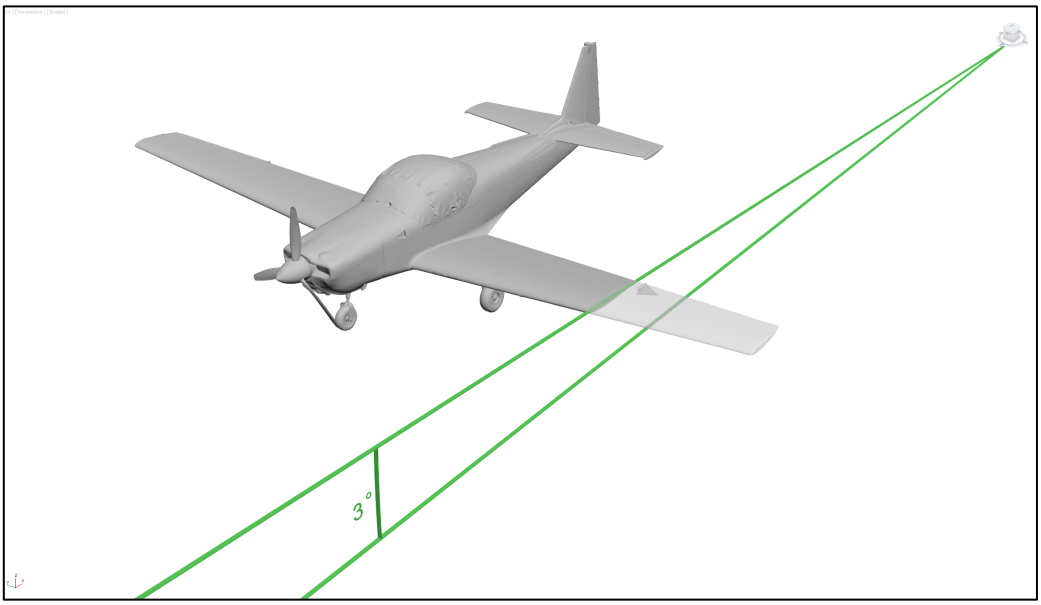

Figure 2. Illustration showing the measurement of wing chord angle using the aeroplane CAD model (created by laser scanning the full-scale aeroplane).

Aeroplane datum was +2 degrees with the Firefly parked in the hangar, measured using a level and the Firefly rigging board for longitudinal leveling (Figure 3).

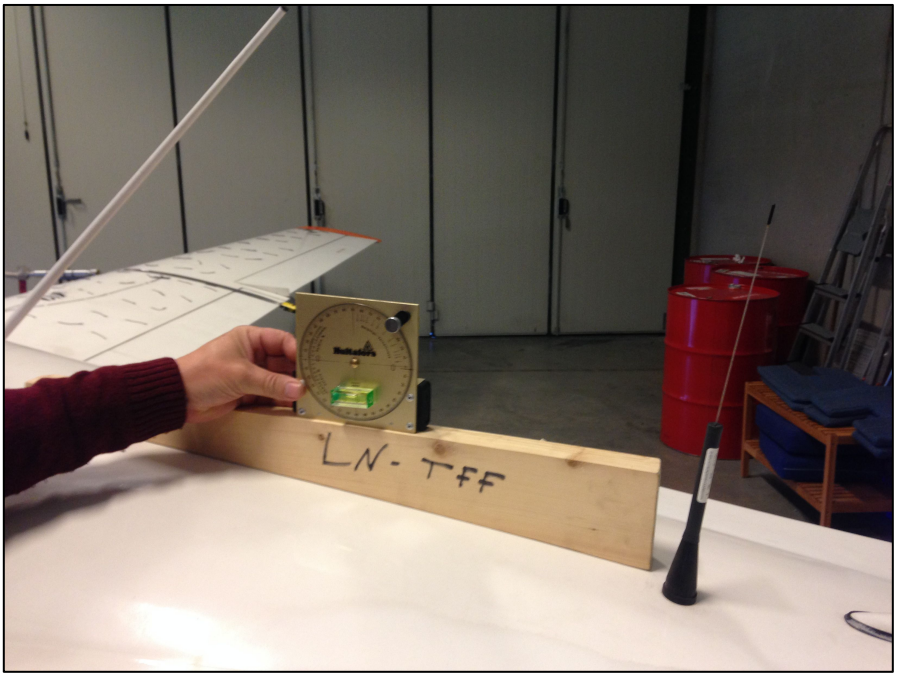

Figure 3. The measurement of aeroplane datum using a level and the appropriate rigging board for longitudinal leveling.

Assuming that the aeroplane flies at datum level when using power for level flight (PLF), the wing chord will then have a theoretical 1 degree AoA at this wing point (WP).

In theory, the ADP will record the following angle in PLF:

1 deg incidence – 6.5 deg (angle between chord and ADP) = -5.5 deg [1]

However, an ADP must be calibrated in flight due to several effects that will influence the local angle of attack measured. This modification of the local angle of attack is mostly due to upwash, but could also be due to probe bending caused by air loads or due to wing flexing [1].

3. Flight calibration of ADP

The same aeroplane mass and CG condition used for the spin research flights was also used for the ADP calibration flights (takeoff mass at 900 kg and CG at 21% MAC). The following maneuver was used for the flight calibration of the ADP:

A power setting of 20 inches of manifold pressure and 2450 propeller RPM was used for PLF resulting in airspeed of approx. 100 kn IAS (97 kn CAS). This setting was confirmed by the MTi-G as 'datum flight' level. Thereafter, the airspeed was reduced at 5 kn intervals. At each intermediate intervals the airspeed was kept as constant as possible and the altitude was kept level throughout. Post flight, the pitch angle (θ) was plotted vs. the local AoA measured by the ADP at each interval and the result is shown in Figure 4.

In addition to the pitch angle measurement by the MTi-G, another source of pitch angle data from the iLevel AHRS-G mini [2] was used for comparison. The reason for obtaining additional pitch angle measurements was due to the difficulty in getting steady pitch angle results from the MTi-G, despite the effort in establishing steady flight conditions between the data points. Based on both of these measurements the following AoA correction equation has been used:

$$\alpha_{corrected} = 1.25\ \alpha_{local} - 2.1 \qquad [2]$$

This slope and bias is also shown in Figure 4 below.

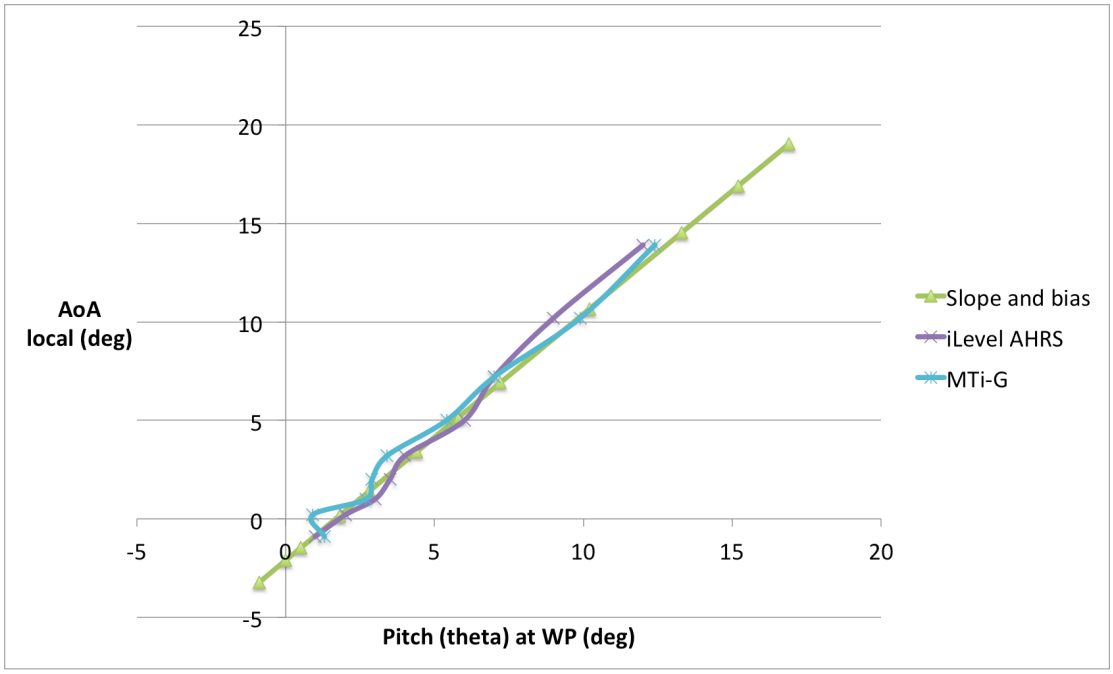

Figure 4. Comparison of pitch angle measured by the MTi-G and iLevel AHRS vs. local AoA measured by the ADP. The suggested slope and bias is shown in the same figure.

[1] Gracey, W. Summary of methods of measuring angle of attack on aircraft, NACA Technical Note 4351, Washington, USA, August 1958

[2] AHRS-G mini, http://www.aviation.levil.com/ahrs-g-mini.html, retrieved 13 October 2014